

MAPPING THE ANKLE JOINTS PASSIVE MOTION AND MEASURING THE EFFECT OF INJURY
ON LIGAMENT CONSTRAINT AT THE ANKLE JOINT

By

Copyright 2011

James Edward West III

Submitted to the graduate degree program in Bioengineering and the Graduate Faculty of
the University of Kansas in partial fulfillment of the requirements for the degree of Master of
Science.

Chairperson Dr. Lorin Maletsky

Dr. Wen Liu

Dr. Sara Wilson

Date Defended: 01/28/2011

The Thesis Committee for Jim West III

certifies that this is the approved version of the following thesis:

MAPPING THE ANKLE JOINTS PASSIVE MOTION AND MEASURING THE EFFECT OF INJURY
ON LIGAMENT CONSTRAINT AT THE ANKLE JOINT

Chairperson Dr. Lorin Maletsky

Dr. Wen Liu

Dr. Sara Wilson

Date approved: 01/28/2011

Abstract

Lateral ankle sprain is one of the most common sports injuries, and having a better understanding of how ligament constraint changes after injury can assist in accurately diagnosing ankle laxity, prevention, and recovery. The objective was to map out the range of motion of the ankle under constant torque loading, and to examine the effect of a lateral ankle sprain level 2 and 3. Nine cadaveric ankles were run through a range of motion where a 6 degree of freedom load cell was used to collect force and torque loads and an Optotrak scanner collected the position of the tibia, talus, and calcaneus. The ankle saw more motion in abduction and inversion than adduction and eversion in the talocrural joint, and the ankle joint complex. The subtalar joint saw no change in inversion or eversion, or adduction, but there was less than four degrees of motion in adduction while the foot was plantarflexed. In general the foot was insensitive to varying torque levels with or without injury except in the talocrural joint where inversion and eversion saw a three to four degree difference after a sprain level 3. It was observed that when ABAD torques were applied the ankle was free to move in INEV, but when INEV torques were applied there was a constraint that limited the motion of the ankle in the ABAD direction. The results from this study show the range of motion of the ankle intact, and with a level 2 and level 3 sprain in the subtalar joint, the talocrural joint, and the ankle joint complex. With knowledge of the ankle's envelope of motion and quantitative assessment of the Taylor tilt test could be created, as well during a total ankle replacement different mid-flexion assessments could be made to create better outcomes for patients.

Acknowledgements

I would first like to thank my loving wife Vanessa for her continued love and support, as well as my advisor Dr. Lorin Maletsky for his thought provoking questions, help, encouragement, and support. I would also like to thank Adam Cyr, Mark Komosa, Kaity Fucinaro, Sami Shalhoub, Amit Mane, Linda Denney and others for their help in figuring out some of the linear algebra, debugging code, providing invaluable feedback, and donating their time helping me to collect data. I would also like to thank the departments of mechanical engineering and bioengineering at KU.

I would like to acknowledge the help of others who had a smaller hand in this thesis as well. Dr. Roeland P. Kleipool for supplying me with raw data from a review paper he authored. Lirel Holt reviewed an early version of my manuscript and gave me invaluable feedback. Andrew Magill provided an excellent picture of the x-ray of an ankle from his foot, which I received permission to use and edit.

Table of Contents

LIST OF FIGURES	IX
LIST OF TABLES	XII
GLOSSARY	XIII
CHAPTER 1 INTRODUCTION	1
1.1 MOTIVATION	1
1.1 OVERVIEW.....	2
CHAPTER 2 BACKGROUND	3
2.1 ANATOMY	3
2.1.1 <i>Bones</i>	3
2.1.2 <i>Joints and Ligaments</i>	4
2.2 ANKLE LIGAMENT INJURY.....	6
2.3 BIOMECHANICS OF THE ANKLE JOINT	8
2.3.1 <i>Range of Motion</i>	8
2.3.2 <i>Joint Kinematics</i>	9
2.3.3 <i>Kinematic Differences among Populations</i>	10
2.3.4 <i>Coordinate System Construction</i>	10
2.3.5 <i>Mathematical Descriptions of Joint Motion</i>	11
2.3.6 <i>Previous Motion Studies</i>	13
CHAPTER 3 MAPPING THE ANKLE JOINTS PASSIVE MOTION AND MEASURING THE EFFECT OF INJURY ON LIGAMENT CONSTRAINT AT THE ANKLE JOINT.....	18
3.1 INTRODUCTION AND BACKGROUND	18
3.2 MATERIALS AND METHODS.....	20
3.2.1 <i>Specimen Preparation</i>	20
3.2.2 <i>Procedure</i>	21
3.2.3 <i>Processing Kinematics</i>	22
3.2.4 <i>Constructing Fixed Coordinate System Axes</i>	22

3.2.5	<i>Equipment</i>	23
3.2.6	<i>Load Cell Analysis</i>	24
3.3	RESULTS	25
3.3.1	<i>Neutral Flexion Path</i>	25
3.3.2	<i>Off Axis Loading</i>	25
3.3.3	<i>Intact Ankle Analysis</i>	26
3.3.4	<i>Sprained Ankle Results</i>	27
3.3.5	<i>Stiffness</i>	29
3.4	DISCUSSION	30
3.4.1	<i>Comparison of Results</i>	32
3.4.2	<i>Sources of Error</i>	34
3.4.3	<i>Future</i>	35
3.5	CONCLUSION	36
CHAPTER 4	CONCLUSION	48
4.1	CONFLICT OF INTEREST STATEMENT AND ROLE OF FUNDING	50
REFERENCES		51
APPENDICES		57
APPENDIX A	TRANSFORMATION EQUATIONS	58
A.1	<i>Load Cell Transformation Equations</i>	58
APPENDIX B	VECTOR TRANSFORMATIONS	60
APPENDIX C	EXAMPLE DATA SETS	63
C.1	<i>Cadaver Details</i>	63
C.2	<i>Representative Data from One Ankle</i>	63
C.2.1	Definition of Coordinate System	64
C.2.2	Kinematic Output and Torque Loading from Applied Motions	65
C.3	<i>Representative Raw Data Points and Line Fits</i>	72
C.4	<i>Positive and Negative Angles vs. PFDF</i>	75

C.4.1	AJC.....	76
C.4.2	TCJ.....	80
C.4.3	STJ.....	84
C.5	<i>Range Angles vs. PFDF</i>	88
C.5.1	AJC.....	89
C.5.2	TCJ.....	93
C.5.3	STJ.....	97
C.6	<i>Off Axis Loading</i>	101
C.6.1	ABAD Motion.....	102
C.6.2	INEV Motion.....	103
APPENDIX D	SENSITIVITY ANALYSIS.....	104
D.1	<i>Neutral Position Repeatability</i>	104
D.2	<i>Fixed CS Construction Sensitivity</i>	105
APPENDIX E	STATISTICAL ANALYSIS.....	108
APPENDIX F	COMPUTATIONAL PROGRAMS.....	109
F.1	<i>Ankle Processing, and Kinematics Transformation Builder Pseudo code</i>	109
F.2	<i>Ankle Processing, and Kinematics Transformation Builder Matlab Code</i>	110
F.2.1	APM.m.....	110
F.2.2	fcn_AnkleProcessMasterLoadData.m.....	111
F.2.3	fcn_transformationbuilder.m.....	117
F.2.4	fcn_transformmcs.m.....	117
F.3	<i>Algorithm for Finding Ankle Axes and Center Pseudo Code</i>	119
F.4	<i>Algorithm for Finding Ankle Axes and Center Matlab Code</i>	120
F.4.1	fcn_buildFixedCS5.m.....	120
F.4.2	fcn_findAnkleAxis10.m.....	122
F.5	<i>Good and Suntay Processing Code</i>	125
F.5.1	fcn_processGS.m.....	125
F.5.2	fcn_gs.m.....	126

F.5.3	fcn_filtersdata.m	127
F.6	<i>Graphical Interfaces</i>	127
F.6.1	gui_bonePositionGrapher3.fig.....	127

List of Figures

- Fig. 2.1: X-Ray image of a left foot showing colored outlines of the bones and joints in the ankle: subtalar joint (red), talocrural joint (green), ankle joint complex (blue) consisting of both the STJ and TCJ. Original X-Ray image provided with permission by Andrew Magill.. 15
- Fig. 2.2: Rotational coordinate system shown for ankle joint complex on a right foot..... 16
- Fig. 2.3: The three bones of the ankle joint. Coloring of A, B, C are represented by articulating bone based on Fig. 1's color coding..... 17
- Fig. 3.1: View of the ankle rig setup. Overlaid on the ankle are a set of probed points indicating each bone in the ankle: tibia (blue), talus (red), and calcaneus (green)..... 37
- Fig. 3.2: Frontal view of the Grood and Suntay Coordinate Axes for each reference frame [1, 24, 56]. The capital letter (XYZ) is the fixed proximal axis, and the lower case letter (xyz) are the fixed distal axis. e1 is the proximal axis. e2 is the floating axis between e1 and e3. e3 is aligned along the long axis of the distal bone. 39
- Fig. 3.3: Surfaces used for axis and joint center finding 40
- Fig. 3.4: PFDF Angle Comparison Between Joints. PFDF range of motion from each ankle joint versus the AJC. For example at -30° PFDF AJC the STJ had -2° PFDF. For consistency all PFDF angles are referenced from the AJC shown in green as a baseline. The average standard deviation for both the TCJ and STJ was less than 0.06 degrees. 41
- Fig. 3.5: Off-axis torque loading of all ankles and all applied loading conditions. Red: torque loading from applied ABAD torques. Blue: torque loading from applied INEV torques. Loadings shown were collected from all subjects and all loading conditions for the intact ankles. 42
- Fig. 3.6: Motion of the intact ankle (n=9) three reference frames showing iso-torque load lines at 3 and 6 Nm. The top green graph (NFP) was the average neutral path subtracted from each ankles motion. The average ankle motions are shown with the top lines being positive rotations, and the bottom lines being negative rotations. The horizontal black line at 0 degrees was the NFP. A, B, and C are applied ABAD motion, while D, E, and F were applied INEV motion. For all angles shown at least six ankles had data across the range shown, this was the reason for some discontinuity in the line at the extremes. The PFDF motion (A-F) are relative to AJC motion and not relative joint motion. The standard deviation across the flexion range was 0.346 for ABAD torques and 0.409 for INEV torques and was less than 0.5 in all joints..... 43
- Fig. 3.7: (shown above) Passive Motion of the injured ankle joint at 3 and 6 Nm in each direction. Three reference frames showing change in iso-torque load lines normalized to the intact ankles passive motion Row 1:ABAD motion, Row 2:INEV motion. Sprain level 2 (talofibular) and Sprain level 3(calcanefibular) refer to the ligament that was cut. ANOVA results indicated by a significant difference between intact/sprain level 2 (Square ■), sprain level 2/sprain level 3 (Diamond ◆), and intact/sprain level 3 (Circle ●). Blue and red symbols indicate a significant difference ($p < 0.05$) from a 3 and 6 Nm torque load, respectively. ANOVA was calculated at five different flexion angles: min

angle for each ankle, -10, 0, 10, and max angle for each ankle. Between -20 and 10 degrees PFDF there were nine ankles, however at the extremes there were a minimum of six ankles.....	44
Fig. 3.8: Average stiffness from applied torque loading. The average stiffness was calculated for each run between -20 and 10 degrees PFDF from 0 to 3 Nm and 3 to 6 Nm.	45
Fig. 3.9: Injured motion of the injured ankle joint with both axes shown. AJC view from applied INEV motion, (top) ABAD motion, (bottom) INEV motion. Eversion has a shift towards inversion which becomes very apparent with sprain level 3.	46
Fig. 3.10: Comparison to previous data formatted and organized in a review article [40]. Error bars represent ± 1 standard deviation [42-45, 47-49, 78].	47
Fig. A.1: View of the load cell CS (top) and the tibia center (bottom). The CS was transformed from the load cell CS to the tibia center.	59
Fig. C.1: Coordinate system definition for ankle number four. Blue is tibia CS, red is the talus CS, and green is the calcaneus CS.....	64
Fig. C.2: Applied motion - Neutral ABAD Path	65
Fig. C.3: Applied motion - Neutral Flexion Path.....	66
Fig. C.4: Applied motion - Neutral INEV Path	67
Fig. C.5: Applied motion - ABAD Rotation.....	68
Fig. C.6: Applied motion - INEV Rotation.....	69
Fig. C.7: Applied motion - ABAD Torque	70
Fig. C.8: Applied motion - INEV Torque.....	71
Fig. C.9: AJC view of the applied 3Nm ABAD torques to the intact ankle condition. Points and line fits vs. PFDF motion. A 5'th order polynomial was used to fit each ankle in both ABAD and INEV to create continuous data sets. Applied adduction torques to the ankle with a threshold selection of 3Nm. showing a healthy intact ankle.....	73
Fig. C.10: AJC view of the applied 3Nm ABAD torques to an ankle that has sustained a level 3 ankle sprain. Points and line fits vs. PFDF motion. A 5'th order polynomial was used to fit each ankle in both ABAD and INEV to create continuous data sets. Applied adduction torques to the ankle with a threshold selection of 3Nm showing the same ankle as Fig. C.1, but with a level 3 ankle sprain.....	74
Fig. C.11: Resulting motion from 3 Nm of ABAD torque in the AJC.....	76
Fig. C.12: Resulting motion from 6 Nm of ABAD torque in the AJC.....	77
Fig. C.13: Resulting motion from 3 Nm of INEV torque in the AJC.....	78
Fig. C.14: Resulting motion from 6 Nm of INEV torque in the AJC.....	79
Fig. C.15: Resulting motion from 3 Nm of ABAD torque in the TCJ.	80
Fig. C.16: Resulting motion from 6 Nm of ABAD torque in the TCJ.	81

Fig. C.17: Resulting motion from 3 Nm of INEV torque in the TCJ.	82
Fig. C.18: Resulting motion from 6 Nm of INEV torque in the TCJ.	83
Fig. C.19: Resulting motion from 3 Nm of ABAD torque in the STJ.....	84
Fig. C.20: Resulting motion from 6 Nm of ABAD torque in the STJ.....	85
Fig. C.21: Resulting motion from 3 Nm of INEV torque in the STJ.....	86
Fig. C.22: Resulting motion from 6 Nm of INEV torque in the STJ.....	87
Fig. C.23: Resulting range of motion from 3 Nm ABAD torque in the AJC.	89
Fig. C.24: Resulting range of motion from 6 Nm ABAD torque in the AJC.	90
Fig. C.25: Resulting range of motion from 3 Nm INEV torque in the AJC.....	91
Fig. C.26: Resulting range of motion from 6 Nm INEV torque in the AJC.....	92
Fig. C.27: Resulting range of motion from 3 Nm ABAD torque in the TCJ.....	93
Fig. C.28: Resulting range of motion from 6 Nm ABAD torque in the TCJ.....	94
Fig. C.29: Resulting range of motion from 3 Nm INEV torque in the TCJ.	95
Fig. C.30: Resulting range of motion from 6 Nm INEV torque in the TCJ.	96
Fig. C.31: Resulting range of motion from 3 Nm ABAD torque in the STJ.....	97
Fig. C.32: Resulting range of motion from 6 Nm ABAD torque in the STJ.....	98
Fig. C.33: Resulting range of motion from 3 Nm INEV torque in the STJ.....	99
Fig. C.34: Resulting range of motion from 6 Nm INEV torque in the STJ.....	100
Fig. C.35: Varying levels of off-axis loading for an applied ABAD motion.	102
Fig. C.36: Varying levels of off-axis loading for an applied INEV torque.	103
Fig. D.1: Repeatability where the neutral position was varied by +/- 3 degrees in 1 degree increments.	106
Fig. F.1: Example view of the bone position grapher written in Matlab and used to validate the kinematics.	128

List of Tables

Tbl. 3.1: Definition of motions (total=15) applied to the ankle. The motions in this table were run for each ankle condition (Intact, sprain level 2, and sprain level 3). Note: The order was not randomized, motions were followed sequentially.	38
Tbl. C.1: Cadaver specimen details	63
Tbl. D.1: Numerical results from repeatability study. Average change in orientation during neutral position was less than 0.03 degrees, while the range of motion was less than 0.10 degrees.	107
Tbl. E.1: Statistical significance of injury modes in the ankle joints based on two torque loading levels (3 and 6 Nm). A confidence interval was constructed from the comparison of group means where a significant difference in means was indicated by a 1. The comparison was done for intact (intact_N), sprain level 2 (S2_N), and sprain level 3 (S3_N), where N is the torque loading level.....	108

Glossary

ABAD – abduction / adduction

Abduction – Rotation away from the midline axis of the body, (positive if L, negative if R).

Adduction – Rotation towards the midline axis of the body, (positive if R, negative if L).

AJC – Ankle joint complex defined as the joints made up of the tibia, fibula, talus, and calcaneus. Specifically it is a combination of the talocrural and subtalar joints.

Anterior – In the sagittal plane towards the front of the body.

AP - Anterior / Posterior

ATFL – Anterior talofibular ligament

CFL – Calcaneofibular ligament

CS – Coordinate system

DOF – Degree of freedom

Dorsiflexion – Extension of the sole of the foot superiorly (positive).

Eversion – Rotation of the foot away from the midline of the body away from the sagittal plane and upward, (positive).

fROM – Functional range of motion

G&S – Grood and Suntay refers to a mathematical method for defining kinematic motion using open chain cylinders [1].

In vitro – Experiment with cadaveric subjects.

In vivo – Clinical experiment with living subjects.

INEV – Inversion / eversion

Inferior – Direction towards the feet in the axial/coronal plane of the body.

Inversion – Rotation of the foot into the midline of the body towards the sagittal plane and upward (negative).

Iso-torque loading – Represents a single torque load. Often this is used to select kinematic data at a specific load.

Lateral – Direction away from the sagittal plane of the body.

LC – Six degree of freedom load cell

Medial – Direction towards the sagittal plane of the body.

ML – Medial / lateral

mROM – Maximal range of motion

NFP – Neutral flexion path

Off-axis torques - Refers to the torque loading in the orthogonal direction.

PFDF – Dorsiflexion / plantarflexion

Plantarflexion – Flexion of the sole of the foot inferiorly, (negative).

Posterior – Direction towards the back of the body in the sagittal plane.

pROM – Passive range of motion

PTFL – Posterior talofibular ligament

SI – Superior / inferior

Sprain2 – Sprain level 2 ankle sprain injury characterized by a tearing or rupture of the anterior talofibular ligament.

Sprain3 – Sprain level 3 ankle sprain injury characterized by a tearing or rupture of the anterior talofibular ligament and the calcaneofibular ligament.

Superior – Direction towards the head in the axial/coronal plane of the body.

STJ – Subtalar joint refers to the articulating surface between the distal side of the talus and the calcaneus.

TAR – Total ankle replacement

TCJ – Talocrural joint refers to the distal end of the tibia and fibula, connecting to the trochlear surface of the talus.

Chapter 1 Introduction

1.1 Motivation

This thesis project was originally inspired by my wife who was a dancer in her youth, and from this has some lingering pain in her knees and ankles. From discussing her time as a ballerina I was inspired to work on the creation of a ballet pointe shoe that would minimize long term injury to the dancers' feet. It was soon discovered that a similar device [2] to what I was proposing was already around and on the market. This discovery led me to take my research on the ballet shoe and dancers' feet and transition it to a general biomechanical analysis of the ankle joint complex.

Ankle sprains are one of the most common types of injuries with between five and nine million cases per year in the United States and accounting for nearly 15-40% of sports injuries [3-5]. Seven to ten percent of all visits to the emergency room are from some sort of ankle sprain injury [6]. The ankle is the most commonly injured joint after the knee [7] and over three quarters of sprains involve the anterior talofibular ligament (ATFL) and/or the calcaneofibular ligament (CFL) [8-9]. The most common predisposition to suffering a lateral ankle sprain is the history of at least one previous ankle sprain [10-14] with a recurrence rate of nine percent [15]. Forty percent of ankle sprains progress to chronic problems due to ligament instability, incomplete rehabilitation, and unrecognized injury [16-17]. Twenty percent of patients with an acute ligament rupture go on to develop chronic ankle instability by either mechanical instability due to ligament lesions, or functional instability with loss of neuromuscular control [18]. The clinical sensitivity for correctly diagnosing ankle sprain injury is only 69% [19].

How can the diagnostic process of ankle injuries be improved? Even better, how can injury modes be better understood and actions taken to prevent ankle injuries from happening in the first place? To address these questions more quantifiable information about the stiffness of the ligaments and how they affect the movement of the ankle joint was needed. A full understanding of how ankle sprains affect the constraint of the ankle would not be possible without first understanding the constraint of the healthy intact ankle.

Objective 1

The first objective was to map out the passive extents of motion along a broad range of the flexion path for an intact ankle and the constraint provided by the soft tissues, and to create a map of the average stiffness of the ankle at discrete torque values.

Objective 2

The second objective was to measure the effect that ankle sprain ligament injury had on the passive range of motion, and to measure how that differed from the intact healthy ankle condition.

1.1 Overview

Chapter 2 is a discussion of the background leading up to this research including anatomy, injury, motion and analysis, as well as a literature review of the subject of ankle biomechanical analysis. In Chapter 3 contains the manuscript: Mapping the ankle joints passive motion and the effect of ligament injury on joint motion. The conclusion and future direction is contained in chapter 4. The appendix contains mathematical derivations, sample code documentation, sample raw data, and more detailed graphs.

Chapter 2 Background

This chapter is separated into three basic categories: anatomy, injury, and biomechanics. Anatomy refers to the physical constructs of the ankle including bones, joints, ligaments, muscles and their basic construction. Injury refers to the types of injury that are common in the ankle joint, how they occur, how they affect motion, and what anatomy they affect. Biomechanics refers to the range of motion of the joints, ways of collecting that information, and mathematical methods for describing kinematic motion.

2.1 Anatomy

2.1.1 Bones

The foot is comprised of 26 bones, 34 joints, and is often divided into the forefoot, midfoot and hindfoot or ankle [20] shown in Fig. 2.1 . More than 100 muscles tendons, and ligaments work in concert to provide the body support, balance and mobility [21]. The forefoot composed of the phalanges and metatarsals (toes) supports weight and balances pressure on the foot. The midfoot acts as a shock absorber and connects the hindfoot to the forefoot (Fig. 2.1).

The ankle is a six DOF joint allowing for rotation and sliding in three dimensions each. The three rotations are: abduction / adduction, inversion / eversion, and plantarflexion / dorsiflexion (Fig. 2.2). The three translations: are superior / inferior, medial / lateral, anterior / posterior (Fig. 2.3A-C).

The ankle consists of four connected bones: tibia, fibula, talus, and calcaneus (Fig. 2.1; Fig. 2.3). The tibia provides the primary weight bearing transfer between the ankle and the superior body features (Fig. 2.3A) [22]. The fibula acts as a strut that is primarily used for

muscle attachment and stability. The medial prominence at the distal base of the tibia is referred to as the medial malleolus, and the lateral prominence at the ankle at the distal base of the fibula is referred to as the lateral malleolus. The distal articular surface of the tibia is referred to as the plafond or pilon and directly articulates with the talus and is also responsible for distributing the stress of weight bearing through the ankle joint [3, 22]. The talus sits between the tibia and the calcaneus, but also articulates with the navicular in the midfoot (Fig. 2.3B). The articulating surface between the tibia and the talus is called the trochlea. The calcaneus is the heel of the foot, the largest of the bones in the foot, and provides skeletal support for the foot. The calcaneus articulates with the both the cuboid, and talus, however while the cuboid has one articulating surface the talus has three [23]. They are the posterior, middle, and anterior articular surfaces with decreasing surface area in the order listed (Fig. 2.3C).

2.1.2 Joints and Ligaments

There are three joints that make up the compound ankle joint complex. They are: the tibiofibular joint, the talocrural joint (TCJ), and the subtalar joint (STJ) (Fig. 2.1). The TCJ and the STJ together create a compound joint called the ankle joint complex (AJC) [24].

The tibiofibular joint is comprised of the distal ends of the tibia and fibula which form a syndesmosis joint providing slight movement held together by three ligaments: the anterior tibiofibular ligament, the interosseous tibiofibular ligament, and the posterior tibiofibular ligament [22, 25]. The anterior tibiofibular ligament has an origin at the anterior distal tibia and an insertion at the anterior distal fibula and distally reinforces the tibiofibular syndesmosis. The interosseous tibiofibular ligament sits between the tibia and the fibula and spans the distance of the tibia and fibula from proximal to distal and provides primarily joint compression[26]. The

posterior tibiofibular ligament has an origin at the anterior distal tibia and an insertion at the anterior distal fibula and reinforces the tibia-fibula joint.

The TCJ is a joint that includes the tibia, fibula, and talus and provides much of the weight bearing and support functions of the ankle. The tibia and fibula act as a cap preventing side to side motion and overhangs the trochlea of the talus which is shaped like a cylinder on its side [22]. The main movements of the TCJ are plantarflexion and dorsiflexion. The ligaments that constrain the TCJ include those in the tibiofibular joint, the medial or deltoid ligament found on the medial side that connects the tibia to the foot, and the lateral collateral ligament of the ankle. The deltoid ligament strengthens the joint and compresses the calcaneus and navicular bones to the talus and is made up of four ligaments [23, 26]. The posterior tibiotalar ligament has an origin at the anterior and posterior colliculus of the medial malleolus, and an insertion at the posterior process of the talus and reinforces the TCJ. This ligament limits talar dorsiflexion and external rotation. The tibiocalcaneal ligament has an origin at the anterior colliculus of the medial malleolus, and an insertion at the sustentaculum tali. The tibiocalcaneal is also the strongest of the deltoid ligaments and limits talar abduction. The tibionavicular ligament has an origin at the anterior colliculus of the medial malleolus, and an insertion at the navicular bone and reinforces the ankle joint. The anterior tibiotalar ligament has an origin at the anterior colliculus of the medial malleolus, and an insertion near the anterior medial aspect of the talus. This ligament limits talar plantarflexion and external rotation.

The lateral ligament prevents inversion and compresses the talus in the AJC. The lateral collateral ligament is not as strong as the deltoid ligament and is made up of three ligaments [23, 26]. The anterior talofibular ligament (ATFL) has an origin at the anterior base of the fibula, and an insertion at the superior anterior aspect of the talus and provides primarily inversion

resistance. The posterior talofibular ligament (PTFL) has an origin at the posterior base of the fibula, and an insertion at the lateral posterior aspect of the talus and primarily limits the endpoint of dorsiflexion and limits internal rotation of the talus. The calcaneofibular ligament (CFL) has an origin at the distal medial aspect of the fibula, and an insertion near the medial calcaneus and provides primarily lateral ankle support.

The STJ is a joint that includes the talus and the calcaneus allowing primarily inversion and eversion movement. The joint is very constrained in plantarflexion and dorsiflexion motion. The STJ is supported medially by the medial, lateral, and posterior talocalcaneal ligaments, and anteriorly by the interosseous talocalcaneal ligament. The talocalcaneal ligaments all work together to limit inversion of the STJ. The medial talocalcaneal ligament has an origin at the posterior process of the talus, and an insertion at the sustentaculum tali and primarily limits inversion in the STJ. The lateral talocalcaneal ligament has an origin at the anterior talus and an insertion at the anterior calcaneus and primarily limits inversion of the STJ. The posterior talocalcaneal ligament has an origin at the posterior process of the talus, and an insertion at the superior calcaneus and primarily limits inversion in the STJ.

The AJC is a compound joint that consists of the TCJ and the STJ (Fig. 2.1). It is often used in practice by doctors and physicians because it obscures the motion of the talus which is very difficult to see without advanced imaging techniques.

2.2 Ankle Ligament Injury

The ankle can be injured in many different ways, but the most common injury is an ankle sprain accounting for more than 80% of all ankle injuries and the most common injury in sports [27]. Of the ankle sprain injuries about 77% consisted of lateral injuries, and 73% had an isolated

rupture or tear to the ATFL [8, 15]. The mechanism in 85% of ankle ligamentous injuries is reported to be inversion [28]. Less frequently the mechanism is supination-internal rotation or supination-plantarflexion [29]. Medial ankle sprains are less common than lateral inversion ankle sprains because of the strong deltoid ligament and bony structure (mortise) of the ankle joint, however when this happens the mechanism is excessive eversion and dorsiflexion [9, 30].

Of the lateral ankle ligaments the ATFL has an ultimate load of approximately 140 N which is about one-half of the PTFL and one-third of the CFL [31], as well the ATFL usually receives higher strains and has faster rates of strain rate loading in sports relative to the other lateral ligaments which could indicate why it is more commonly injured [32]. From a purely mechanical perspective this correlates with the order of injury as well by studies that show the ATFL is the first ligament to be damaged while receiving a lateral ankle sprain, and followed by the CFL [33-34]. Reports of injuries to the CFL without injury to the ATFL is very rare [35], and is injured in 40% of ATFL injuries [28]. The PTFL is the least likely to be injured, because the PTFL is the strongest of the lateral complex and is rarely injured in an inversion sprain [36].

There are three levels of classifications or grades for lateral ankle sprain injury. A level 1 sprain is traditionally defined as a stretching of the ATFL and CFL ligaments [9, 37]. This is a common injury and does not always require hospital treatment or medical treatment. There is usually very little or no functional loss, and no mechanical instability. A level 2 sprain is defined as a partial tear of the ATFL and a stretch of the CFL [9, 37]. There is usually mild to moderate instability in the joint. A grade III sprain is rare and uncommon [38], but is characterized by a rupture of the ATFL and CFL with partial tearing of the posterior talofibular and tibiofibular ligaments [9, 37]. A level 3 sprain usually requires fixation of the ankle and possibly surgical

intervention to stabilize the ankle joint, but is fortunately fairly rare. There is a full loss of function and motion, mechanical instability, and severe swelling of the joint.

2.3 Biomechanics of the Ankle Joint

There are many ways that have been used historically to analyze the biomechanics of the ankle joint including range of motion of the joints, sliding motion of the joints, stiffness of the ligaments, and force generation [39-40]. Studies looking at biomechanics can take two forms: in vitro and in vivo. In vivo studies usually take place by looking at a live subject using their ankle, or using their feedback systems like pain, proprioception, and muscle activation while in vitro studies take place outside of a living organism, usually using cadaveric tissue and lack a direct feedback system [41].

2.3.1 Range of Motion

A functional range of motion (fROM) is one where the muscles are actively engaged in the system like in walking, running, squatting, or when walking up or down stairs [42-45]. Past studies have looked at the range of motion during walking, running, and playing different sports. Muscle activities are different for every person and in athletes are heavily dependent on training and the sport played [46]. Some of the difficulties of performing fROM deal with the inability to take invasive measurements during activity, like exact position of the bones, pressure in the joint capsule and strain on the ligaments. An advantage of the fROM studies are that the joint can be subjected to "real world" scenarios.

A passive range of motion (pROM), sometimes called functional range of motion (fROM) is one where the soft tissue constraints like the ligaments, skin and fascia restrain the motion of the joint [47-49]. The effect of muscles and tendons are removed from the experiment.

Another use of this term is maximal range of motion (mROM) where the maximum force that the joint can safely take is applied. This term is not rigorously defined and can be performed both in vitro and in vivo. This has been performed by Tuijthof in vivo using a board strapped to a patient's foot in an MRI and pulling towards the patient by hanging weights on strings until the patient said it became uncomfortable [48]. Another in vivo experiment by Allinger created an ankle rig that would measure the range of motion of a relaxed patient [50].

2.3.2 Joint Kinematics

Motion of the foot is a complicated coordination between the tibia, fibula, talus, calcaneus, the midfoot and the forefoot, with an interplay of bone articulation surface geometry, ligaments, and muscle-tendon units in the joints [51]. An attempt has been made to circumvent this difficulty by describing the complex movement in the talocrural and the subtalar joint as a movement of one universal joint, the ankle joint complex [52-53]. However in the last 20-30 years it has been determined sufficiently that the ankle joint complex cannot be easily described in this manner, rather it is a complex joint which had axis of rotation changes during the movement by shifting from anterior to posterior during plantarflexion and dorsiflexion [39]. In 1988 Chen and Siegler wrote a two part paper on 3D ankle joint kinematics where they were the first to show that the ankle joint is not an ideal hinge joint where the subtalar joint provides pure IE motion and the talocrural joint provides pure PD motion, but rather a more complicated joint where compound motions occur [47]. That same year Engsberg et al. looked into the relationship between the TCJ and STJ and created a description of specific joint motion [54].

2.3.3 Kinematic Differences among Populations

In the population there exists great variance among individuals and even among single individuals over time. Women in general have a greater range of motion than men as young adults, but among the elderly there is little variation among the populations [55]. Women have a ROM approximately eight degrees smaller in dorsiflexion, and eight degrees higher in plantarflexion than men [55]. Due to these anatomical differences and variations data must be looked at based on the age group, and possibly even the gender of the person. For example, even in the use of goniometers, there is evidence of large intra-subject variation and large fluctuations observed over time when analyzing joint motion [41].

2.3.4 Coordinate System Construction

It is difficult to directly compare kinematic results in the AJC, the STJ, and the TCJ due to variations in CS construction, variation in methods, and lack of rigorous standardized definitions for translations and rotations [24, 39, 52, 55-62]. It is difficult to find consistent coordinate systems that work both in vitro [63-64] and in vivo [65-66]. Active motion studies that use surface identification markers are common for in vivo studies and have because there are serious issues with the incorrect identification of landmarks in the construction of reference frames [58]. and There is also evidence that the axes of rotation changes during motion further complicating analysis [67]. To record kinematic data there are several common methods including the use of: bone sonic digitizers [52, 68], optical light systems using active cameras [69-70] or active sensors [58, 71] which can record the exact position of 3d markers [45] and specific points that can be probed, fluoroscopy, magnetic sensors [72], goniometers [41], and inertial accelerometers [73]. Using internal marker that are fixed to bone tend to be more

accurate than surface skin based markers due to the fact that there are artifacts introduced from moving skin and soft tissue between the marker and the bone [45, 74-75].

There are many different ways to get points that can be used to construct a joint coordinate system. In the simplest form external points on the surface of the skin can be collected and the CS can be built off of those points [71]. A more detailed version would be using internal features of the bones themselves to define a CS based off dissected bones, or to build points based off of CT or MRI scanned slices of the bone from which you can build a 3d model of the bone non-invasively [76]. The difficulty in these methods is in accurately reproducing points across subjects due to changes in anatomy, difficulty in precision of point definitions, and even within patient reproducibility errors. In at least one case tantalum beads were inserted into the bony surfaces of several live subjects which would show up under x-ray [67].

Some experimenters that use robotics, actuators, motors, and loading platforms make use of the equipment being used to define their coordinate systems [49, 61, 68, 77]. The bone geometry features are used to define features [76, 78], or a helical axis method [48, 57, 79], or bone surface geometry. Another common method, especially in clinical use is to use externally probed points [80]. The disadvantage of external probed points is that all motion of the talus is lost and the CS only works in the AJC reference view.

2.3.5 Mathematical Descriptions of Joint Motion

In the field of biomechanics there are several ways to analyze the kinematic motion between two bodies in space. The common methods of describing kinematic motion are:

Euler/Cardan angles [81-82], screw axis or helical axis [83-84], quaternion angles [85-86], dual Euler angles [60-62], and Grood and Suntay angles [1, 24, 56].

Euler/Cardan angles are a series of three rotations carried out in sequence. A serious drawback to Euler/Cardan angles is that it is very difficult to derive clinical meaning from the results since the angles are sequence dependent, and are dependent on the changing coordinate system. Another issues with Euler angles is the presence of a gimbal-lock where under certain conditions of rotation the axes lock and prevent accurate description of the motion.

The screw axis method [87] consists of finding an instant center that can rotate and translate. This is useful because they are defined by the motion and not on variable probed points. Unfortunately this advantage also has a disadvantage in that the resulting motions might have no clinical corollaries. Another drawback is that if the joint is not well “hinged” there can be translation in the joint (the instant center will travel) deriving clinical relevance becomes challenging.

In quaternions rotations four parameters define the rotation. A big advantage to using quaternions is being able to avoid the gimbal-lock common to Euler rotations; however quaternions suffer from a similar application perspective as the screw axis method. It defines rotations in four dimensions where the reference axes are constantly shifting and as such is difficult to derive clinical meaning.

In 1983, Grood and Suntay bridged the gap between engineers and doctors by defining a series of rotations about a non-orthogonal coordinate system and applying it to the knee. With G&S the proximal axis is selected on the proximal bone, and a distal axis is selected on the distal bone. A floating axis is then created between these two axes allowing clinical meaning along

with scientifically measurable parameters. A big drawback to the G&S system is when using it to predict joint forces and moments [88].

Dual Euler angles are similar to Euler/Cardan angles in that they are also sequence dependent; however they present a clearer connection for the clinical descriptions of joint movement. They are orthogonal and can be used in situations where G&S cannot like determining moments and forces in the joint. In essence the dual Euler method consists of a sequence of three screw motions along three pre-defined axes.

For the purposes of this thesis only the G&S angles method will be considered. It has been used extensively in the past to describe complicated 3D joint motion, it is easy to translate and understand the results, and it will be easier to compare output to previous studies for comparison.

2.3.6 Previous Motion Studies

A review article by Kleipool and Blankevoort (2010) collected a range of studies that analyzed the motion of the STJ and TCJ. The types of applied motion were separated into fROM and mROM. fROM is the motion seen during certain physiological activities such as walking, and running, while mROM is loosely defined as the maximum extent to which the joint can move before joint damage occurs. Of particular interest were the mROM studies because they most closely match the current study, and are most useful for analyzing ankle injury where there is a need to move beyond physiological movement to find changes in motion. Comparing the data between fROM and mROM could be used to help diagnose unstable ankle conditions however more data is needed to account for the great variations in anatomy between subjects. It is important to look at both range and deviation from the neutral position. Range was less

susceptible to variations in CS, and neutral position definitions, while deviation can provide insight into specific changes in motion. The CS used by de Asla [78] was very similar to the one used in this study which used a geometric CS by fitting a cylinder to the talar dome. The CS used by Tuijthof [48] was a finite helical axis based on talar geometry. The CS by Weindel [49] was generated by the machine applying pure motions, details not given. They applied 2.5 Nm for PFDF and INEV while applying 10Nm for ABAD. The CS used by Siegler [47] was based on Grood and Suntay and only had pure rotations applied.

In the study by Tuijthof [48] mROM was determined in vivo by attaching a board to the foot and pulling the board in certain directions until the patient felt discomfort. In the study by Weindel [49] a force controlled gimbal actuator was used to apply rotations to the foot in vitro. Finally in the study by de Asla patients used their own muscle force to generate a mROM. In the present study motion was selected at 6 Nm of torque in the applied direction.

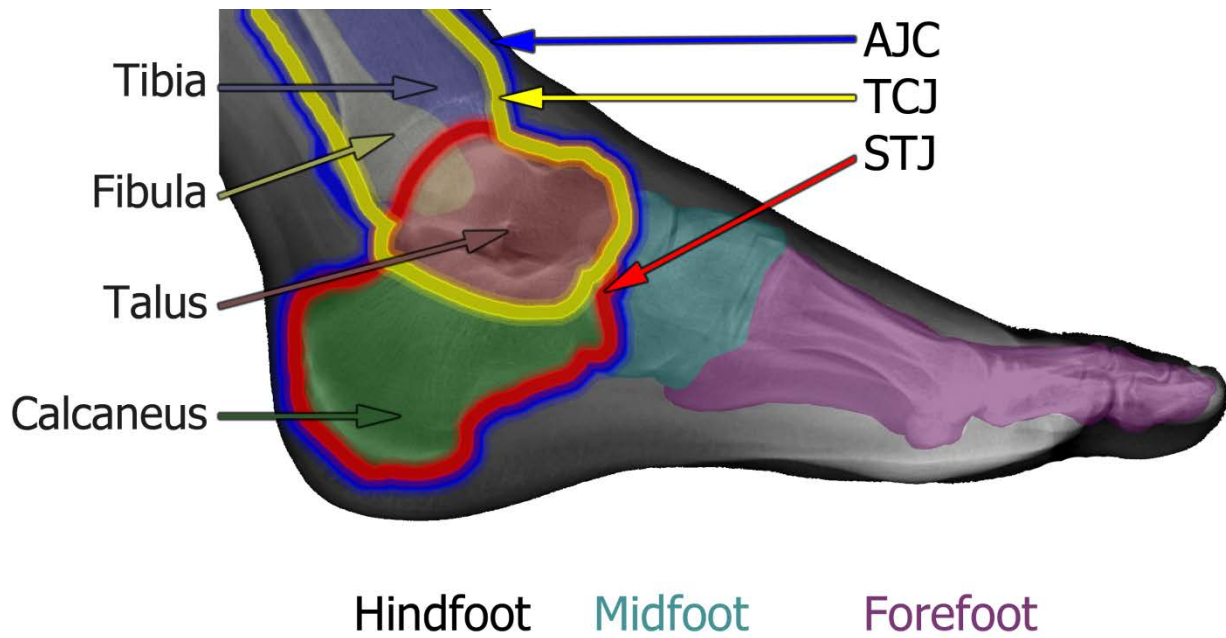


Fig. 2.1: X-Ray image of a left foot showing colored outlines of the bones and joints in the ankle: subtalar joint (red), talocrural joint (green), ankle joint complex (blue) consisting of both the STJ and TCJ. Original X-Ray image provided with permission by Andrew Magill.

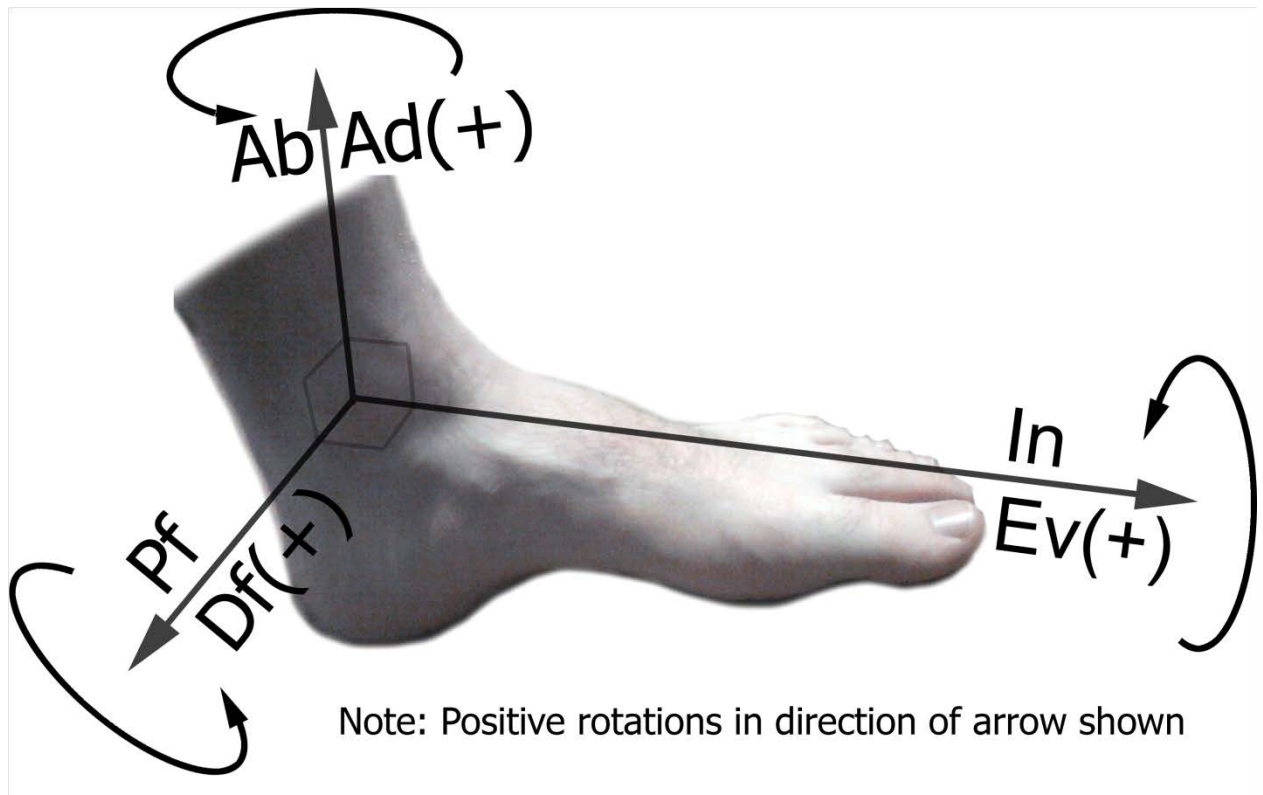


Fig. 2.2: Rotational coordinate system shown for ankle joint complex on a right foot.

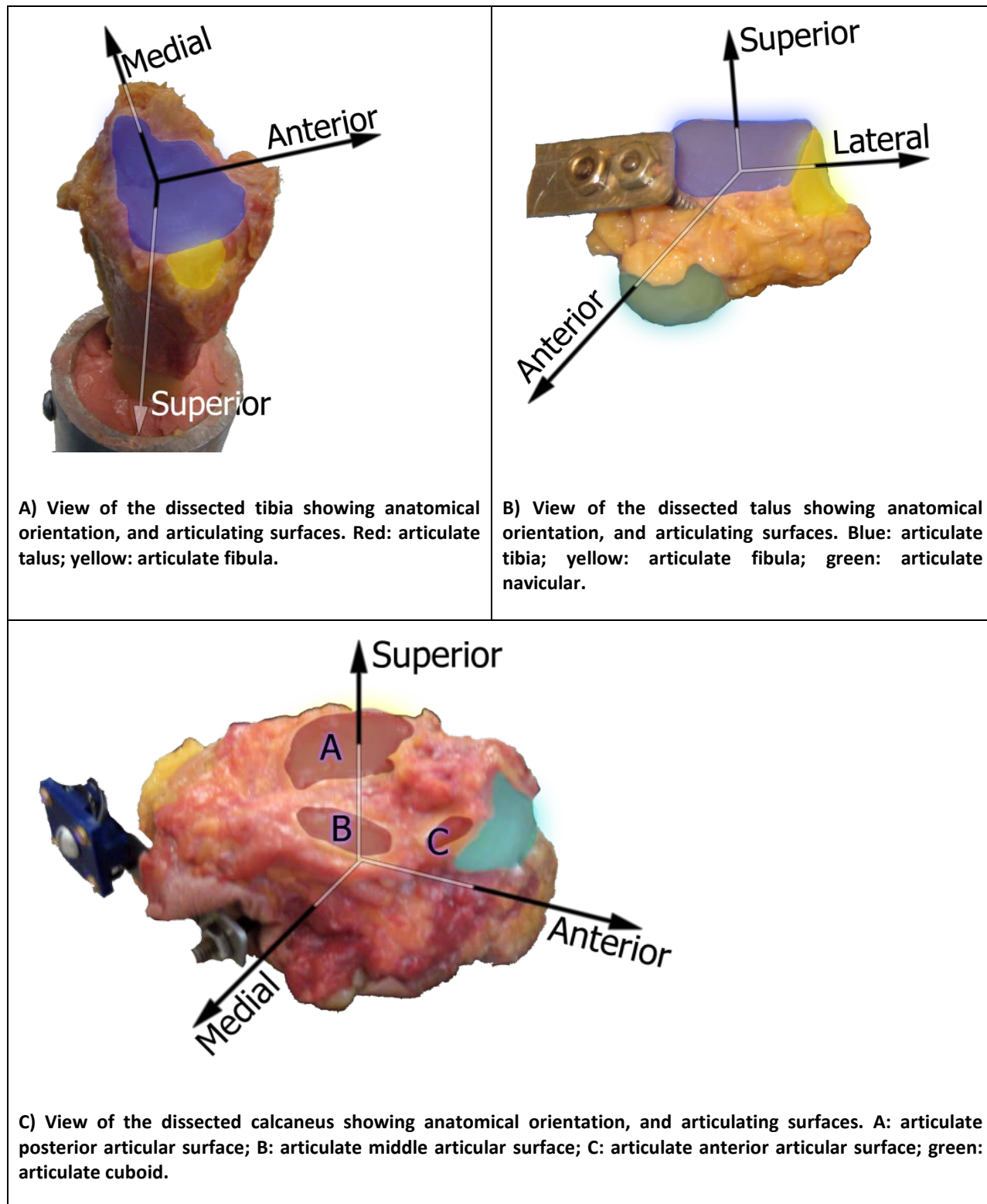


Fig. 2.3: The three bones of the ankle joint. Coloring of A, B, C are represented by articulating bone based on Fig. 1's color coding.

Chapter 3 MAPPING THE ANKLE JOINTS PASSIVE MOTION AND MEASURING THE EFFECT OF INJURY ON LIGAMENT CONSTRAINT AT THE ANKLE JOINT

3.1 Introduction and Background

In the United States, ankle sprains account for 7% to 10% of all visits to the emergency room, and account for 10% to 15% of all sport-related injuries [6]. Most of these ankle injuries are sustained during contact and pivoting sports [38]. The most common acute injury to the ankle is the lateral ankle sprain [9]. There are three lateral ankle ligaments that work together to constrain the motion of the ankle: anterior talofibular ligament (ATFL), calcaneofibular ligament (CFL), and the posterior talofibular ligament (PTFL) [89].

The ankle joint complex (AJC) is a compound joint visualized as movement of the tibia and the calcaneus and has been used extensively in clinical practice due to the ease of measurement with external markers and visual cues. The AJC is made up of three joints: the distal tibiofibular syndesmosis joint made up of the distal ends of the tibia and the fibula, the talocrural joint (TCJ) made up of the tibia and the talus, and the subtalar joint (STJ) made up of the talus and the calcaneus [90]. Traditionally the TCJ is seen as where the primary motion of plantarflexion / dorsiflexion (PFDF) and abduction / adduction (ABAD) motion occurs, while inversion / eversion (INEV) occurs more in the STJ [47].

There are three levels of sprain that are common in the ankle [9, 91]. Sprain level 1 is a partial tear or stretching of a ligament usually either ATFL, CFL or a combination of both. Sprain level 2 is an incomplete/partial tear of a ligament usually the ATFL. Sprain level 3 is a complete rupture of the ATFL and CFL as well as stretching of the PTFL. The following three contributors stabilize the ankle joint: bone geometry interaction, ligament constraint, and muscle

unit interaction which perform dynamic stabilization of the joint [90]. When the ligaments are injured the static constraint of the ankle is changed and becomes more lax. There are three primary rotations that the ankle exhibits: plantarflexion/dorsiflexion (PFDF) which is a rotation of the ankle looking at the sagittal plane, inversion/eversion (INEV) which is a rotation in the axial plane, and abduction/adduction (ABAD) which is a rotation in the frontal plane. It is not fully understood how the interaction of ligament injury affects the subsequent motions of the AJC, STJ and TCJ.

There are several ways that have been developed to analyze the motion of the AJC in vitro [47, 52, 62, 74, 92] and in vivo [48, 93-96] using a variety of techniques such as: surface markers, x-rays, fluoroscopy, MRI, sonic bone markers, optical bone markers, magnetic sensors, goniometers, and others. Collected data can roughly be separated into two groups: functional range of motion (fROM), and maximal range of motion (mROM) [40]. fROM is the extent of the motion during physiological activity, commonly walking or running. mROM is the extent the joint can move in any direction, and is not related to a physiological movement, but that extent is not well defined. Passive range of motion (pROM) is a subset of mROM of motion without muscle activation; however the loading level is variable. The present study looks at pROM under specific torque loadings.

The first objective was to map out the passive extents of motion along a broad range of the flexion path for an intact ankle and the constraint provided by the soft tissues, and to create a map of the average stiffness of the ankle at discrete torque values. The second objective was to measure the effect that ankle sprain ligament injury had on the passive range of motion, and to measure how that differed from the intact healthy ankle condition.

3.2 Materials and Methods

Nine fresh frozen cadaver specimens with no history of ankle injury were used to in this study (Appendix C). The average age of subjects was 61 years (s.d.=9 years), with a minimum age of 41 and a maximum age of 69. The average BMI was 26 (s.d.=6.2). Eight of the subjects were male, and four of the ankles were right.

3.2.1 Specimen Preparation

To test the ankle laxity and ligament constraint, each ankle was thawed approximately twelve hours to room temperature after having been used but not injured in a previous experiment. It should be noted however that each specimen had been thawed previously for approximately 36 hours, kept well irrigated, sectioned mid-tibia and refrozen prior to use. Soft tissue was cut down to be 2.5” above the medial malleolus with 3” of bone extending outward to attach the tibial cylinder to the tibia (Fig. 3.1). The tibia was aligned in the cylinder using a bubble level and cemented using Poly methyl methacrylate (PMMA). The talus and calcaneus bones both had two screwposts inserted to which infrared LED (iRED) rigid body markers were affixed. The calcaneus sensor was placed 1.5” anterior and superior from the most distal posterior point on the medial side, while the talus was placed 0.4” below the edge of the tibial bone in full dorsiflexion on the medial side. The foot rig was then attached to the load cell and connected to the table. A flat board attached by three screws through the calcaneus at opposing angles and a foot strap of zip-ties locking the forefoot down was used to apply direct motion to the foot.

3.2.2 Procedure

To map the constraint of the ankle, seven types of motion (60 seconds each) were applied to the intact ankle (Tbl. 3.1). The neutral position of the ankle was identified by making the tibia perpendicular to the ground using a bubble level, and then making the bottom of the foot level by putting the foot in roughly 90 degrees of flexion with no extraneous INEV or ABAD rotations. The bubble level was used to set INEV to 0 degrees, while ABAD was set to the best of the operator's ability. The neutral paths (1-3) were performed one time each, and the compound motions (4-7) were done three times each. The experiment was performed by one individual for all tests to minimize intraoperator error. The ankles were forced into to specific orientations and the resulting torques and positions were recorded. The way that loading is applied can affect the output kinematics. Due to the viscoelasticity of ligaments the ligament can become stiffer if the loading is too fast. These effects were minimized by the slow loading of the ligaments with an average loading cycle of 5.5 seconds per torque.

To reproduce a simulated ankle sprain in-vitro across all ankles, only sprain level 2 and 3 were simulated because they deal primarily with a rupture of a specific ligament. A level 1 sprain was not simulated because it deals with a weakening of the ligaments, and would be difficult to reproduce across specimens. A level 2 sprain (sprain level 2) consists of a rupture of the ATFL from a small incision just anterior of the fibula ATFL insertion. A level 3 sprain consists of a rupture of the ATFL and CFL from a small incision just anterior to the CFL insertion. Once all the motions had been performed and collected a level 2 ankle sprain (sprain 2) was applied and the envelopes were repeated. Finally a level 3 ankle sprain (sprain 3) was applied and the envelopes were repeated a final time.

3.2.3 Processing Kinematics

The kinematic analysis was performed using a modified version of the [1] joint coordinate systems defined by the ISB in 2002 for the AJC and custom definitions for the TCJ and STJ shown in Fig. 3.2 [1, 24, 56]. The motivation for using a custom definition was partly because the ISB definition [24] is incomplete addressing only the AJC, but also that the floating axis is poorly defined and not consistent with the intentions of Grood and Suntay [56]. The last rotation in the chain (e_3) should be about the long axis of the distal segment as this provides a better clinical interpretation of the output. Using Baker's methodology of the third rotation about the long axis of the distal segment a consistent G&S CS for each joint was defined (Fig. 3.2; Appendix B).

The three rotation angles are defined globally in the AJC as: PF(-) DF(+) as a rotation in the sagittal plane of the tibia; AB(-) AD(+) as the floating axis between e_1 and e_3 ; and IN(-) EV(+) as a rotation about the long axis of the calcaneus.

3.2.4 Constructing Fixed Coordinate System Axes

A logical coordinate system (CS) for the bones in the AJC was defined from the "neutral" position. The center portion of the trochlea of the talus is cylindrical in shape. An optimization algorithm was used to find the center of a cylinder fit to the shape of the dome based on collected probed points of the talar dome and its orientation which was set as the ML axis (Appendix E). This axis was transformed to the tibia through a transformation of the neutral position and a line from the distal center to the proximal center of the bone was used as a construction SI axis. These were crossed to get the AP axis, and crossed again to get the final SI axis. The position of the fixed CS was determined by fitting a cylinder to the points of the trochlea for the talus, the

points of the posterior talar articular surface of the calcaneus for the calcaneus, and the inferior articular surface of the tibia for the tibia (Fig. 3.3). The body fixed CS was defined generally as ADAB (X), and INEV (Y), PFDF (Z). The reason for using bone geometry instead of probed articular points was that finding points that could be repeatably probed across different ankles was very challenging due to variations in bone geometry. Using articular surface geometry reduces the effect of variation from the researcher.

3.2.5 Equipment

For this experiment an NDI Optotrak model 3020 was used with Infrared Light Emitting Diodes (IRED's) attached to rigid body markers inserted into the tibia, talus, and calcaneus. A custom Labview script, was used to collect 3D bone position data at 100 Hz, and the corresponding torque data, while Matlab r2010 was used to process all collected data (Appendix E). A custom fixator interfaced the tibia to a JR3 Tri-Axial Load Cell, Woodland CA and was fixed to the table through a vice (Fig. 3.1). The long axis of the tibia bone was aligned by hand to be parallel and central to the fixator and held in place by PMMA denture dental cement. To move the foot in a consistent manner a flat rectangular piece of wood was attached to the foot using three screws inserted at different orientations through the calcaneus bone to allow direct manipulation of the calcaneus. The forefoot was fixed to the front of the board by two cable ties and the board was used as a reference plane to define the neutral position using a bubble level. Kinematic constraints were kept to a minimum allowing the ankle to have a full six degree of freedom (DOF) range of motion.

3.2.6 Load Cell Analysis

Force and torque data were collected and transformed from the origin of the load cell (LC) to the coordinate system axis of the tibia using the calculated location of the ankle center (Fig. 3.2A, Appendix A) with the origin at the neutral position relative to the load cell. The torque and load data were filtered using a low-pass Butterworth filter (order 2, and a cutoff frequency of 0.28). The data were identified into interpolated torque loading values of 3 Nm, and 6 Nm for ABAD and INEV motion which was used to construct the range of motion (PFDF vs. INEV and ABAD) at specified loading levels called iso-torque lines. Hysteresis (decreasing load) torques were removed from the analysis by only selecting the data that consisted of increasing load. Off axis torques (ABAD torque on INEV movement, and vice versa) were removed if the torque was more than 1.5 times the primary axis torque loading (C.6). A torque load was specified and data points (PFDF vs. INEV and ABAD) were collected. A fifth order polynomial had been used in similar analysis in the past with an average r^2 value of 0.67 and a s.d. of 0.24 (Appendix C). The curve was used to interpolate the data and define discrete data points which could be used for analysis. A curve was not fit if there were less than six data points to use. Iso-torque loadings were defined as the position of the ankle at a specific torque load. For example, if ABAD rotation was used, every time there was a torque of 3 or 6Nm the position of the ankle was collected, and when these were taken together and fitted with a curve they create an isoline.

3.3 Results

3.3.1 Neutral Flexion Path

When analyzing the movement of a specific joint for simplicity and clarity PFDF movement are only studied in relation to the AJC. The PFDF movement at the TCJ and STJ can be correlated using Fig. 3.4 which shows the specific joint angle versus the global AJC angle. The TCJ very nearly describes the AJC PFDF motion, while the STJ has a very limited PFDF motion, showing highly constrained motion. The primary motions that were looked at were ABAD and INEV from 0 to 3, and 3 to 6 Nm of torque loading. For example, when the ankle had 20 degrees of dorsiflexion the TCJ had 18 degrees of dorsiflexion and the STJ had 6 degrees of dorsiflexion (Fig. 3.4).

3.3.2 Off Axis Loading

The effect of off axis torque loading was an effect of the ankle constraint and was different in INEV and ABAD (Fig. 3.5). Off axis loading was where a load applied in one direction caused part of the load to be transferred to a different direction. The off axis torque loading was an effect of the ankle constraint and bone geometry. With ABAD torque loading the off axis torque showed a bowtie band with both positive and negative loading in either abduction or adduction. This meant that the ankle was not constrained in either inversion or eversion when moving with applied ABAD torques. With INEV torque loading the off axis torques followed a slightly different pattern where in eversion there was primarily abduction torque loading, and in inversion there was primarily adduction torque loading.

3.3.3 Intact Ankle Analysis

There was large variability in the ROM between ankles outside of this range with the average ROM of 64.0 degrees (s.d.=17.1 degrees). The maximum angle was 43.6 degrees, and the average maximum was 25.4 degrees (s.d.=14.7 degrees). The deepest plantarflexion angle was -51.6 degrees, and the average minimum was -38.6 degrees (s.d.=7.5 degrees) (Appendix C). To minimize variability between subjects a neutral flexion path was subtracted from each ankles motion to account for differences in specimen motion. This neutral path consisted of moving the foot through the PFDF range minimizing ABAD and INEV motion. The excursion from the neutral flexion path of specified iso-torque lines at both 3 and 6 Nm of INEV or ABAD torque at each joint in the ankle is shown in Fig. 3.6. In each figure the top green line shows the average applied PFDF neutral path that the ankles followed with the standard deviation shown in green. A total of nine ankles were analyzed and all had at minimum a PFDF range between -20 and 10 degrees in the AJC (Global) reference frame. When applying ABAD rotation or torques to the ankle there was more abduction occurring than adduction, except in the TCJ in deep dorsiflexion (Fig. 3.6A-C). In the AJC and TCJ adduction motion was very similar, but became slightly more lax above 10 degrees PFDF in the AJC. The STJ showed high stiffness and low laxity across the flexion range except in high flexion. Abduction was nearly equal in low flexion in the TCJ and STJ, however the STJ was mostly horizontal indicating that its laxity was nearly unchanging and the ligament constraint is relatively unaffected by PFDF angle. The TCJ shows a constant positive slope nearly reaching 0 degrees ABAD in high flexion which indicated an interaction of geometry, or possibly an effect of changing ligament length.

When applying INEV rotation or torques to the ankle there was very little motion occurring at the TCJ indicating that it was stiff with low laxity and unaffected by flexion angle

(Fig. 3.6E). Eversion happens almost exclusively in the STJ and was clearly evidenced by comparing the AJC and STJ eversion iso-torque lines (Fig. 3.6D,F). The TCJ has virtually no eversion motion, and shows very high stiffness and very low laxity. Eversion has a slightly positive slope with lower stiffness and lower laxity in low flexion, while being higher in high flexion. Inversion rotation was similar to eversion in the TCJ with high stiffness and low laxity. The STJ has similar stiffness across the flexion range, however in low flexion the joint was 30-50% higher than high flexion and even higher in the AJC.

3.3.4 Sprained Ankle Results

The affect of ligament constraint on the injured ankle was analyzed by first cutting the talofibular ligament creating sprain level 2, and then subsequently by cutting the calcaneofibular ligament creating sprain level 3. The change in motion relative to the intact ankle condition shown in Fig. 3.7. In the AJC and TCJ changes from the ligaments are nearly the same, while the STJ was very stiff, and has had relatively little change based on these ligament injuries. The jumps in values seen at the extremes of the PFDF range are were due to loss of ankles at certain ranges. The minimum number of ankles at any given PFDF range was six, and the maximum was nine.

Applied ABAD motion versus PFDF showed a change in the AJC as a whole, and it was clear that the TCJ was the sub-joint where most of the excess motion occurred (Fig. 3.7A-B). There was very little change in motion between loading levels (3 and 6 Nm) as indicated by the similarly colored lines with very little separation indicating high stiffness in the ABAD direction. There was strong conformity in all joints between -10 and 10 degrees PFDF with little effect from torque level. In the AJC and TCJ there were larger motions at the extremes of the motion

based on torque loading where there was possibly less geometric conformity. The STJ was very constrained in all motion having nearly no change based on condition or torque level except for adduction at high dorsiflexion which showed a larger relative change in motion (Fig. 3.7C).

Applied INEV motion versus PFDF shows a similar effect to ABAD motion where most of the motion occurs in the TCJ represents most of the motion of the AJC (Fig. 3.7D-E). The sprain level 2 had high stiffness and conformity with no effect from the sprain in eversion indicated by the horizontal line at 0 degrees eversion across the flexion range. Inversion had a positive slope across the PFDF range indicating a larger range at high plantarflexion, and high conformity at deep dorsiflexion with no change in motion at 20 degrees PFDF and no effect based on torque loading level. Sprain level 3 in eversion showed a change in motion relative to sprain level 2 from -30 to 10 degrees PFDF moving towards conformity above 10 degrees PFDF. Inversion had a change in motion across the flexion range, and based on torque loading level. There was an effect on both motions from applied torque loading across the range. The STJ showed very little change in motion based on either ligament injury or torque loading level in both inversion and eversion (Fig. 3.7F).

An analysis of variance (ANOVA) was performed on the excursion data to determine which injury modes were statistically significant to the change in motion based on sprain level (Fig. 3.7). The statistically significant difference was defined as $p < 0.05$ (Appendix E). A multiple comparison procedure was run to determine with 95% confidence the range of the true mean between two groups. Intact, sprain level 2 and sprain level 3 were analyzed at 3 and 6 Nm of torque loading. If the difference between the estimation of the true means was greater than zero then there was a statistically significant difference between the means.

3.3.5 Stiffness

Stiffness was defined as the change in torque divided by the change in rotation.

$$\mathbf{Stiffness} = \frac{\Delta\mathbf{Moment}}{\Delta\mathbf{Rotation}} \quad \text{Eq. 1}$$

The stiffness can be interpreted as a combined effect of ligaments working together to prevent movement. The average stiffness based on torque loading, for each injury mode is shown in Fig. 3.8. The stiffness was calculated at between 0 and 3 Nm, and 3 and 6 Nm using the data between -20 and 10 degrees ankle flexion which indicates the change in stiffness due to ankle injury in each joint.

Abduction stiffness showed almost no change based on injury from 0 to 3 Nm in all reference frames. When the torque was increased to 3 to 6 Nm the AJC stiffness was the same from intact to sprain 2, and had a 28% from sprain2 to sprain level 3. The TCJ showed a decrease and then an increase in stiffness which meant that there were other effects affecting the motion. In the STJ the stiffness increased by 60% from intact to sprain 3 with little change between sprain 2 and sprain 3.

Adduction stiffness was consistent from 0 to 3 Nm in all reference frames being a 40% and 60% drop from intact for sprain 2 and sprain 3 respectively. From 3 to 6 Nm there was no change between intact healthy and sprain 2 in all reference frames, however a drop of 30% occurred in both the AJC and TCJ, while the STJ remained relatively unchanged between sprain 2 and sprain 3.

In inversion from 0 to 3 Nm there was a steady trend to less stiff across all ankle conditions seen mostly in the TCJ, but also in the AJC to a lesser degree. The STJ was almost

flat having very little change in stiffness based on injury, however the large standard deviation with sprain level 3 indicates that there is a changing stiffness in some ankles. From 3 to 6 Nm the AJC and the STJ are similar in change where there was relatively no change between intact and sprain 2, while there was a drop of about 50% and 22% respectively. The TCJ saw a rapid decrease in stiffness based on injury with a drop of about 50% and 80% between sprain 2 and sprain level 3 injuries compared to the intact.

Eversion at 0 and 3 Nm saw no significant changes between intact and sprain 2 for any of the reference frames. There was a strong jump of more than 200% and 46% in the AJC and TCJ when moving from a sprain level 2 to a sprain level 3 injury, while the STJ saw very little change in stiffness. From 3 to 6 Nm there was a consistent drop in stiffness across all reference frames of about 10-20% for intact to sprain 2 and 40% from sprain 2 to sprain 3.

3.4 Discussion

The first objective of the present study was to provide a complete envelope describing the motion of the ankle joint at discrete dorsiflexion plantarflexion values (Fig. 3.6). Along with this description of motion was a description of how that envelope changes across the flexion range. When looking at the intact ankle motion (Fig. 3.6) it was clear that the TCJ provided nearly all the adduction motion, while abduction motion was shared between both the TCJ and the STJ. When looking at INEV motion, nearly all the motion happened in the STJ, and the TCJ provided relatively little motion. This observation coincides with past research in this area [40, 42-45, 47-50, 60, 78].

The second objective of the study was to analyze the effect of ligament sprain injury on the pROM. While the STJ has a slight increase in motion, it was clear that the ligament injury

affects primarily the TCJ for both ABAD and INEV which could be expected by the attachment sites of the affected ligaments. The ABAD TCJ injuries were unaffected by the amount of applied torque to motion within our range, except for inversion which was strongly affected by the amount of applied torque, and eversion which was somewhat affected by the amount of applied torque. In the most extreme cases of the STJ abduction in plantarflexion had a significant change in motion from healthy to sprain level 3 which indicated that even though the ligaments primarily protect the TCJ there are some changes as well in the STJ.

There was one artifact from Fig. 3.7D and E which showed that the extent of eversion was being shifted towards inversion below the neutral line with a level 3 ankle sprain. To determine the cause of this shift Fig. 3.7D was analyzed with the off axis graphed as well (Fig. 3.9). There was a shift towards adduction (top graph) which directly correlates with the drop in eversion (bottom graph). This shift toward of the eversion towards inversion appeared to be an artifact of the cross coupling in the joints.

The study also successfully implemented a modified version of the G&S coordinate system the ISB standard definition of the ankle joint [1, 24]. This was necessary because the ISB standards neglected to create a recommendation for the TCJ and the STJ and never provided the followup to the joints in the ankle. There are several advantages to using this modified CS versus other systems. The output from this system is readily accessible to clinicians and surgeons because the rotations are similar to how they describe the motions while other methods like the helical axis, and Euler angles force the description into an orthogonal system limiting the translation to the clinic. The definition is fixed to the long axis of the distal segment creating a logical fixed axis based on the primary motion of the bones.

3.4.1 Comparison of Results

A review done in 2010 by Kleipool and Blankevoort gives a set of data to compare the present study against [40]. The data sets were divided into functional range of motion (fROM) and maximal range of motion (mROM) and shows data from both the STJ and the TCJ.

The rotations in the subtalar joint showing rotation relative to a neutral position are shown in Fig. 3.10A. There are fewer studies showing this based on how other researchers reported their findings. The values relative to a neutral position show interesting results. PFDF was on average between -5 and 5 degrees, while Siegler [47] saw 9 degrees plantarflexion and Tuijthof [48] showed a very limited range, probably due to the Finite Helical Axis method used. INEV saw very strong congruity for inversion while eversion was more constrained than that shown by previous studies. ABAD was also more constrained overall than previous studies. The injured ankle showed very little change between ABAD, and showed an increase of 2 degrees adduction with a sprain level 3. Inversion showed an increase of 3 degrees from intact to sprain level 2, and an increase of 1 degree from sprain level 2 to sprain level 3

The rotations in the subtalar joint showing rotation relative to a neutral position are shown in Fig. 3.10B. The TCJ was free to move in PFDF and ABAD as well as inversion, while being highly constrained in eversion. PFDF very closely agrees with the results found by Tuijthof [48] and was almost 2 to 3 times the values found during normal walking exercises. INEV was found to be almost equal to the walking studies and much less than the study by Tuijthof, while ABAD was found to be almost three times as large as walking and only slightly greater than Tuijthof. There was lower eversion than Siegler [47] or Thuijthof [48], however inversion and adduction was nearly equal to Siegler while Tuijthof was nearly three times larger

in inversion and both were larger in abduction. There was no change in eversion across any injury in the TCJ, however inversion had a strong change of 4 degrees from intact to sprain level 2, and a change of 15 degrees from sprain level 2 to sprain level 3. Both abduction and adduction increased across all levels with a 4 degree increase in both abduction and adduction from intact to sprain level 2, and a 9 degree increase in abduction and a 3 degree increase in adduction from sprain level 2 to sprain level 3.

The study by Siegler [47] applied only pure moment rotations, equivalent to the neutral flexion path, the neutral ABAD path, and the neutral INEV path. The coordinate systems in Siegler were defined by the machine used to perform the testing, and as such did not guarantee that the motions were truly aligned with the bones. The present study provides a deeper understanding of joint motion by applying a larger variety of motions than the study by Siegler. Tuijthof was a mROM study that used finite helical axes based on MRI scans of the subjects' feet at the maximal positions. A board was strapped to subjects' feet and the board was pulled in different rotations until the subject expressed discomfort and then an MRI scan was taken. Due to this setup, it is possible that muscle reflexes could shift the result without the subjects' knowledge or intent. Nester was a cadaveric study with a dynamic rig applying muscle activation, and Arndt used intracortical pins in the bones of live subjects to record joint motion.

With the information from the present study the breadth of knowledge concerning the motion of the sub-joints in the ankle as well as the change in motion based on ankle sprain injuries is better understood. The data from the present study correlates very well with the Taylor tilt test which is commonly used along with the anterior drawer test to determine the level of sprain injury. There are already quantitative measures of the anterior drawer test, but nothing exists for the Taylor tilt test. This research could be applied to create a device which could be

used help to determine the level of ankle sprain injury in a person by helping to create a quantitative assessment of the Taylor tilt test with the help of the contralateral ankle. The best angle to measure inversion change is at 20 degrees plantarflexion where inversion has the greatest range (Fig. 3.7D). A value of approximately 7 degrees extra inversion compared to the contralateral would indicate the possibility of a sprain level 2, while a value of 20 degrees would indicate a sprain level 3.

Since the last 1970's there has been a new option for people with ankle arthritis providing an alternative to fusing the ankle providing the option to get a total ankle replacement (TAR). During the TAR the foot is rigidly held in a neutral position while the surgery is performed and the surgeon works to remove the talus, and then replace the implant from the anterior direction [97]. During a total knee replacement the surgeon performs the surgery and checks the range of motion at 90 degrees flexion sometimes at full extension, but usually skipping mid-flexion ranges, which has been shown to lead to unnatural ligament constraint causing instability in the knee at these other flexion ranges [98]. This could also be related to the ankle joint where to the author's knowledge during the total ankle replacement surgery the surgeon does not check critical midflexion ranges. Inversion in the AJC changes drastically from plantarflexion to dorsiflexion. When testing the TAR the surgeon should verify that inversion in plantarflexion is around 350% greater than in dorsiflexion (Fig. 3.6D).

3.4.2 Sources of Error

The definition of the neutral position was one consideration for sources of error. The largest sources of error in the present study would be the use of the neutral flexion path which was only collected once, but used to create all the motion graphs. The free floating fibula was

another source of error in the study which could greatly impact the kinematics. Another source of error could be operator error in inconsistent loading patterns. Interoperator and intraoperator variability for finding the neutral position was determined to be less than 1 degree with three standard deviations for all measured angles (n=5, repetitions=5). Other sources of error include the fixation of the foot, and a wide range of morphological and biological differences between subjects affect all aspects of analysis. The Achilles tendon was not under tension in the present study due to sectioning the tibia, this lack of tension would also affect the motion of the calcaneus. There were some instances where after a level 3 sprain was applied motion became so large that it was difficult to work within the constraints of the testing area. The cadaveric tissue used in the study had a longer chance to degrade compared to other studies since part of the specimen had been used in a previous experiment. This degradation could affect the stiffness of the ligaments and surrounding tissues.

3.4.3 Future

Future efforts to expand this research should include a broader selection of ankle ligaments to resect including the PTFL, the deltoid ligaments, and the syndesmotric ligaments which act in concert to constrain the ankle joint. To get a better understanding of ligament constrain the insertion and origin of the ligaments should be taken along with the cross sectional area of the ligaments. This would help for developing computer models and simulations. A machine to apply pre-specified motions to the ankle that is repeatable and less susceptible to human error would be an elegant way to deal with the error in the torque input. A surgeon who could repair the ankle after the injury has been applied would be able to quantitatively validate how well ankle reconstruction works, and identify areas where surgical methods could be improved. A surgeon could also perform a total ankle replacement and compare the pROM of the

new ankle joints to the originals to aid in the design of future TAR revisions. For both surgical options the mid flexion ranges are pretty similar in the AJC except for inversion which has a 6 degree shift towards eversion at 20 degrees dorsiflexion, and a six degree shift towards inversion at 30 degrees plantarflexion from the neutral position. Future work with the surgeons can determine if the mid flexion ranges are similar after surgery.

3.5 Conclusion

The present study has looked at the passive range of motion of the ankle envelope and created a map of the ankles envelope of motion across a broad flexion range. The effect lateral ligament injury was also mapped to create a detailed map of ankle motion before and after injury in the AJC, TCJ, and the STJ. A map of the average stiffness in ABAD and INEV was created showing where the stiffness changed after ligament injury. Steps were proposed to improve the analysis of ankle injury by creating a quantitative element to the Taylor tilt test, and a possible method for improving the outcome of total ankle replacement surgery was proposed.

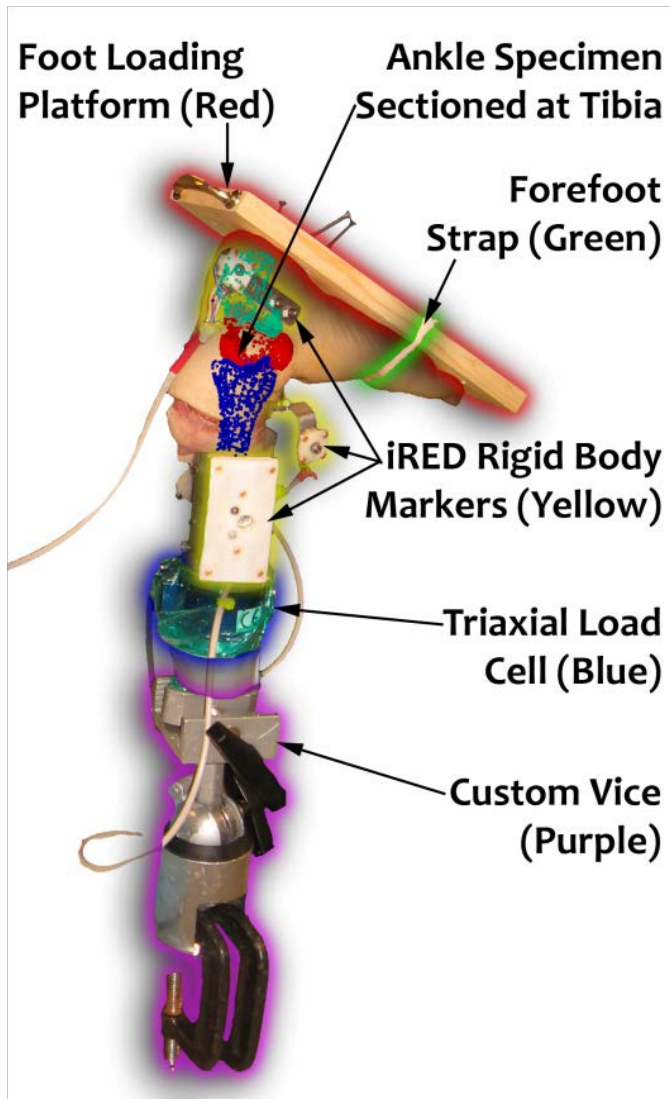


Fig. 3.1: View of the ankle rig setup. Overlaid on the ankle are a set of probed points indicating each bone in the ankle: tibia (blue), talus (red), and calcaneus (green).

Tbl. 3.1: Definition of motions (total=15) applied to the ankle. The motions in this table were run for each ankle condition (Intact, sprain level 2, and sprain level 3). Note: The order was not randomized, motions were followed sequentially.

#	Title	Repeat	Description
1	Neutral Flexion Path (NFP)	1	Foot is moved in pure PFDF rotation from the neutral position
2	Neutral ABAD Path	1	Foot is moved in pure ABAD rotation from the neutral position
3	Neutral INEV Path	1	Foot is moved in pure INEV rotation from the neutral position
4	ABAD Rotation	3	ABAD rotations are applied at different flexion angles
5	INEV Rotation	3	INEV rotations are applied at different flexion angles
6	ABAD Torque	3	Constant ABAD torque across flexion range
7	INEV Torque	3	Constant INEV torque across flexion range

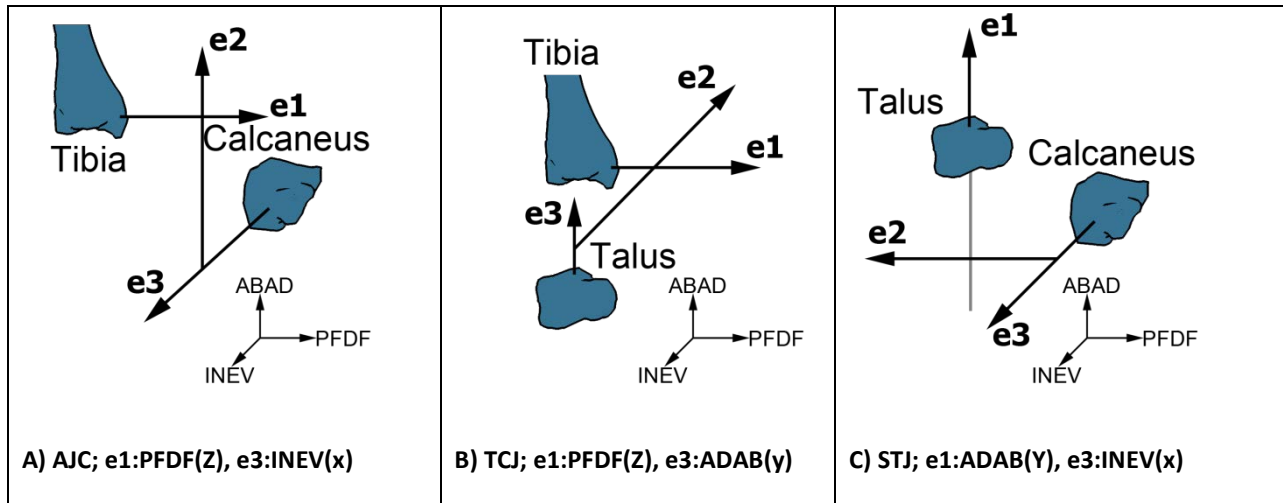


Fig. 3.2: Frontal view of the Grood and Suntay Coordinate Axes for each reference frame [1, 24, 56]. The capital letter (XYZ) is the fixed proximal axis, and the lower case letter (xyz) are the fixed distal axis. e_1 is the proximal axis. e_2 is the floating axis between e_1 and e_3 . e_3 is aligned along the long axis of the distal bone.

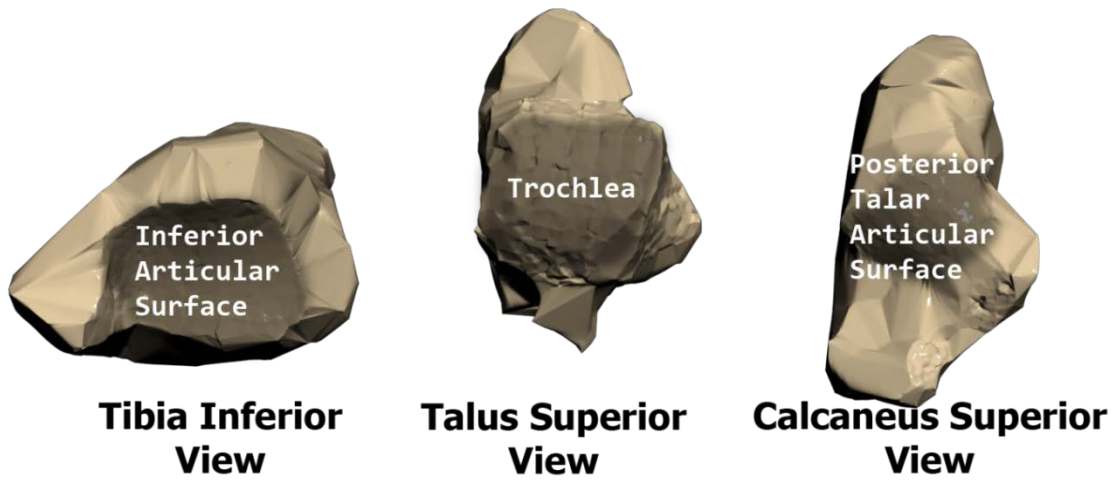


Fig. 3.3: Surfaces used for axis and joint center finding

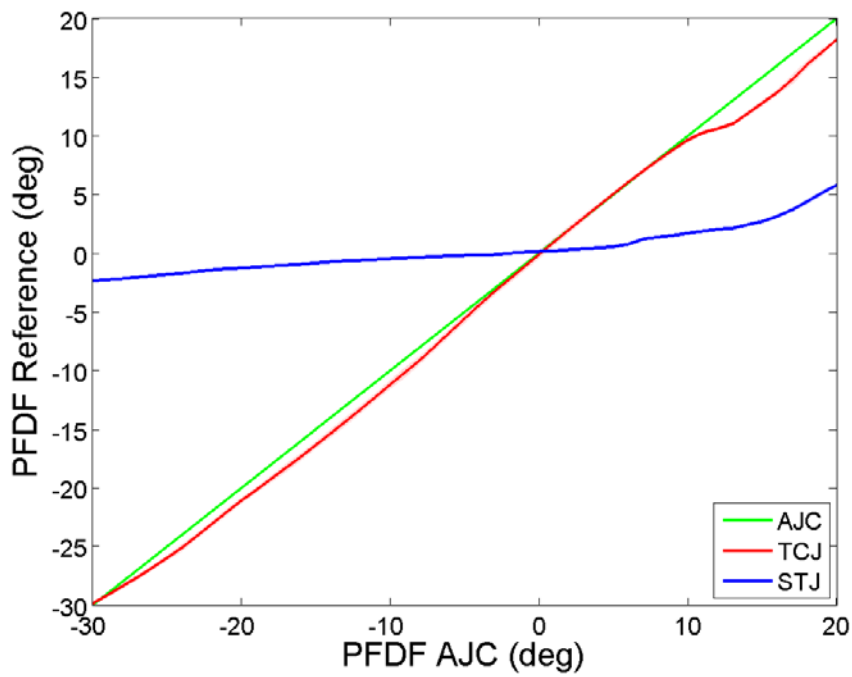


Fig. 3.4: PFDF Angle Comparison Between Joints. PFDF range of motion from each ankle joint versus the AJC. For example at -30° PFDF AJC the STJ had -2° PFDF. For consistency all PFDF angles are referenced from the AJC shown in green as a baseline. The average standard deviation for both the TCJ and STJ was less than 0.06 degrees.

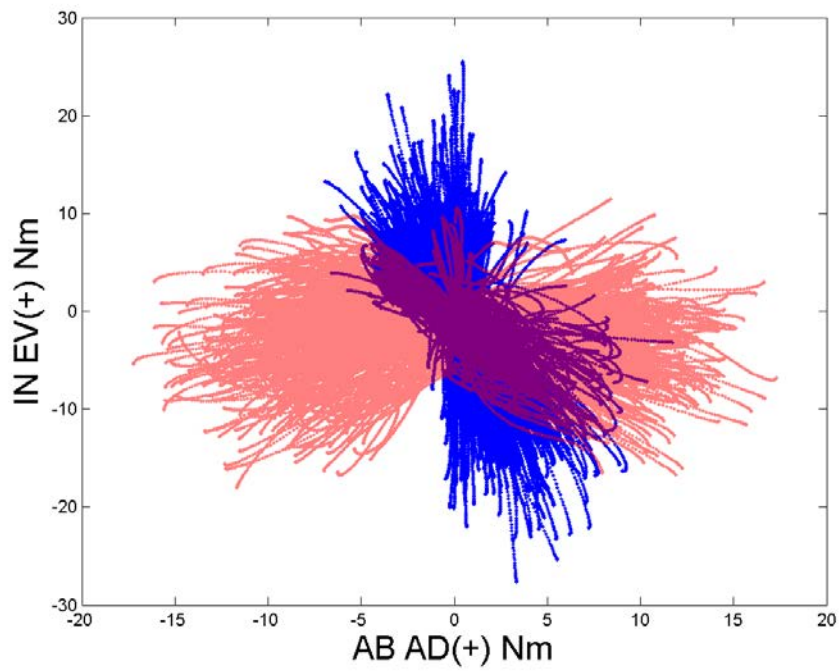


Fig. 3.5: Off-axis torque loading of all ankles and all applied loading conditions. Red: torque loading from applied ABAD torques. Blue: torque loading from applied INEV torques. Loadings shown were collected from all subjects and all loading conditions for the intact ankles.

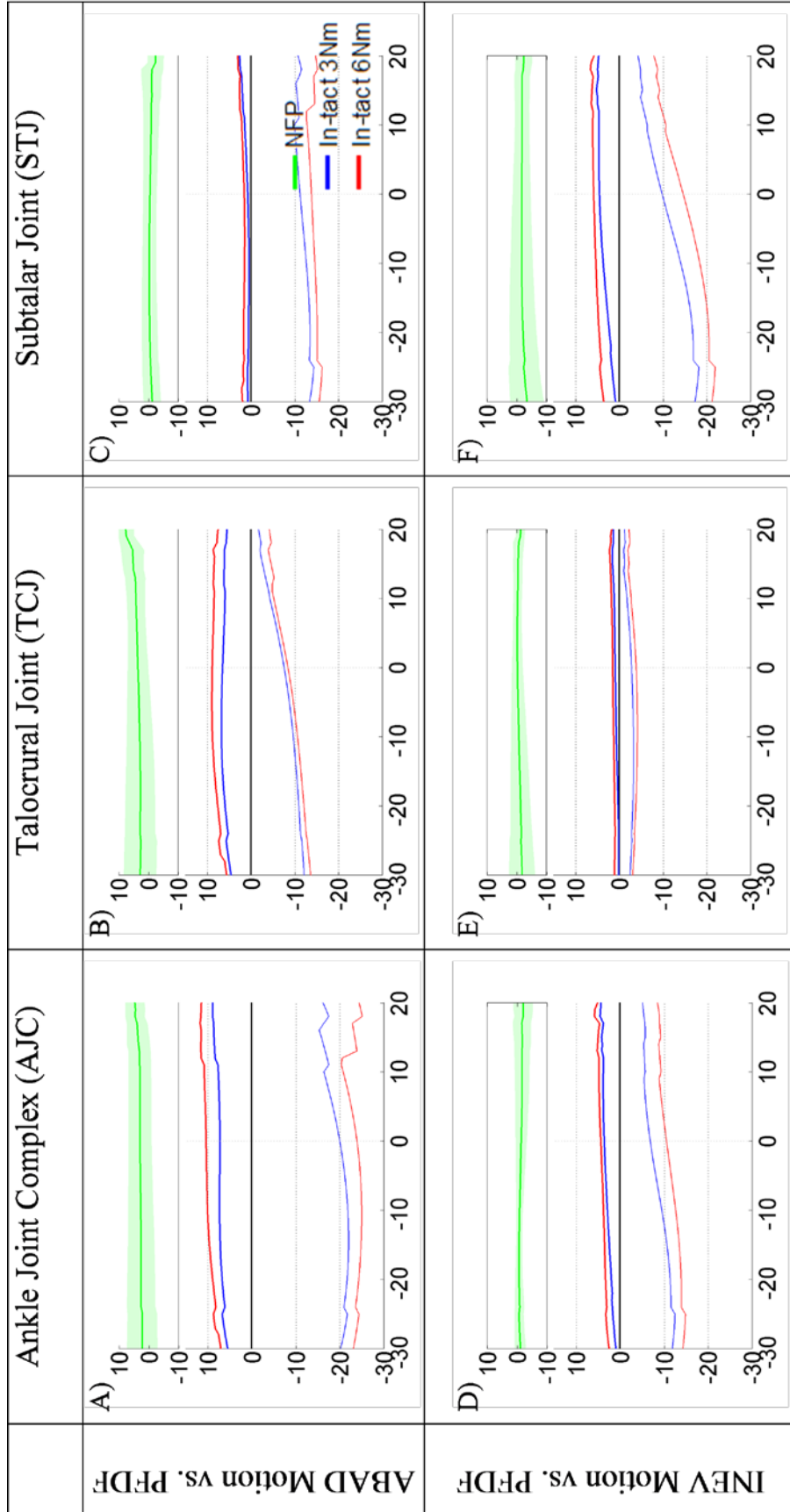


Fig 3.6 Motion of the intact ankle (n=9) three reference frames showing iso-torque load lines at 3 and 6 Nm. The top green graph (NFP) was the average neutral path subtracted from each ankles motion. The average ankle motions are shown with the top lines being positive rotations, and the bottom lines being negative rotations. The horizontal black line at 0 degrees was the NFP. A, B, and C are applied ABAD motion, while D, E, and F were applied INEV motion. For all angles shown at least 6 ankles had data across the range shown, this was the reason for some discontinuity in the line at the extremes. The PPDF motion (A-F) are relative to AJC motion and not relative joint motion. The standard deviation across the flexion range was 0.346 for ABAD torques and 0.409 for INEV torques and was less than 0.5 in all joints.

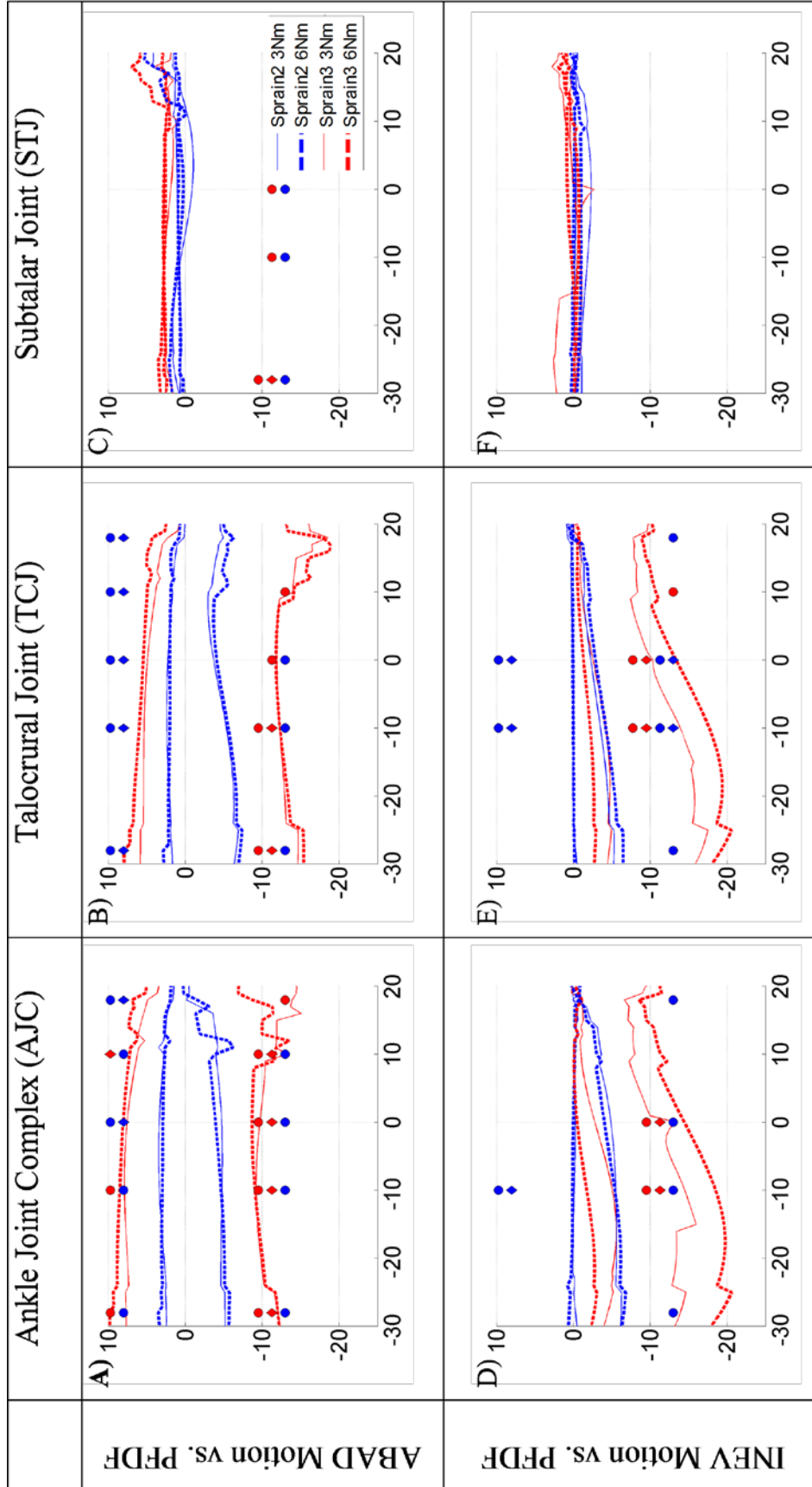


Fig. 3.7: Passive Motion of the injured ankle joint at 3 and 6 Nm in each direction. Three reference frames showing change in iso-torque load lines normalized to the intact ankles passive motion Row 1: ABAD motion, Row 2: INEV motion, Row 3: talofibular and Sprain level 2 (calcaneofibular) refer to the ligament that was cut. ANOVA results indicated by a significant difference between intact/sprain level 2 (Square ■), sprain level 2/sprain level 3 (Diamond ◆), and intact/sprain level 3 (Circle ●). Blue and red symbols indicate a significant difference (p<0.05) from a 3 and 6 Nm torque load, respectively. ANOVA was calculated at five different flexion angles: min angle for each ankle, -10, 0, 10, and max angle for each ankle. Between -20 and 10 degrees PFDF there were nine ankles, however at the extremes there were a minimum of six ankles.

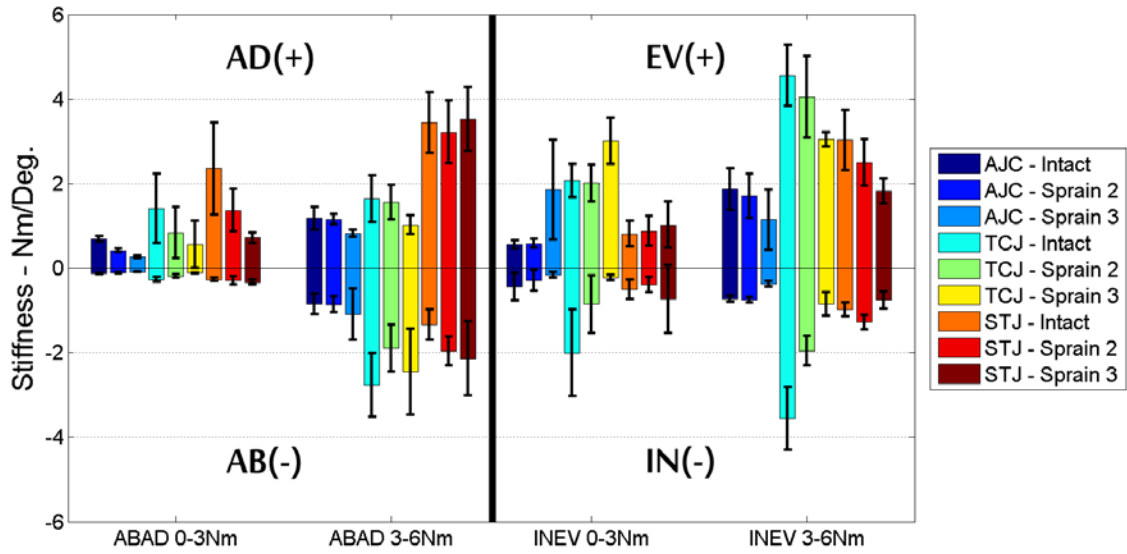


Fig. 3.8: Average stiffness from applied torque loading. The average stiffness was calculated for each run between -20 and 10 degrees PFDf from 0 to 3 Nm and 3 to 6 Nm.

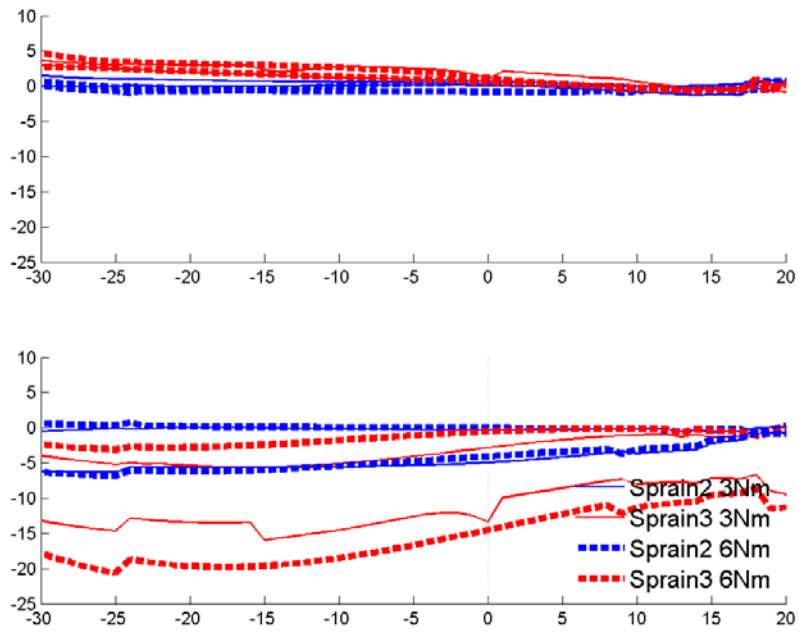


Fig. 3.9: Injured motion of the injured ankle joint with both axes shown. AJC view from applied INEV motion, (top) ABAD motion, (bottom) INEV motion versus PFDF angle. Eversion has a shift towards inversion which becomes very apparent with sprain level 3.

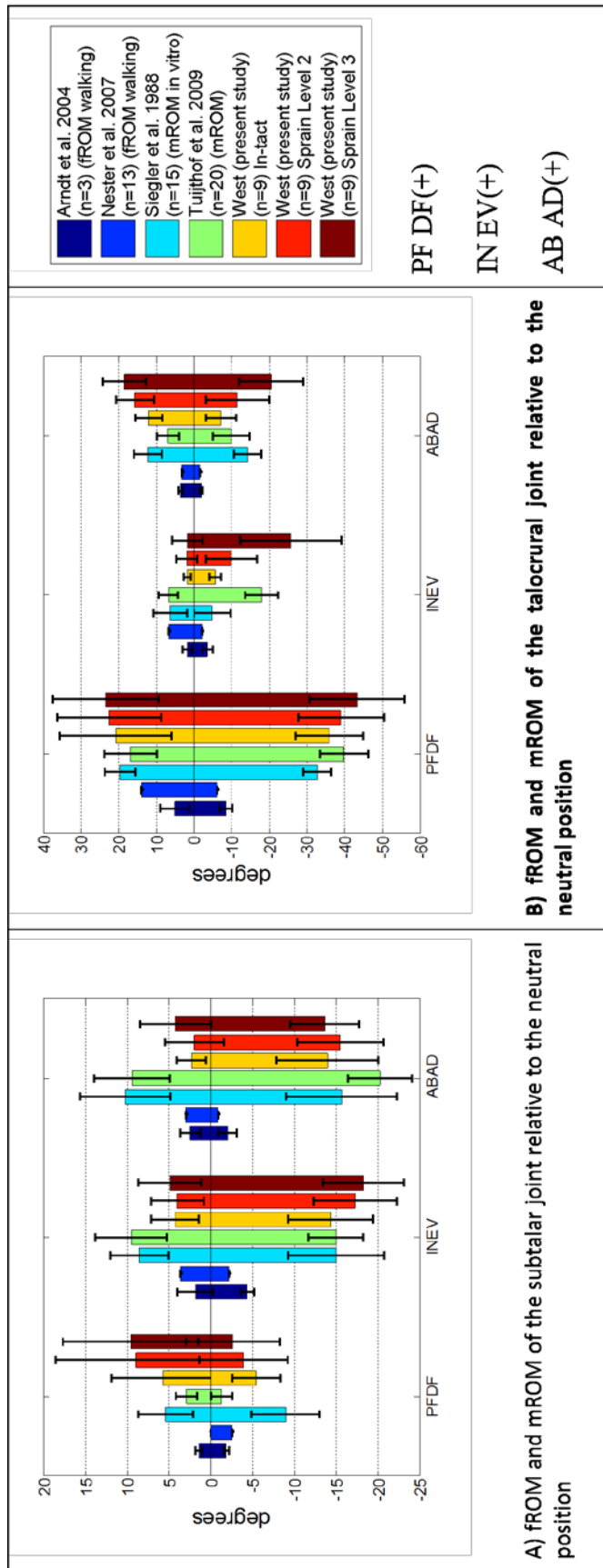


Fig. 3.10: Comparison to previous data formatted and organized in a review article [40]. Error bars represent ± 1 standard deviation [42-45, 47-49, 78].

Chapter 4 Conclusion

The present study consisted of nine ankle specimens that were tested for stiffness, and passive range of motion at specified torque levels of 3 and 6 Nm. The ATFL and then the CFL were both severed to analyze the change in motion based on ankle sprain injury. The effect of level 2 and level 3 ankle sprains and their effect on the stiffness and constraint on the AJC, TCJ and the STJ were analyzed by severing the ATFL and the CFL respectively. A method was developed to find the kinematic orientations at specific iso-torque loads, as well as a new application of generating bone based coordinate systems and a modified description of the G&S system for the ankle subjoints.

Some of the key results from the study show that the laxity occurs primarily in the TCJ leaving the STJ relatively stable, but not unchanged. Even though methodologies were different there was parity in the resulting motions with previous studies. From ankle sprain injury abduction and inversion had an overall greater change in range than adduction, and eversion which had a smaller change in motion. This is expected because abduction and inversion are restrained by the lateral ligaments. What was interesting was the overall change in motions constrained by the medial ligaments in the TCJ. At high dorsiflexion, eversion had no change based on injury level.

There are several areas where learning could be applied for the future. The following future suggestions falls into three categories: specimen and cadaver preparation; data collection; and data analysis.

Specimen and cadaver preparation could be enhanced by obtaining a detailed CT or MRI scan of the ankle. This led to a difficulty where it was impossible to have a detailed model of the

ankle, but lack of CT or MRI data made it impossible to achieve this, and even detailed probing is not enough to get a good description. A protocol should be created with an exclusion criterion to verify that an ankle is acceptable for testing. There were several specimens that were significantly more lax than others leading to problems with rigid bodies impinging bone, and having so much movement that the ankle became completely unstable at sprain level 3 in certain rotations, primarily inversion and abduction. Some specimens also showed poor bone quality making solid fixation of the rigid bodies challenging. One of the limitations of the present study was the free-floating fibula. Designing a method for the fibula to be consistently restrained would be important for future studies.

To improve data collection more time should be spent collecting this motion, because the neutral flexion path ended up being of great value. It was only collected once for 60 seconds in the present study. A robot or machine that could repeatably apply dynamic motion similar to the KKS would help in collecting more useable data points, and remove the difficulty of off axis torque loading. In the future probing the insertion and origin of the ligaments and measuring their cross sectional area could be used to input future computer models. With this data variations in origin and insertion might illuminate other factors affecting motion. In the present study the envelope was created by applying rotations to the ankle joint. In future studies applying motions similar to the anterior drawer test and other sliding motions could be recorded as well to create an expanded envelope of sliding and rotation motion. This could also be helped by the use of a machine to apply the motion. If a rigid body was inserted into the fibula the motion of all the joints in the hindfoot could be understood.

Data analysis could be improved by making the process simpler and more streamlined. This might not be feasible but if the lab agreed on a format for processing data, then a generic

kinematic solver could be created that could process, visualize and analyze whatever joint data is inputted into it. This would however deprive future graduate students the opportunity to program vector kinematics themselves.

4.1 Conflict of interest statement and role of funding

The authors did not have any financial and personal relationships with other people or organizations that could inappropriately influence (bias) their work.

References

- [1] Grood, E. S., and Suntay, W. J., 1983, "A joint coordinate system for the clinical description of three-dimensional motions: application to the knee," *J Biomech Eng*, 105(2), pp. 136-144.
- [2] Capulet, 2008, "Juliet D3o Ballet Dance Shoe," <http://www.capuletworld.com/>.
- [3] Griffin, L. Y., 2005, *Essentials of musculoskeletal care.*, Amer Academy of Orthopaedic.
- [4] Hannafin, J. A., Kitaoka, H. B., and Panagis, J. S., 2010, "Questions and Answers Sprains and Strains," Webpage and booklet, http://www.niams.nih.gov/Health_Info/Sprains_Strains/default.asp.
- [5] Hootman, J. M., Dick, R., and Agel, J., 2007, "Epidemiology of collegiate injuries for 15 sports: summary and recommendations for injury prevention initiatives," *J Athl Train*, 42(2), pp. 311-319.
- [6] Viljakka, T., and Rokkanen, P., 1983, "The treatment of ankle sprain by bandaging and antiphlogistic drugs," *Ann Chir Gynaecol*, 72(2), pp. 66-70.
- [7] Fong, D. T., Hong, Y., Chan, L. K., Yung, P. S., and Chan, K. M., 2007, "A systematic review on ankle injury and ankle sprain in sports," *Sports Med*, 37(1), pp. 73-94.
- [8] Renstrom, P. A., and Konradsen, L., 1997, "Ankle ligament injuries," *Br J Sports Med*, 31(1), pp. 11-20.
- [9] Wolfe, M. W., Uhl, T. L., Mattacola, C. G., and McCluskey, L. C., 2001, "Management of ankle sprains," *Am Fam Physician*, 63(1), pp. 93-104.
- [10] Bahr, R., and Bahr, I. A., 1997, "Incidence of acute volleyball injuries: a prospective cohort study of injury mechanisms and risk factors," *Scand J Med Sci Sports*, 7(3), pp. 166-171.
- [11] Ekstrand, J., and Tropp, H., 1990, "The incidence of ankle sprains in soccer," *Foot Ankle*, 11(1), pp. 41-44.
- [12] McKay, G. D., Goldie, P. A., Payne, W. R., and Oakes, B. W., 2001, "Ankle injuries in basketball: injury rate and risk factors," *Br J Sports Med*, 35(2), pp. 103-108.
- [13] Milgrom, C., Shlamkovitch, N., Finestone, A., Eldad, A., Laor, A., Danon, Y. L., Lavie, O., Wosk, J., and Simkin, A., 1991, "Risk factors for lateral ankle sprain: a prospective study among military recruits," *Foot Ankle*, 12(1), pp. 26-30.
- [14] Smith, R. W., and Reischl, S. F., 1986, "Treatment of ankle sprains in young athletes," *Am J Sports Med*, 14(6), pp. 465-471.
- [15] Woods, C., Hawkins, R., Hulse, M., and Hodson, A., 2003, "The Football Association Medical Research Programme: an audit of injuries in professional football: an analysis of ankle sprains," *Br J Sports Med*, 37(3), pp. 233-238.
- [16] Cass, J. R., Morrey, B. F., Katoh, Y., and Chao, E. Y., 1985, "Ankle instability: comparison of primary repair and delayed reconstruction after long-term follow-up study," *Clin Orthop Relat Res*(198), pp. 110-117.

- [17] Mizel, M. S., Hecht, P. J., Marymont, J. V., and Temple, H. T., 2004, "Evaluation and treatment of chronic ankle pain," *Instr Course Lect*, 53, pp. 311-321.
- [18] Krips, R., de Vries, J., and van Dijk, C. N., 2006, "Ankle instability," *Foot Ankle Clin*, 11(2), pp. 311-329, vi.
- [19] Lucchesi, G. M., Jackson, R. E., Peacock, W. F., Cerasani, C., and Swor, R. A., 1995, "Sensitivity of the Ottawa rules," *Ann Emerg Med*, 26(1), pp. 1-5.
- [20] Thordarson, D., 2004, *Foot and ankle*, Lippincott Williams & Wilkins, Philadelphia.
- [21] Swierzweski, J. J., 2000, "Foot & Ankle Anatomy - Foot Anatomy," <http://www.podiatrychannel.com/anatomy/index.shtml>.
- [22] Saladin, K. S., 2006, *Anatomy & Physiology The Unity of Form And Function*, McGraw-Hill Science Engineering.
- [23] Netter, F., 1989, *Atlas of human anatomy*, Ciba-Geigy Corp., Summit N.J.
- [24] Wu, G., Siegler, S., Allard, P., Kirtley, C., Leardini, A., Rosenbaum, D., Whittle, M., D'Lima, D. D., Cristofolini, L., Witte, H., Schmid, O., and Stokes, I., 2002, "ISB recommendation on definitions of joint coordinate system of various joints for the reporting of human joint motion--part I: ankle, hip, and spine. International Society of Biomechanics," *J Biomech*, 35(4), pp. 543-548.
- [25] Monk, C. J., 1969, "Injuries of the tibio-fibular ligaments," *J Bone Joint Surg Br*, 51(2), pp. 330-337.
- [26] McGlamry, E., 2001, *McGlamry's comprehensive textbook of foot and ankle surgery*, Lippincott Williams & Wilkins, Philadelphia.
- [27] Garrick, J. G., and Requa, R. K., 1988, "The epidemiology of foot and ankle injuries in sports," *Clin Sports Med*, 7(1), pp. 29-36.
- [28] Bytowski, J., 2010, *Oxford American handbook of sports medicine*, Oxford University Press, New York.
- [29] Nyska, M., 2002, *The unstable ankle*, Human Kinetics, Champaign IL.
- [30] Anderson, M., 2003, *Fundamentals of sports injury management*, Lippincott Williams & Wilkins, Philadelphia.
- [31] Attarian, D. E., McCrackin, H. J., Devito, D. P., McElhaney, J. H., and Garrett, W. E., Jr., 1985, "A biomechanical study of human lateral ankle ligaments and autogenous reconstructive grafts," *Am J Sports Med*, 13(6), pp. 377-381.
- [32] Fong, D. T., Chan, Y. Y., Mok, K. M., Yung, P., and Chan, K. M., 2009, "Understanding acute ankle ligamentous sprain injury in sports," *Sports Med Arthrosc Rehabil Ther Technol*, 1, p. 14.
- [33] Brostroem, L., 1964, "Sprained Ankles. I. Anatomic Lesions in Recent Sprains," *Acta Chir Scand*, 128, pp. 483-495.
- [34] Staples, O. S., 1975, "Ruptures of the fibular collateral ligaments of the ankle. Result study of immediate surgical treatment," *J Bone Joint Surg Am*, 57(1), pp. 101-107.

- [35] Spouge, A., 2001, Practical MRI of the foot and ankle, CRC Press % @ 9780849302817, Boca Raton.
- [36] Hintermann, B., 1999, "Biomechanics of the unstable ankle joint and clinical implications," *Med Sci Sports Exerc*, 31(7 Suppl), pp. S459-469.
- [37] Organization, W. L. D. I.-P. F. P., 2008, "Ankle & foot (acute & chronic)," <http://www.guidelines.gov/content.aspx?id=12657&search=ankle+sprain>.
- [38] Gotlin, R., 2008, Sports injuries guidebook, Human Kinetics, Champaign IL.
- [39] Michael, J. M., Golshani, A., Gargac, S., and Goswami, T., 2008, "Biomechanics of the ankle joint and clinical outcomes of total ankle replacement," *J Mech Behav Biomed Mater*, 1(4), pp. 276-294.
- [40] Kleipool, R. P., and Blankevoort, L., 2010, "The relation between geometry and function of the ankle joint complex: a biomechanical review," *Knee Surg Sports Traumatol Arthrosc*, 18(5), pp. 618-627.
- [41] Gajdosik, R. L., and Bohannon, R. W., 1987, "Clinical measurement of range of motion. Review of goniometry emphasizing reliability and validity," *Phys Ther*, 67(12), pp. 1867-1872.
- [42] Arndt, A., Westblad, P., Winson, I., Hashimoto, T., and Lundberg, A., 2004, "Ankle and subtalar kinematics measured with intracortical pins during the stance phase of walking," *Foot Ankle Int*, 25(5), pp. 357-364.
- [43] Arndt, A., Wolf, P., Liu, A., Nester, C., Stacoff, A., Jones, R., Lundgren, P., and Lundberg, A., 2007, "Intrinsic foot kinematics measured in vivo during the stance phase of slow running," *J Biomech*, 40(12), pp. 2672-2678.
- [44] Lundgren, P., Nester, C., Liu, A., Arndt, A., Jones, R., Stacoff, A., Wolf, P., and Lundberg, A., 2008, "Invasive in vivo measurement of rear-, mid- and forefoot motion during walking," *Gait Posture*, 28(1), pp. 93-100.
- [45] Nester, C. J., Liu, A. M., Ward, E., Howard, D., Cocheba, J., Derrick, T., and Patterson, P., 2007, "In vitro study of foot kinematics using a dynamic walking cadaver model," *J Biomech*, 40(9), pp. 1927-1937.
- [46] Aruin, A. S., and Zatsiorsky, V. M., 1984, "Biomechanical characteristics of human ankle-joint muscles," *Eur J Appl Physiol Occup Physiol*, 52(4), pp. 400-406.
- [47] Siegler, S., Chen, J., and Schneck, C. D., 1988, "The three-dimensional kinematics and flexibility characteristics of the human ankle and subtalar joints--Part I: Kinematics," *J Biomech Eng*, 110(4), pp. 364-373.
- [48] Tuijthof, G. J., Zengerink, M., Beimers, L., Jonges, R., Maas, M., van Dijk, C. N., and Blankevoort, L., 2009, "Determination of consistent patterns of range of motion in the ankle joint with a computed tomography stress-test," *Clin Biomech (Bristol, Avon)*, 24(6), pp. 517-523.
- [49] Weindel, S., Schmidt, R., Rammelt, S., Claes, L., v Campe, A., and Rein, S., 2010, "Subtalar instability: a biomechanical cadaver study," *Arch Orthop Trauma Surg*, 130(3), pp. 313-319.
- [50] Allinger, T. L., and Engsborg, J. R., 1993, "A method to determine the range of motion of the ankle joint complex, in vivo," *J Biomech*, 26(1), pp. 69-76.

- [51] Stormont, D. M., Morrey, B. F., An, K. N., and Cass, J. R., 1985, "Stability of the loaded ankle. Relation between articular restraint and primary and secondary static restraints," *Am J Sports Med*, 13(5), pp. 295-300.
- [52] Engsberg, J. R., 1987, "A biomechanical analysis of the talocalcaneal joint--in vitro," *J Biomech*, 20(4), pp. 429-442.
- [53] Wright, D. G., Desai, S. M., and Henderson, W. H., 1964, "Action of the Subtalar and Ankle-Joint Complex during the Stance Phase of Walking," *J Bone Joint Surg Am*, 46, pp. 361-382.
- [54] Engsberg, J. R., Grimston, S. K., and Wackwitz, J. H., 1988, "Predicting talocalcaneal joint orientations from talocalcaneal/talocrural joint orientations," *J Orthop Res*, 6(5), pp. 749-757.
- [55] Nigg, B. M., Fisher, V., Allinger, T. L., Ronsky, J. R., and Engsberg, J. R., 1992, "Range of motion of the foot as a function of age," *Foot Ankle*, 13(6), pp. 336-343.
- [56] Baker, R., 2003, "ISB recommendation on definition of joint coordinate systems for the reporting of human joint motion-part I: ankle, hip and spine," *J Biomech*, 36(2), pp. 300-302; author reply 303-304.
- [57] Beimers, L., Tuijthof, G. J., Blankevoort, L., Jonges, R., Maas, M., and van Dijk, C. N., 2008, "In-vivo range of motion of the subtalar joint using computed tomography," *J Biomech*, 41(7), pp. 1390-1397.
- [58] Conti, G., Cristofolini, L., Juszczak, M., Leardini, A., and Viceconti, M., 2008, "Comparison of three standard anatomical reference frames for the tibia-fibula complex," *J Biomech*, 41(16), pp. 3384-3389.
- [59] Rome, K., 1996, "Ankle joint dorsiflexion measurement studies. A review of the literature," *J Am Podiatr Med Assoc*, 86(5), pp. 205-211.
- [60] Wong, Y., Kim, W., and Ying, N., 2005, "Passive motion characteristics of the talocrural and the subtalar joint by dual Euler angles," *J Biomech*, 38(12), pp. 2480-2485.
- [61] Ying, N., and Kim, W., 2002, "Use of dual Euler angles to quantify the three-dimensional joint motion and its application to the ankle joint complex," *J Biomech*, 35(12), pp. 1647-1657.
- [62] Ying, N., Kim, W., Wong, Y., and Kam, B. H., 2004, "Analysis of passive motion characteristics of the ankle joint complex using dual Euler angle parameters," *Clin Biomech (Bristol, Avon)*, 19(2), pp. 153-160.
- [63] Cristofolini, L., and Viceconti, M., 2000, "Mechanical validation of whole bone composite tibia models," *J Biomech*, 33(3), pp. 279-288.
- [64] Gray, H. A., Taddei, F., Zavatsky, A. B., Cristofolini, L., and Gill, H. S., 2008, "Experimental validation of a finite element model of a human cadaveric tibia," *J Biomech Eng*, 130(3), p. 031016.
- [65] Della Croce, U., Leardini, A., Chiari, L., and Cappozzo, A., 2005, "Human movement analysis using stereophotogrammetry. Part 4: assessment of anatomical landmark misplacement and its effects on joint kinematics," *Gait Posture*, 21(2), pp. 226-237.

- [66] Thewlis, D., Richards, J., and Bower, J., 2008, "Discrepancies in knee joint moments using common anatomical frames defined by different palpable landmarks," *J Appl Biomech*, 24(2), pp. 185-190.
- [67] Lundberg, A., Svensson, O. K., Nemeth, G., and Selvik, G., 1989, "The axis of rotation of the ankle joint," *J Bone Joint Surg Br*, 71(1), pp. 94-99.
- [68] Siegler, S., Lapointe, S., Nobilini, R., and Berman, A. T., 1996, "A six-degrees-of-freedom instrumented linkage for measuring the flexibility characteristics of the ankle joint complex," *J Biomech*, 29(7), pp. 943-947.
- [69] Arampatzis, A., Bruggemann, G. P., and Klapsing, G. M., 2002, "A three-dimensional shank-foot model to determine the foot motion during landings," *Med Sci Sports Exerc*, 34(1), pp. 130-138.
- [70] Bruening, D. A., Crewe, A. N., and Buczek, F. L., 2008, "A simple, anatomically based correction to the conventional ankle joint center," *Clin Biomech (Bristol, Avon)*, 23(10), pp. 1299-1302.
- [71] Franci, R., Parenti-Castelli, V., Belvedere, C., and Leardini, A., 2009, "A new one-DOF fully parallel mechanism for modelling passive motion at the human tibiotalar joint," *J Biomech*, 42(10), pp. 1403-1408.
- [72] O'Donovan, K. J., Kamnik, R., O'Keefe, D. T., and Lyons, G. M., 2007, "An inertial and magnetic sensor based technique for joint angle measurement," *J Biomech*, 40(12), pp. 2604-2611.
- [73] Favre, J., Aissaoui, R., Jolles, B. M., de Guise, J. A., and Aminian, K., 2009, "Functional calibration procedure for 3D knee joint angle description using inertial sensors," *J Biomech*, 42(14), pp. 2330-2335.
- [74] Leardini, A., O'Connor, J. J., Catani, F., and Giannini, S., 1999, "Kinematics of the human ankle complex in passive flexion; a single degree of freedom system," *J Biomech*, 32(2), pp. 111-118.
- [75] Maletsky, L. P., Sun, J., and Morton, N. A., 2007, "Accuracy of an optical active-marker system to track the relative motion of rigid bodies," *J Biomech*, 40(3), pp. 682-685.
- [76] Hayes, A., Tochigi, Y., and Saltzman, C. L., 2006, "Ankle morphometry on 3D-CT images," *Iowa Orthop J*, 26, pp. 1-4.
- [77] Chen, J., Siegler, S., and Schneck, C. D., 1988, "The three-dimensional kinematics and flexibility characteristics of the human ankle and subtalar joint--Part II: Flexibility characteristics," *J Biomech Eng*, 110(4), pp. 374-385.
- [78] de Asla, R. J., Wan, L., Rubash, H. E., and Li, G., 2006, "Six DOF in vivo kinematics of the ankle joint complex: Application of a combined dual-orthogonal fluoroscopic and magnetic resonance imaging technique," *J Orthop Res*, 24(5), pp. 1019-1027.
- [79] Woltring, H. J., 1994, "3-D attitude representation of human joints: a standardization proposal," *J Biomech*, 27(12), pp. 1399-1414.
- [80] Dul, J., and Johnson, G. E., 1985, "A kinematic model of the human ankle," *J Biomed Eng*, 7(2), pp. 137-143.

- [81] Chao, E. Y., 1980, "Justification of triaxial goniometer for the measurement of joint rotation," *J Biomech*, 13(12), pp. 989-1006.
- [82] Tupling, S. J., and Pierrynowski, M. R., 1987, "Use of cardan angles to locate rigid bodies in three-dimensional space," *Med Biol Eng Comput*, 25(5), pp. 527-532.
- [83] Blankevoort, L., Huiskes, R., and de Lange, A., 1990, "Helical axes of passive knee joint motions," *J Biomech*, 23(12), pp. 1219-1229.
- [84] Kinzel, G. L., Hall, A. S., Jr., and Hillberry, B. M., 1972, "Measurement of the total motion between two body segments. I. Analytical development," *J Biomech*, 5(1), pp. 93-105.
- [85] Kuipers, J., 1999, *Quaternions and rotation sequences : a primer with applications to orbits, aerospace, and virtual reality*, Princeton University Press, Princeton N.J.
- [86] Tong, K. Y., and Mak, A. F., 2001, "Development of computer-based environment for simulating the voluntary upper-limb movements of persons with disability," *Med Biol Eng Comput*, 39(4), pp. 414-421.
- [87] Ball, R. S., 1876, *The Theory of Screws: A study in the dynamics of a rigid body*, Hodges, Foster, and Co., Grafton-Street, Dublin.
- [88] Zatsiorsky, V., 1998, *Kinematics of human motion*, Human Kinetics, Champaign IL.
- [89] Ellis, H., 2010, *Clinical anatomy : applied anatomy for students and junior doctors*, Wiley-Blackwell, Chichester West Sussex ;;Hoboken NJ.
- [90] Hertel, J., 2002, "Functional Anatomy, Pathomechanics, and Pathophysiology of Lateral Ankle Instability," *J Athl Train*, 37(4), pp. 364-375.
- [91] Litt, J. C., 1992, "The sprained ankle. Diagnosis and management of lateral ligament injuries," *Aust Fam Physician*, 21(4), pp. 447, 452-446.
- [92] Stahelin, T., Nigg, B. M., Stefanyshyn, D. J., van den Bogert, A. J., and Kim, S. J., 1997, "A method to determine bone movement in the ankle joint complex in vitro," *J Biomech*, 30(5), pp. 513-516.
- [93] Buczek, F. L., and Cavanagh, P. R., 1990, "Stance phase knee and ankle kinematics and kinetics during level and downhill running," *Med Sci Sports Exerc*, 22(5), pp. 669-677.
- [94] Kepple, T. M., Stanhope, S. J., Lohmann, K. N., and Roman, N. L., 1990, "A video-based technique for measuring ankle-subtalar motion during stance," *J Biomed Eng*, 12(4), pp. 273-280.
- [95] Kitaoka, H. B., Luo, Z. P., and An, K. N., 1997, "Three-dimensional analysis of normal ankle and foot mobility," *Am J Sports Med*, 25(2), pp. 238-242.
- [96] Lundberg, A., 1989, "Kinematics of the ankle and foot. In vivo roentgen stereophotogrammetry," *Acta Orthop Scand Suppl*, 233, pp. 1-24.
- [97] Wright, 2011, "INBONE Total Ankle Replacement," <http://www.wmt.com/footandankle/FA214-408.asp>.
- [98] Cooper, D. E., 1991, "Tests for posterolateral instability of the knee in normal subjects. Results of examination under anesthesia," *J Bone Joint Surg Am*, 73(1), pp. 30-36.

Appendices

The appendices A-E provide supplemental information as follows:

APPENDIX A TRANSFORMATION EQUATIONS

APPENDIX B VECTOR TRANSFORMATIONS

APPENDIX C EXAMPLE DATA SETS

APPENDIX D SENSITIVITY ANALYSIS

APPENDIX E STATISTICAL ANALYSIS

APPENDIX F COMPUTATIONAL PROGRAMS

The equations cover the basic equations used during the paper. Example data sets provide a more detailed look at the data and how it was processed. A sensitivity analysis was performed to test for the repeatability of the construction of the CS. Computational programs offers a glimpse at the code that was used to process the data as well as easier to read accompanying pseudo code that walks through the logic of the programs.

Appendix A Transformation Equations

A.1 Load Cell Transformation Equations

The following are the list of equations used to transform the load cell to the ankle joint. It was also necessary to transform the coordinate systems along with the transformations of the torques and forces (Fig. A.1). Once equations A1-A6 have been applied to the load cell data the transformation matrix defining the tibial CS could be used to find the torques and forces in each orthogonal rotation (PFDF, ABAD, INEV).

A.1.1 Force Translations:

$$F_{XAnkle} = F_{xLC} \quad \text{Eq. A-1}$$

$$F_{YAnkle} = F_{yLC} \quad \text{Eq. A-2}$$

$$F_{ZAnkle} = F_{zLC} \quad \text{Eq. A-3}$$

A.1.2 Torque Translations:

$$T_{XAnkle} = F_{yAnkle} d_y + F_{zAnkle} d_z + T_x \quad \text{Eq. A-4}$$

$$T_{YAnkle} = F_{xAnkle} d_x + F_{zAnkle} d_z + T_y \quad \text{Eq. A-5}$$

$$T_{ZAnkle} = F_{xAnkle} d_x + F_{yAnkle} d_y + T_z \quad \text{Eq. A-6}$$

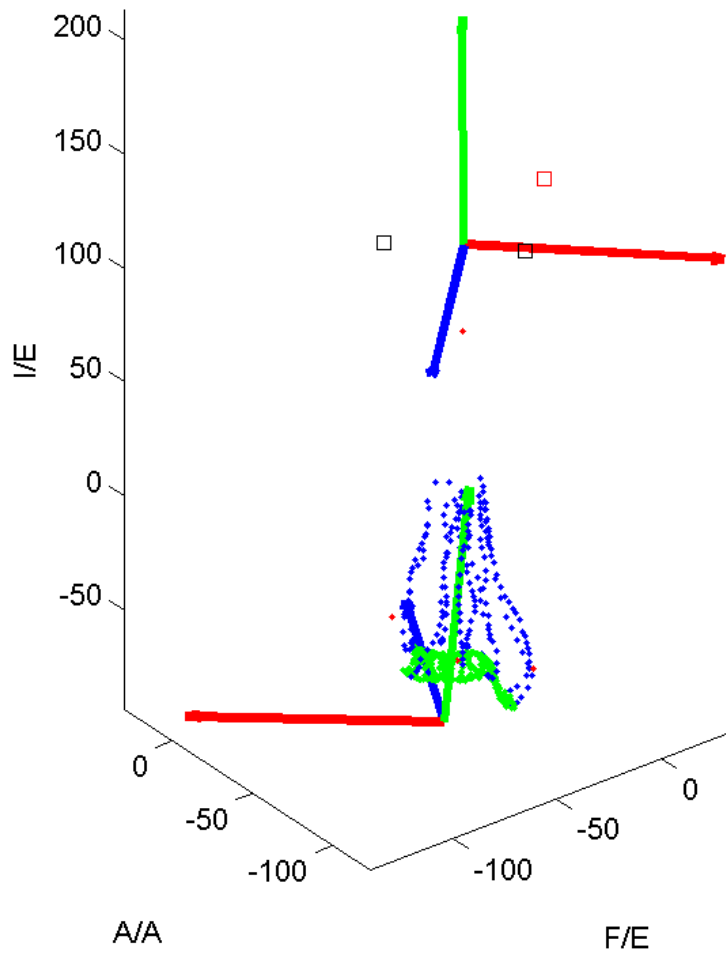


Fig. A.1: View of the load cell CS (top) and the tibia center (bottom). The CS was transformed from the load cell CS to the tibia center.

Appendix B Vector Transformations

The following is a description of the equations used to determine the kinematic joint angles using the mathematics originally defined by Grood and Suntay [1]. The first two inputs are the coordinate system vectors (CS) for A and B defining the position of the CS in the rigid body reference frame relative to the global system (Eq. B1). The second two inputs are the position vectors (P) denoting the position of A and B relative to the global at a fixed point in time. Before the angles can be calculated the inputs need to be conditioned to be a transformation matrix of distal (A) relative to the fixed origin proximal (B) (Eq. B2-B3). There are four inputs required to calculate one set of angles. All inputs are 4x4 transformation matrices denoting position and rotation.

Given:

$$\text{Proximal Axis: } e1 = I; e1^r = J$$

$$\text{Distal Axis: } e3 = k; e3^r = j$$

Where $e1^r$ and $e3^r$ denote the reference axis.

$$\overline{CS}^B = {}^0T^B = \vec{I} = \begin{pmatrix} 1 & 0 & 0 & 0 \\ 0 & 1 & 0 & 0 \\ 0 & 0 & 1 & 0 \\ 0 & 0 & 0 & 1 \end{pmatrix} \quad \text{Eq. B-1}$$

$${}^A\vec{T}^B = \overline{CS}^B \vec{I} * (\vec{P}^B \setminus \vec{P}^A) * \overline{CS}^A \quad \text{Eq. B-2}$$

$${}^A\vec{T}^B = \begin{pmatrix} 1 & 0 & 0 & 0 \\ \vec{P}_{OS} & \vec{R} & & \end{pmatrix} = \begin{matrix} T_{11} & T_{12} & T_{13} & T_{14} \\ T_{21} & T_{22} & T_{23} & T_{24} \\ T_{31} & T_{32} & T_{33} & T_{34} \\ T_{41} & T_{42} & T_{43} & T_{44} \end{matrix} \quad \text{Eq. B-3}$$

*where X\Y indicates inv(X)*Y. Vector CS denotes the rigid body coordinate system relative to the global system. Vector P denotes the current position of the rigid body relative to the global system.

From Eq. B-3 the rotation matrix R has the following vector components relating the proximal to the distal bone segment.

$$\vec{R} = \begin{matrix} I \cdot i & J \cdot i & K \cdot i \\ I \cdot j & J \cdot j & K \cdot j \\ I \cdot k & J \cdot k & K \cdot k \end{matrix} \quad \text{Eq. B-4}$$

The first angle is a rotation about e2, the floating axis (beta).

$$\cos \beta = e1 \cdot e3 = I \cdot k = R_{31} \quad \text{Eq. B-5}$$

$$\beta = \cos^{-1}(I \cdot k) = \frac{\pi}{2} - \cos^{-1} R_{31} \quad \text{Eq. B-6}$$

The second angle is a rotation about e1, the proximal axis (alpha).

$$\tan \alpha = \frac{\sin \alpha}{\cos \alpha} = \frac{\sin \beta \sin \alpha}{\sin \beta \cos \alpha} = \frac{J \cdot k}{K \cdot k} = \frac{R_{32}}{R_{33}} \quad \text{Eq. B-7}$$

$$\alpha = \tan^{-1} \frac{R_{32}}{R_{33}} \quad \text{Eq. B-8}$$

The third angle is a rotation about e_3 , the axis about the long axis of the distal bone (gamma).

$$\tan \gamma = \frac{\sin \gamma}{\cos \gamma} = \frac{\sin \gamma \sin \beta}{\cos \gamma \sin \beta} = \frac{l \cdot j}{l \cdot i} = \frac{R_{21}}{R_{11}} \quad \text{Eq. B-9}$$

$$\gamma = \tan^{-1} \frac{R_{21}}{R_{11}} \quad \text{Eq. B-10}$$

Using equations B-6, B-8, and B-10 the G&S joint angles can be directly calculated.

Appendix C Example Data Sets

C.1 Cadaver Details

The cadaveric specimens used in the study had an average age of 61 years, and a BMI score of 26.0. All but one was male. Each ankle was thawed approximately twelve hours to room temperature after having been used but not injured in a previous experiment having been thawed for approximately 36 hours.

Tbl. C.1: Cadaver specimen details

Number	R/L	Sex	Age (years)	Height (m)	Weight (kg)	BMI
1	R	M	63	1.85	77.1	22.4
2	L	M	69	1.83	65.8	19.7
3	L	M	68	1.83	100.0	29.9
4	R	M	65	1.85	83.9	24.4
5	R	M	67	1.83	79.4	23.7
6	L	F	59	1.70	55.3	19.1
7	R	M	57	1.75	108.9	35.4
8	L	M	57	1.75	108.9	35.4
9	L	M	41	1.83	79.9	23.9
Total	4 Right	8 Male	60.7	1.8	84.3	26.0
Std Dev			8.7	0.1	18.5	6.2

C.2 Representative Data from One Ankle

Ankle number four was chosen to give a representation of what the output data looks like. Included are the coordinate system definitions (Fig. C.1), a comparison of the motions applied to the ankle and their corresponding torque loads and kinematic output over time (Fig. C.2-C.8).

C.2.1 Definition of Coordinate System

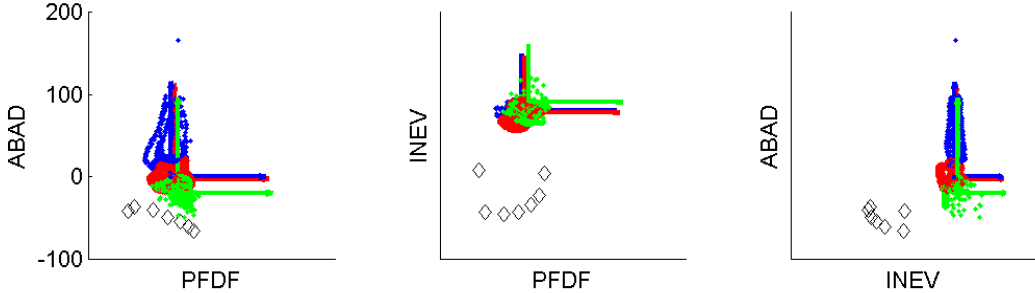


Fig. C.1: Coordinate system definition for ankle number four. Blue is tibia CS, red is the talus CS, and green is the calcaneus CS.

C.2.2 Kinematic Output and Torque Loading from Applied Motions

Representative data set from ankle number four showing G&S rotations (blue) and torque loading levels (green) versus time in seconds.

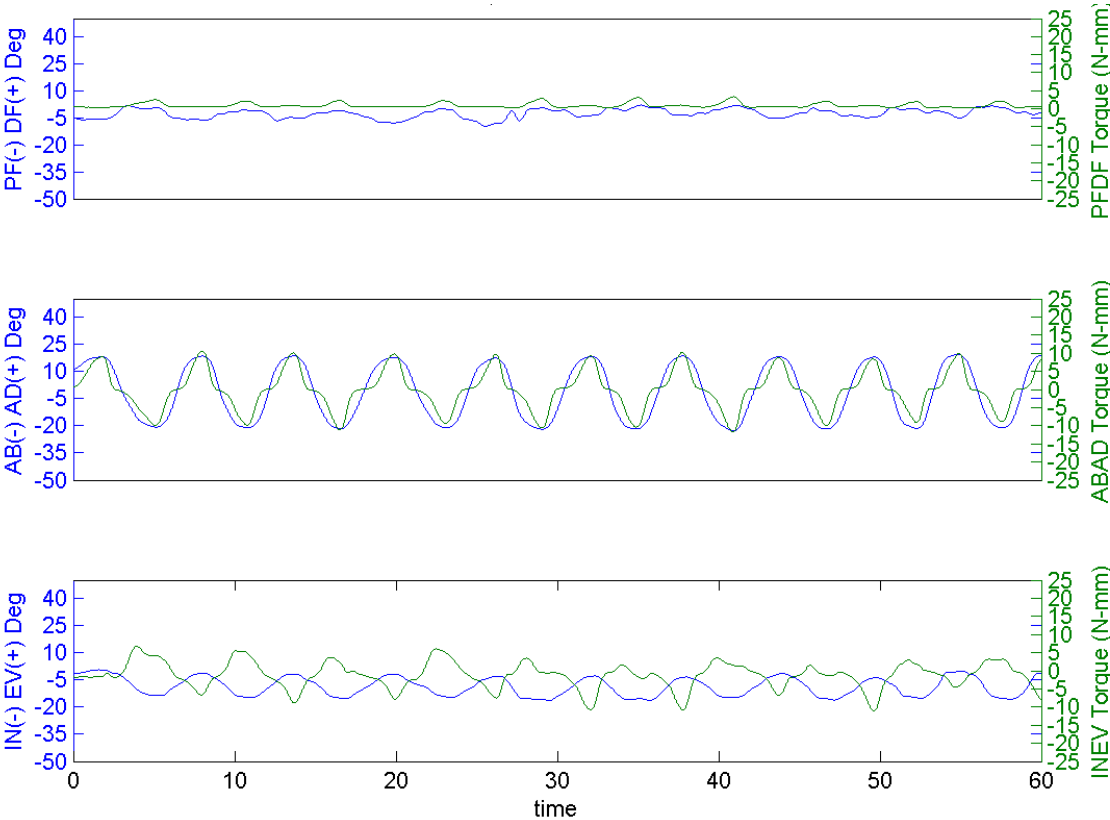


Fig. C.2: Applied motion - Neutral ABAD Path

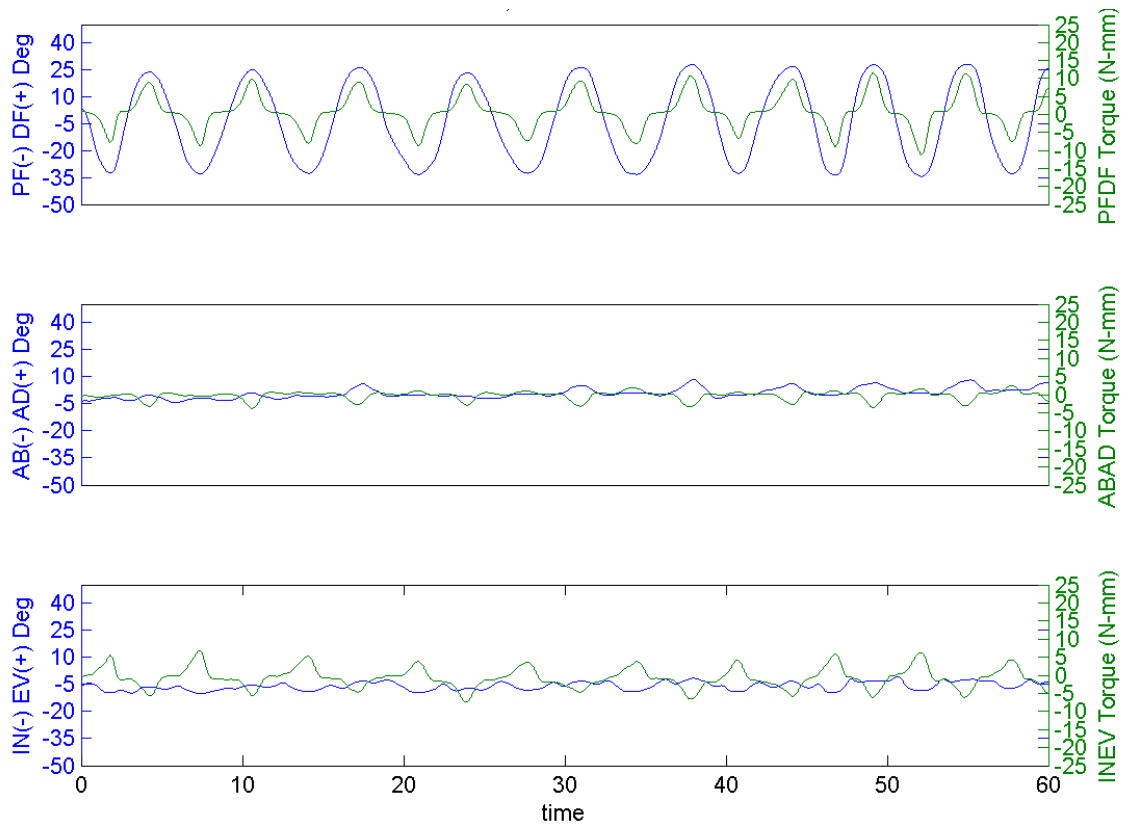


Fig. C.3: Applied motion - Neutral Flexion Path

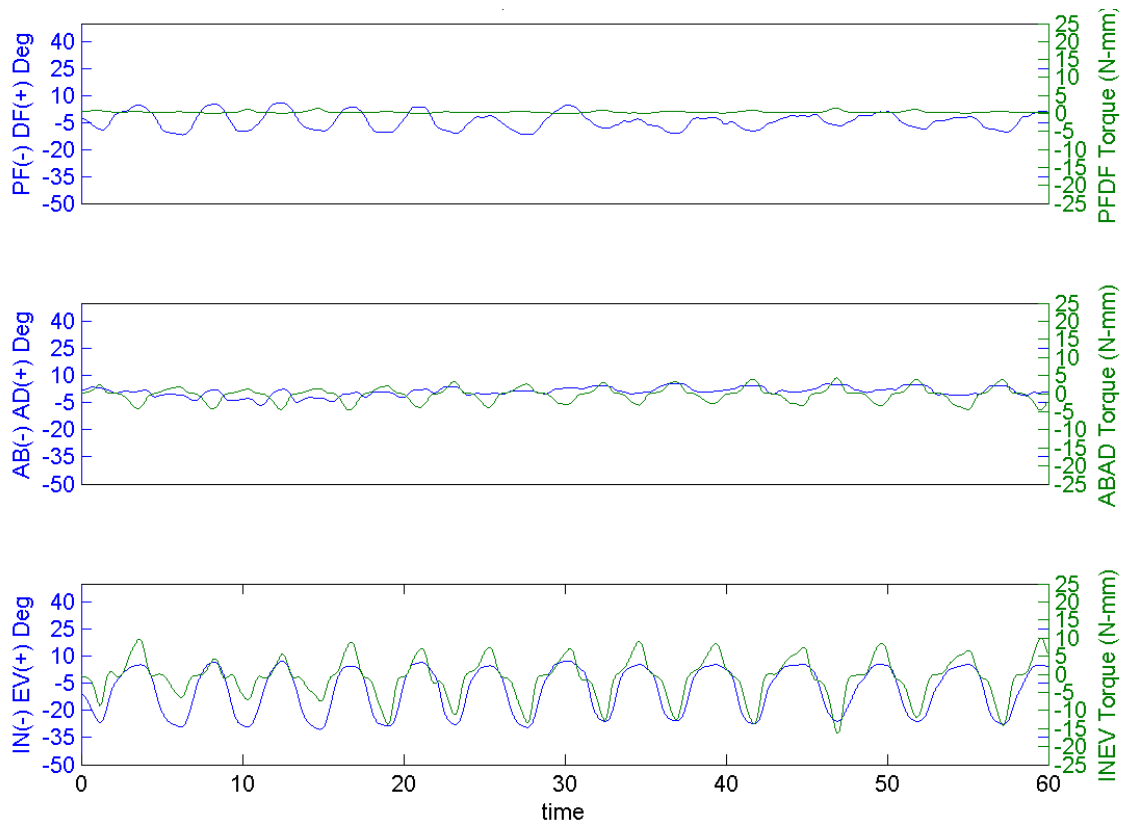


Fig. C.4: Applied motion - Neutral INEV Path

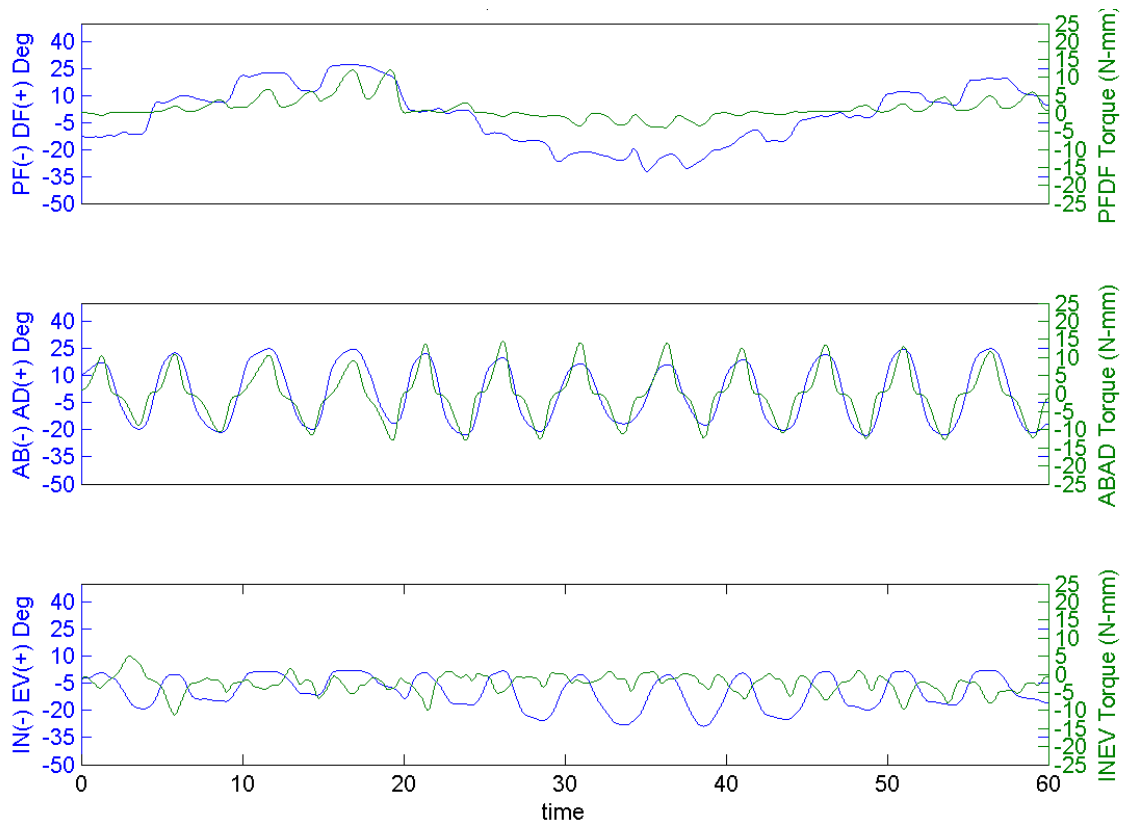


Fig. C.5: Applied motion - ABAD Rotation

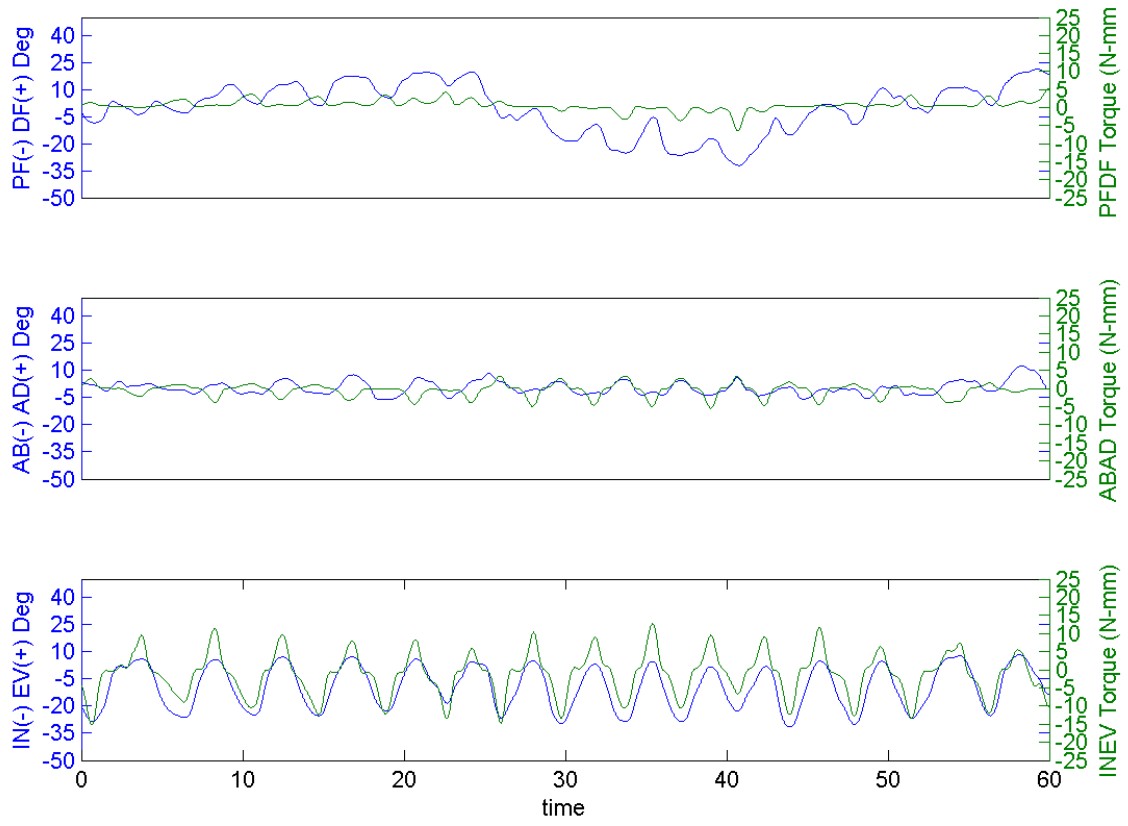


Fig. C.6: Applied motion - INEV Rotation

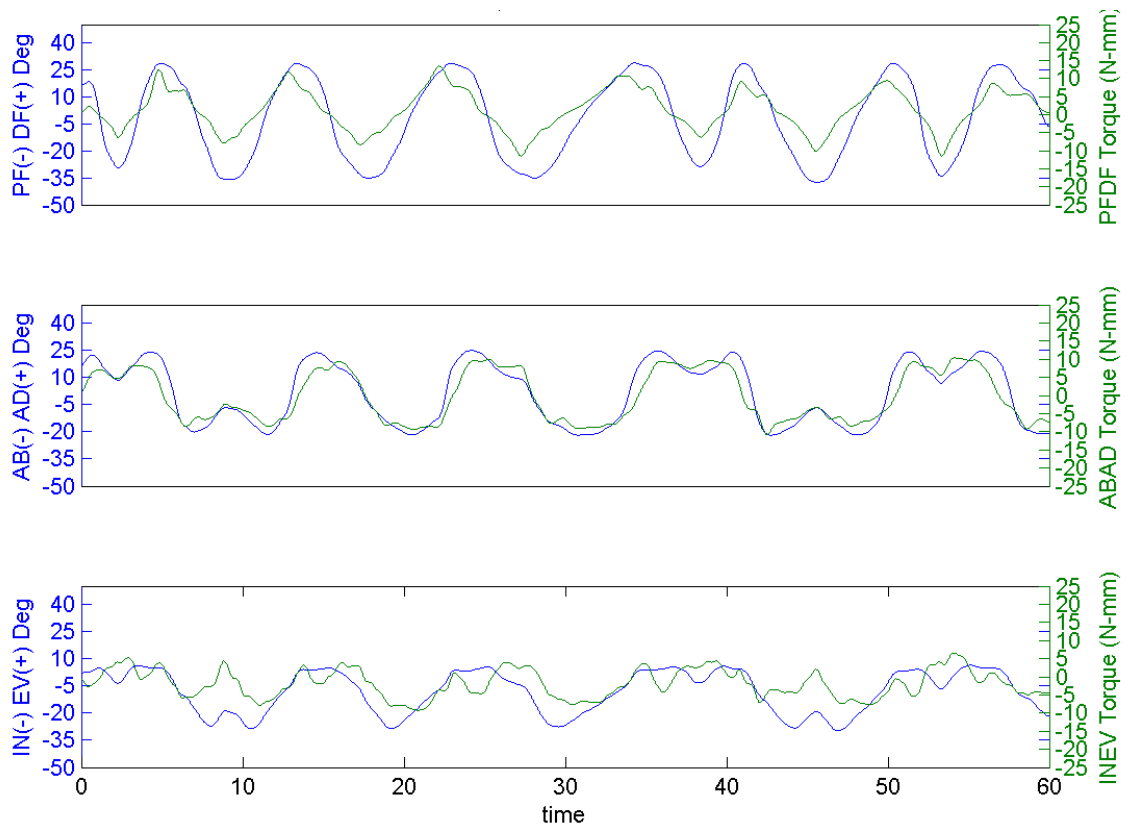


Fig. C.7: Applied motion - ABAD Torque

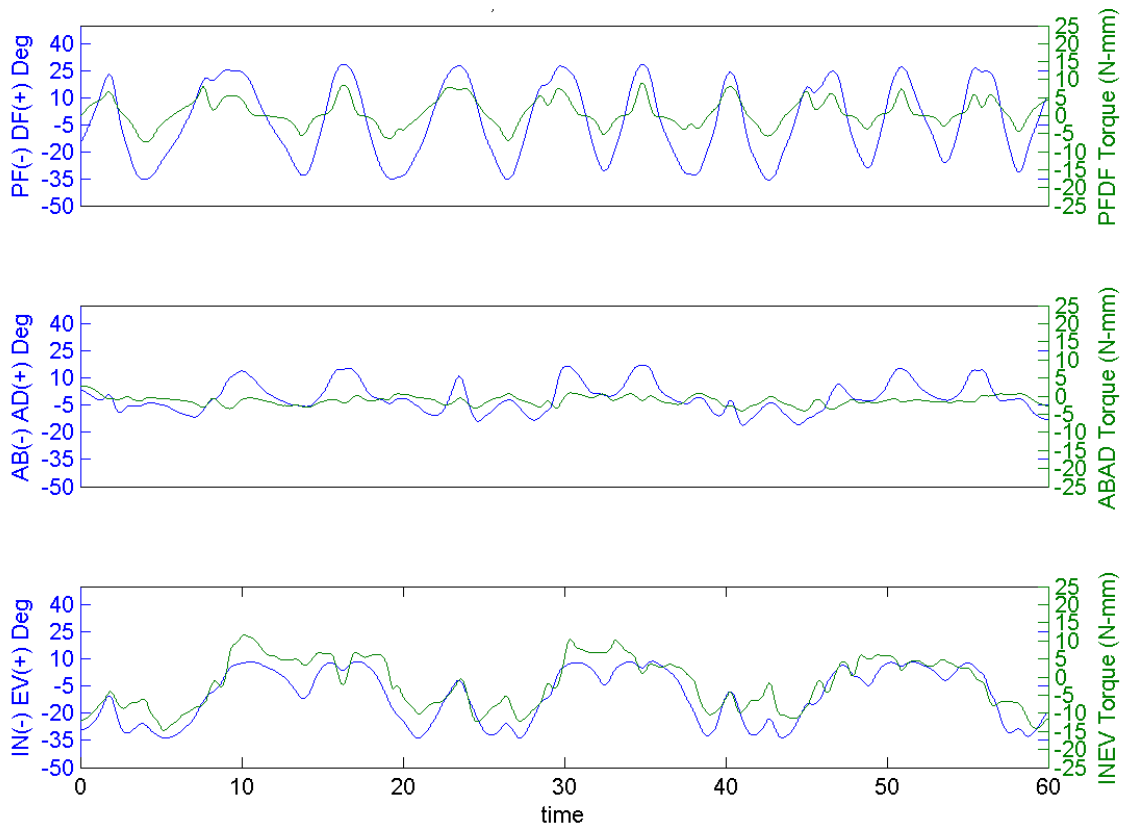


Fig. C.8: Applied motion - INEV Torque

C.3 Representative Raw Data Points and Line Fits

Each ankle listed below had a different PFDF range and had different INEV and ABAD ranges as well. For both runs shown below, an iso-torque load of 3 Nm was selected, with an applied ABAD torque load in the AJC reference view. The points are interpolated values collected from the kinematics when the torque load crossed the 3 Nm threshold. The top portion of the graph shows ABAD vs. PFDF and the bottom portion shows INEV vs. PFDF. Taken together this represents a three dimensional view of the ankle rotations. The legend to the right of the plots shows the ankles corresponding color in the graph, as well as its r-squared value which represents a goodness of fit with 1.00 being a perfect fit.

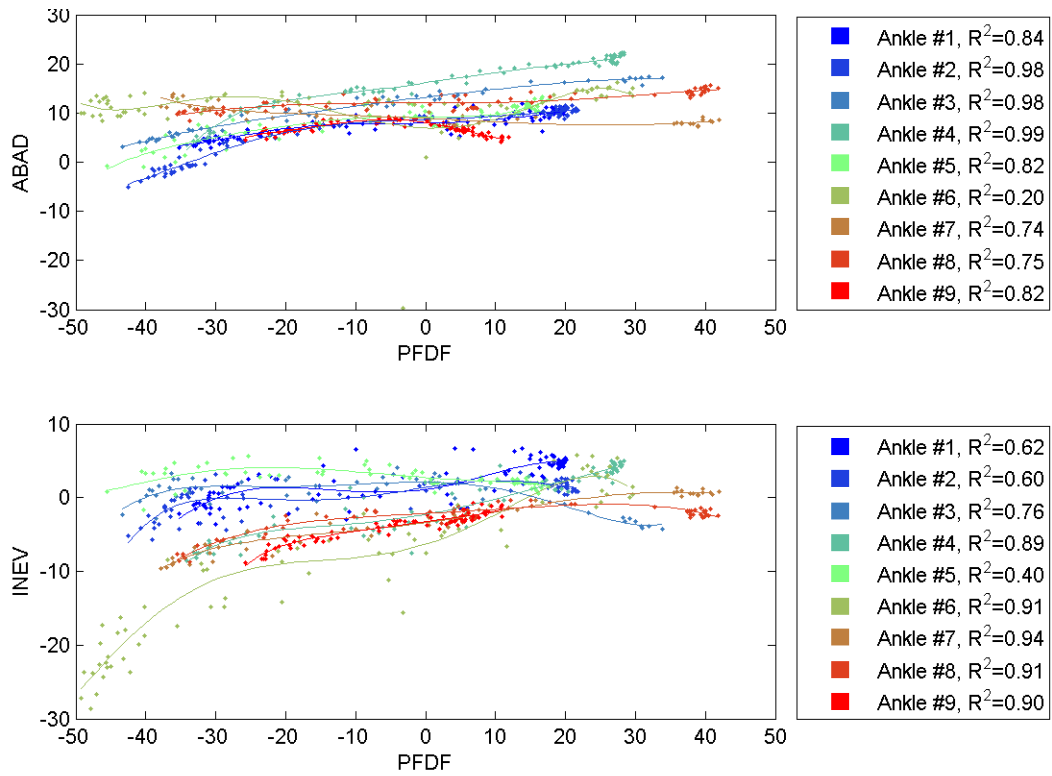


Fig. C.9: AJC view of the applied 3Nm ABAD torques to the intact ankle condition. Points and line fits vs. PFD motion. A 5'th order polynomial was used to fit each ankle in both ABAD and INEV to create continuous data sets. Applied adduction torques to the ankle with a threshold selection of 3Nm. showing a healthy intact ankle.

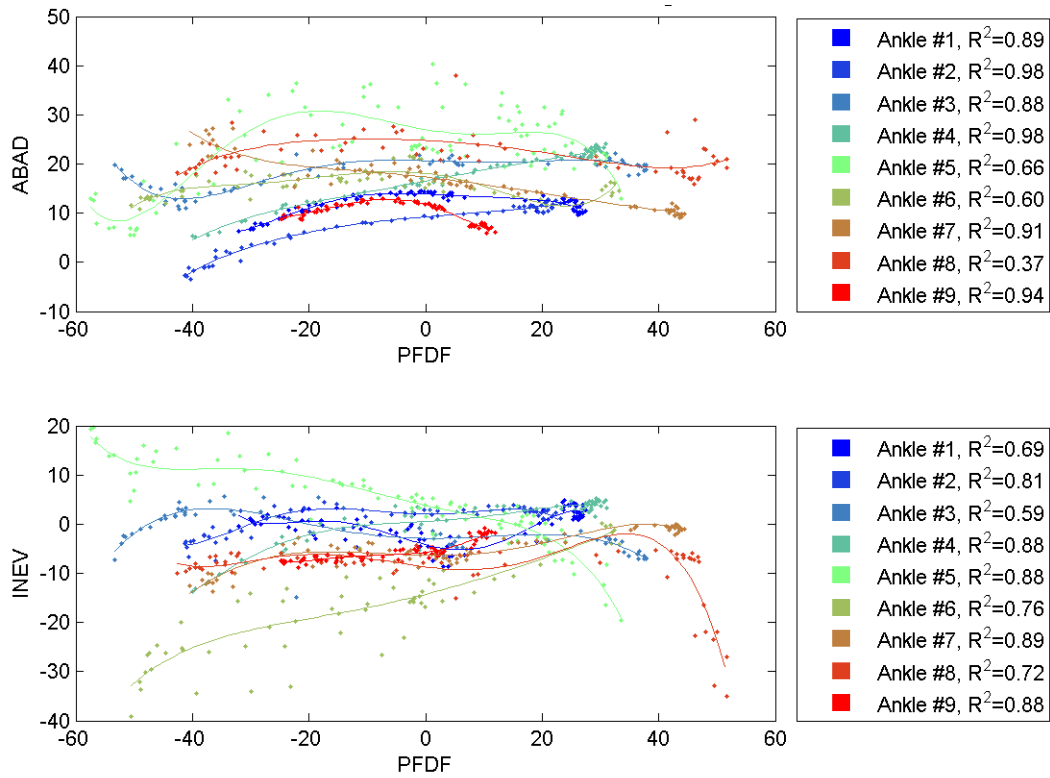


Fig. C.10: AJC view of the applied 3Nm ABAD torques to an ankle that has sustained a level 3 ankle sprain. Points and line fits vs. PFDF motion. A 5'th order polynomial was used to fit each ankle in both ABAD and INEV to create continuous data sets. Applied adduction torques to the ankle with a threshold selection of 3Nm showing the same ankle as Fig. C.1, but with a level 3 ankle sprain.

C.4 Positive and Negative Angles vs. PFDF

After the data points were collected and continuous lines were fit (section 4.1C.3), it was possible to average all the rotation information together to find average position and standard deviation at specific flexion angles. The positive and negative rotations versus PFDF for all ankles with standard deviations shown in the matching color. Blue (intact), green (sprain2), and red (sprain3). The following figures represent all three reference frames (AJC, TCJ, STJ), two torque levels (3 and 6 Nm), and both INEV and ABAD applied torque motion. The colored numbers above and below represent the number of ankles that contributed to that calculation and had data at the specified PFDF angle and torque threshold. For example in Fig. C.11A, at -40 degrees PFDF, adduction had four, four, and six ankles moving from intact to sprain3 respectively. The ankle had more range of motion with a sprain level 3 and two ankles that weren't moving that far previously shifted after the injury.

C.4.1 AJC

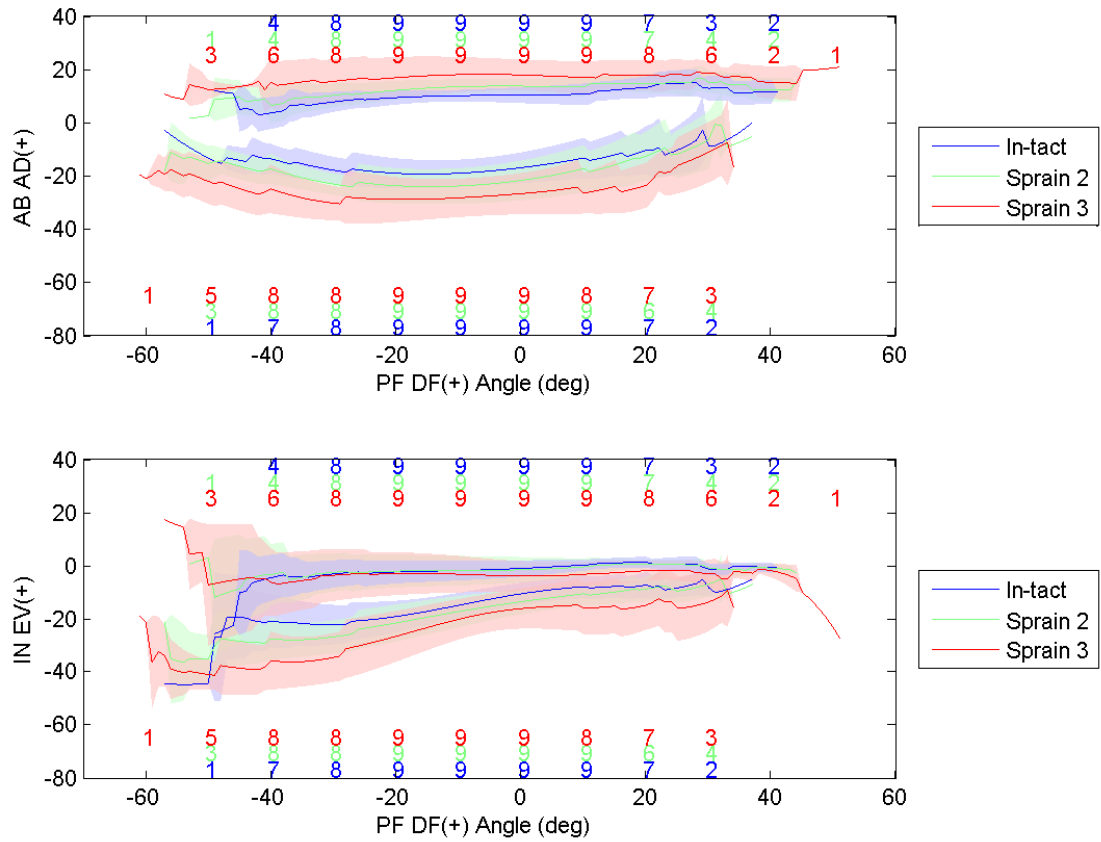


Fig. C.11: Resulting motion from 3 Nm of ABAD torque in the AJC.

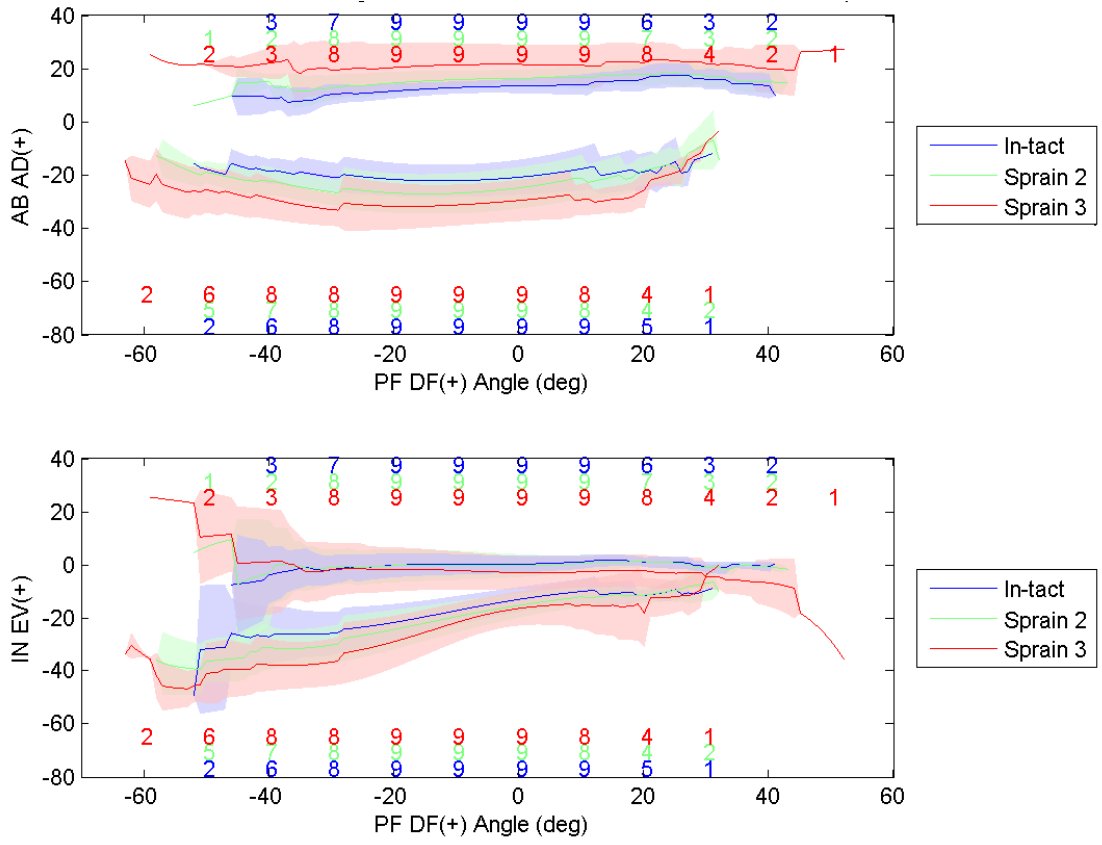


Fig. C.12: Resulting motion from 6 Nm of ABAD torque in the AJC.

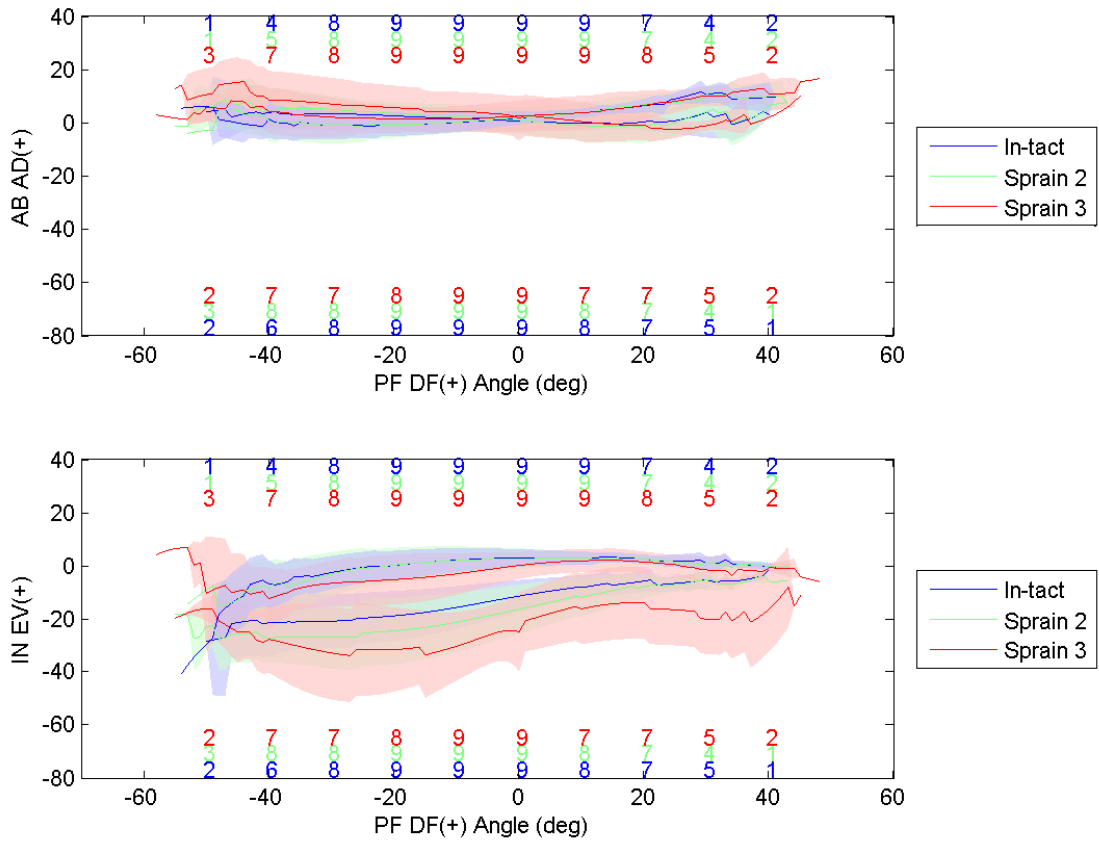


Fig. C.13: Resulting motion from 3 Nm of INEV torque in the AJC.

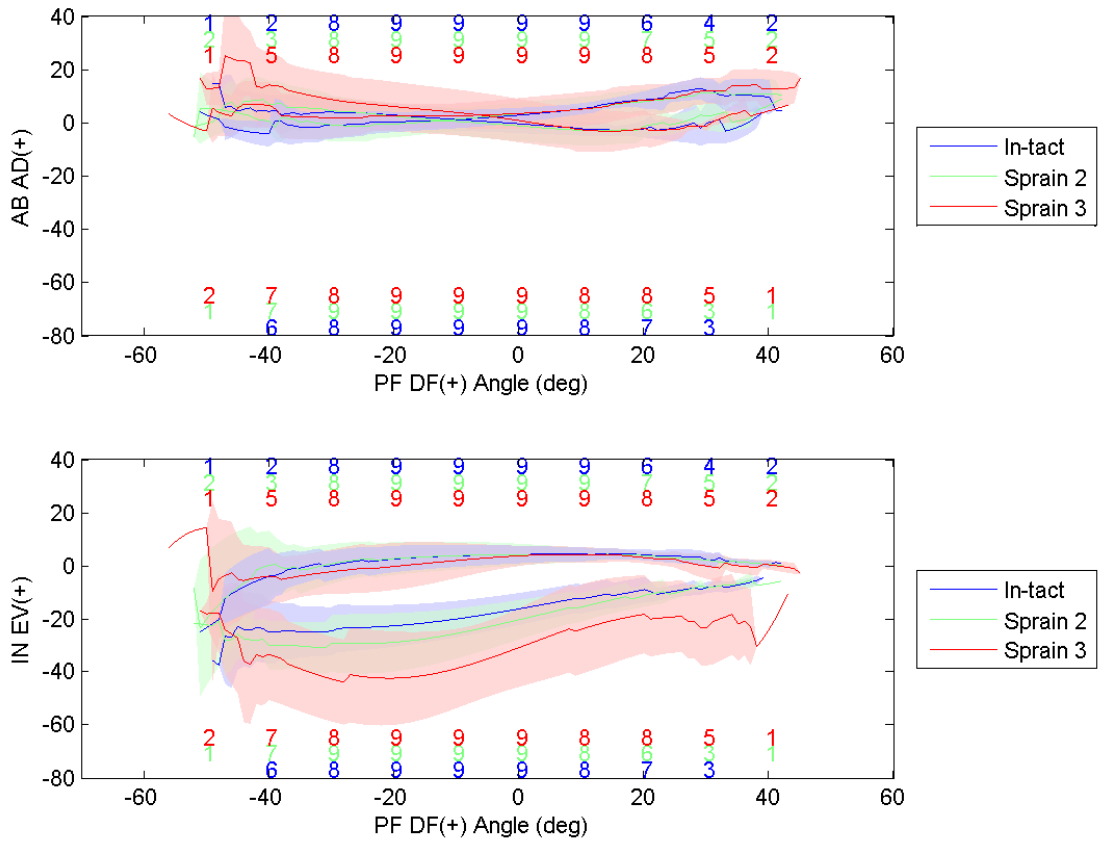


Fig. C.14: Resulting motion from 6 Nm of INEV torque in the AJC.

C.4.2 TCJ

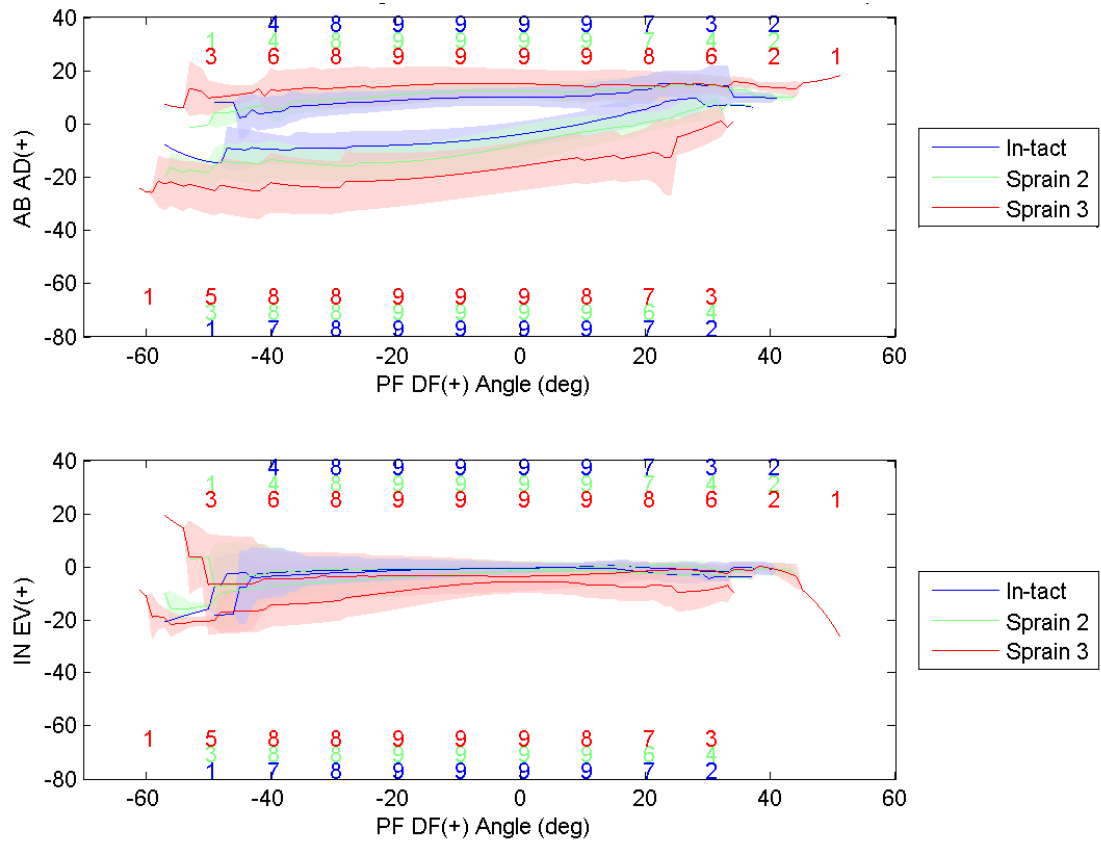


Fig. C.15: Resulting motion from 3 Nm of ABAD torque in the TCJ.

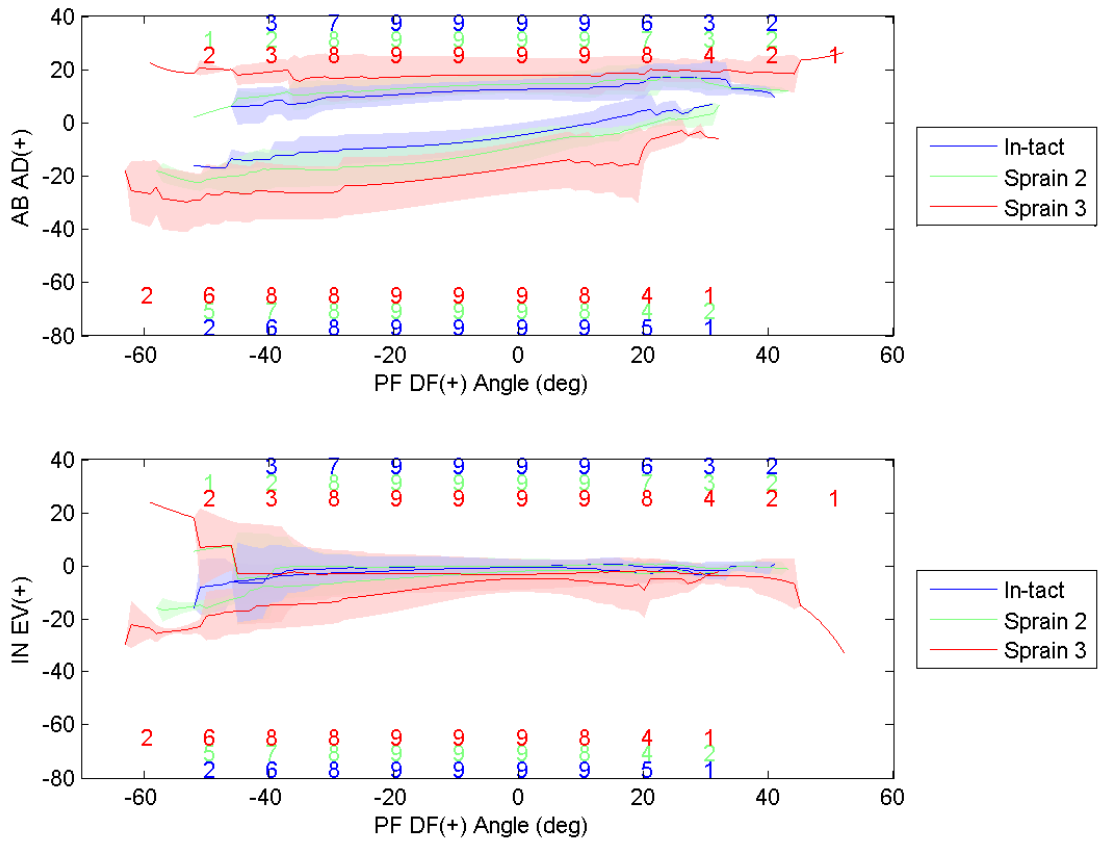


Fig. C.16: Resulting motion from 6 Nm of ABAD torque in the TCJ.

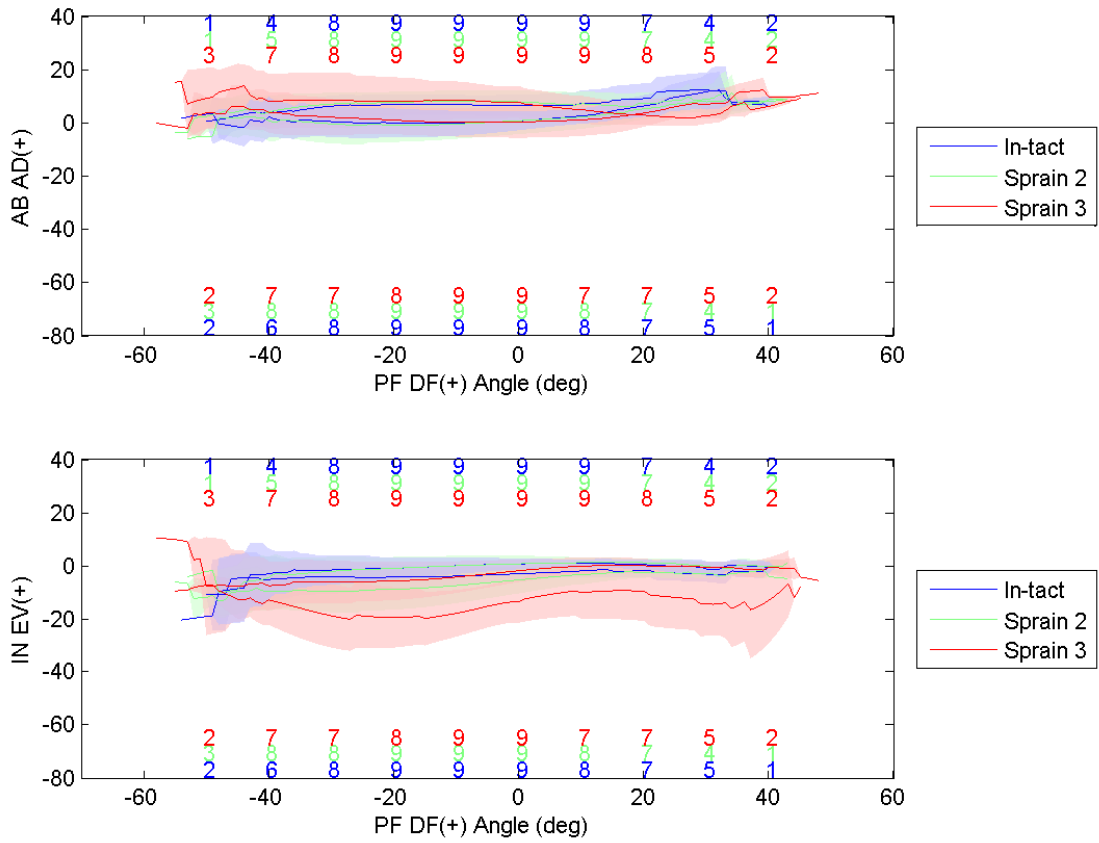


Fig. C.17: Resulting motion from 3 Nm of INEV torque in the TCJ.

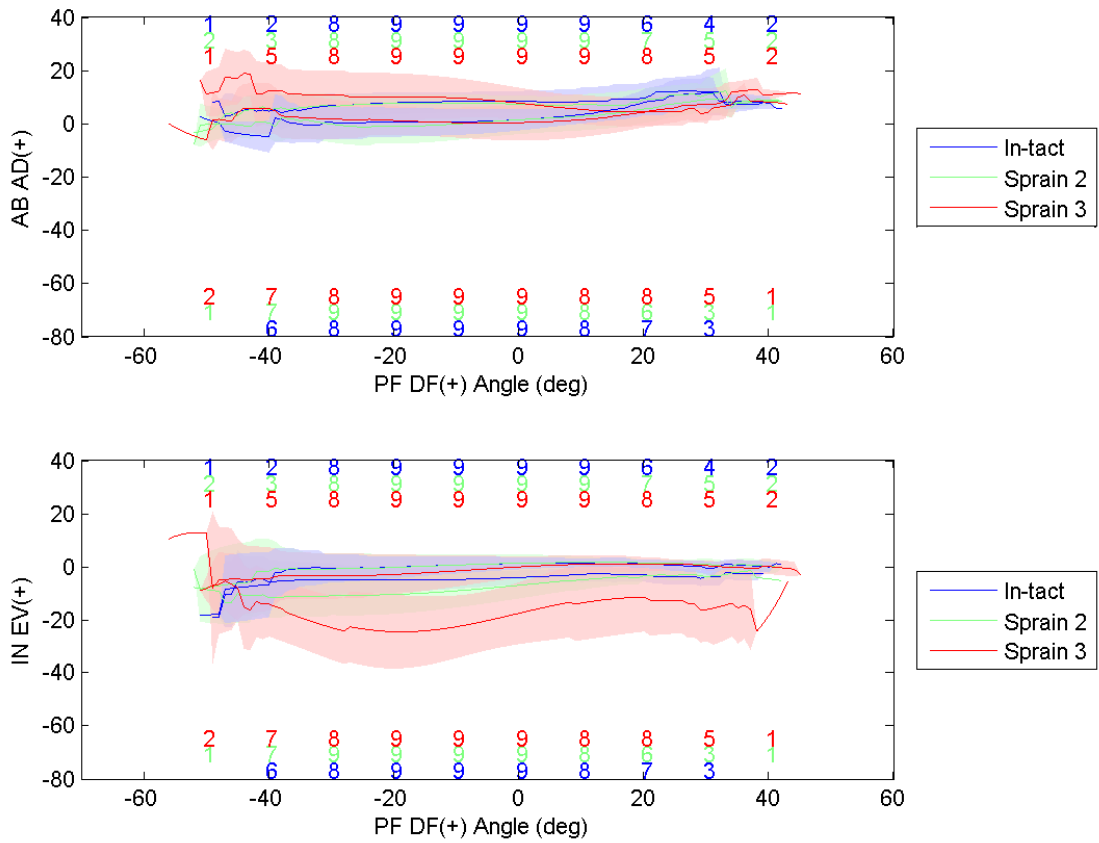


Fig. C.18: Resulting motion from 6 Nm of INEV torque in the TCJ.

C.4.3 STJ

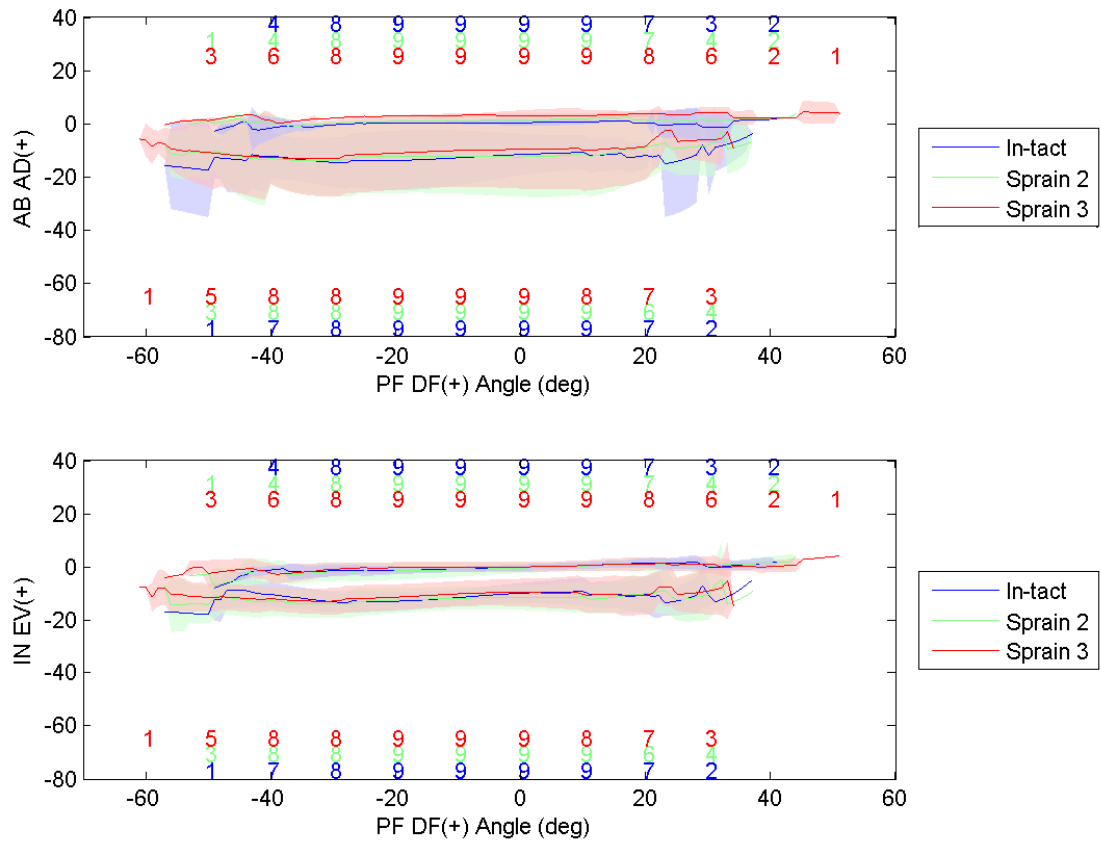


Fig. C.19: Resulting motion from 3 Nm of ABAD torque in the STJ.

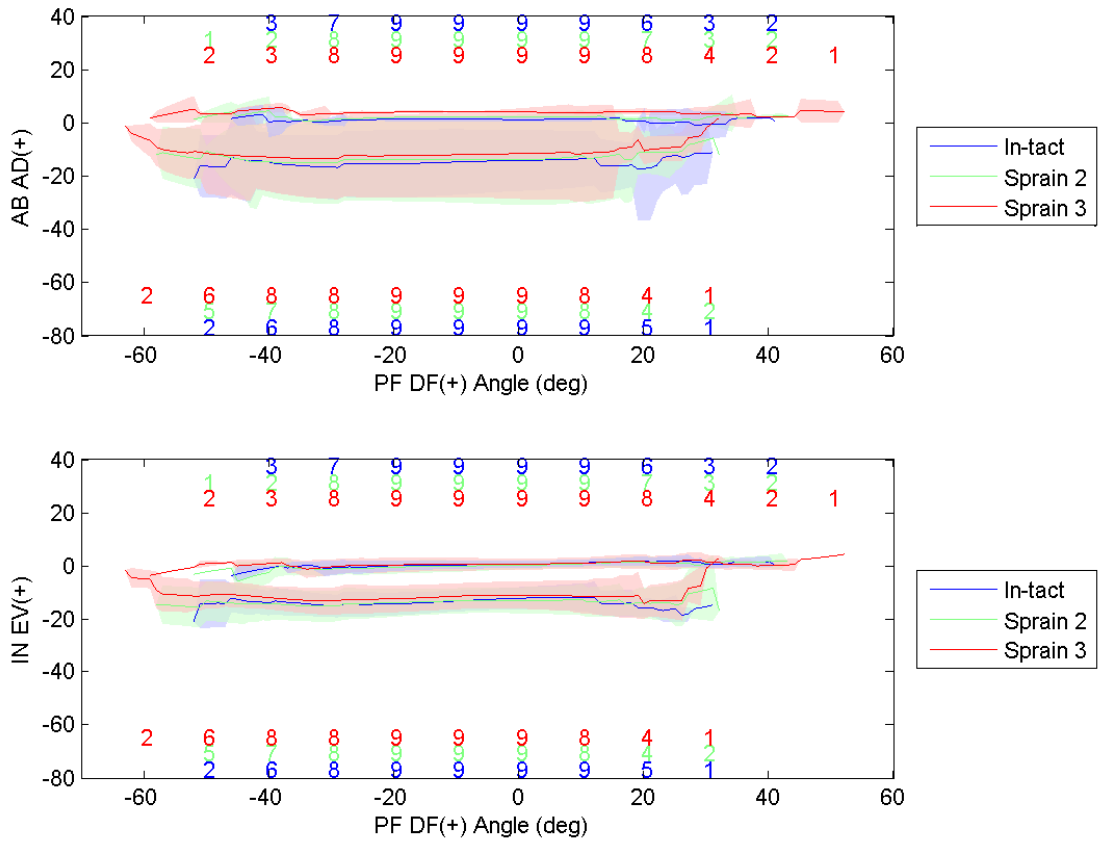


Fig. C.20: Resulting motion from 6 Nm of ABAD torque in the STJ.

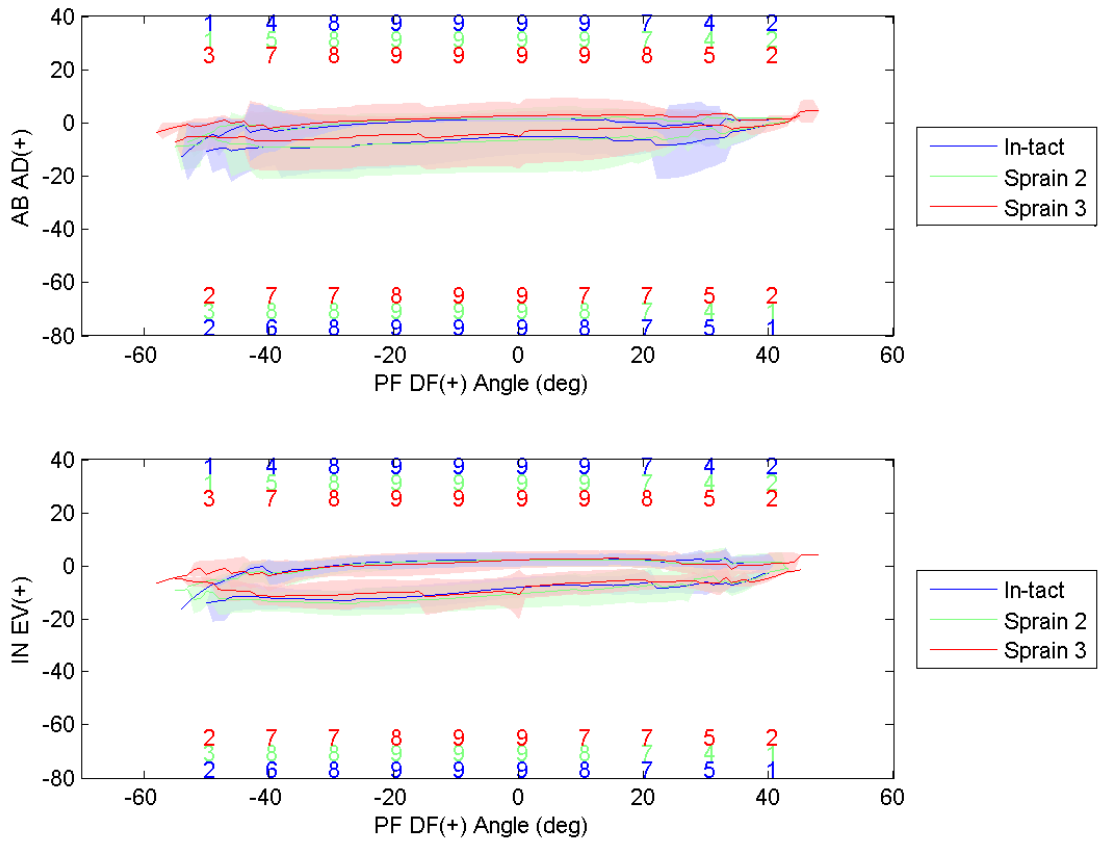


Fig. C.21: Resulting motion from 3 Nm of INEV torque in the STJ.

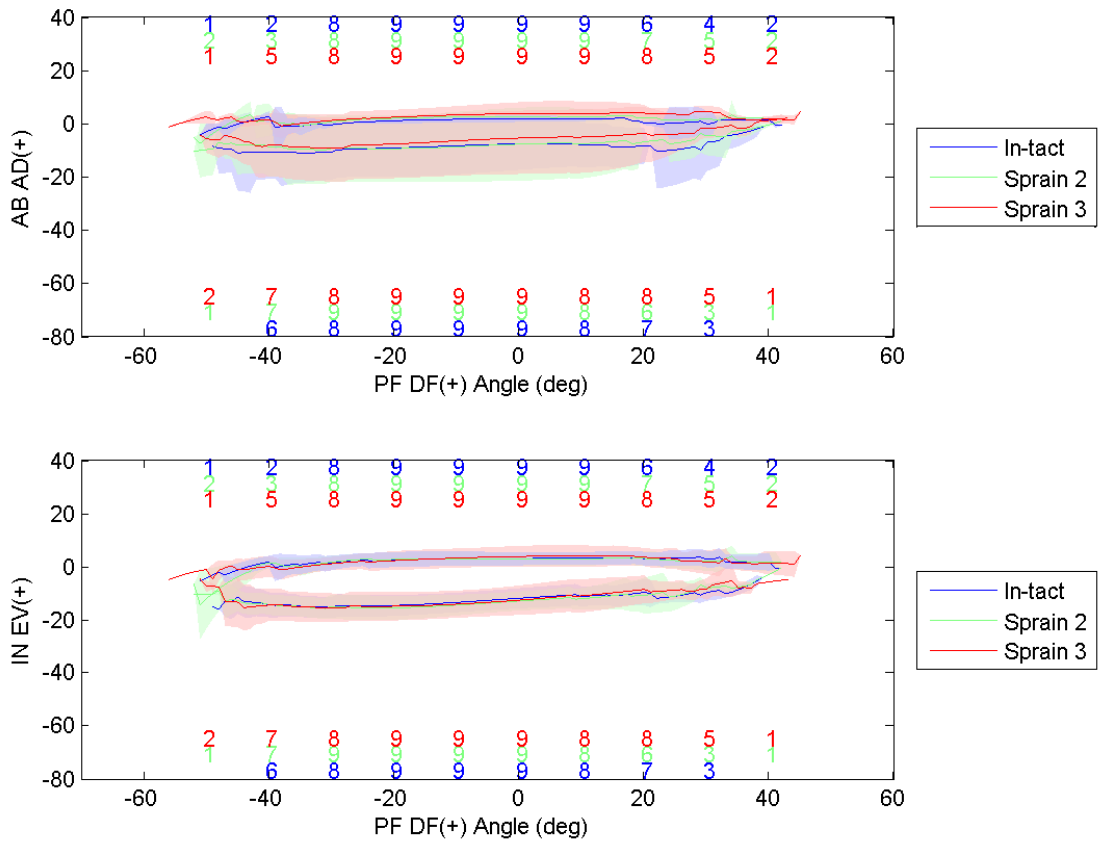


Fig. C.22: Resulting motion from 6 Nm of INEV torque in the STJ.

C.5 Range Angles vs. PFDF

The range of motion in ABAD and INEV versus PFDF for all ankles with standard deviations shown in the appropriate color. Blue (intact), green (sprain2), and red (sprain3). The colored numbers above and below represent the number of data points (ankles) that had data at the specified PFDF angle. The formatting of the following graphs is identical to that found in section 4.1C.4, but now the range is shown. The range was calculated by subtracting the negative rotation from the positive rotation. The range is good for viewing trends in the data along the flexion range.

C.5.1 AJC

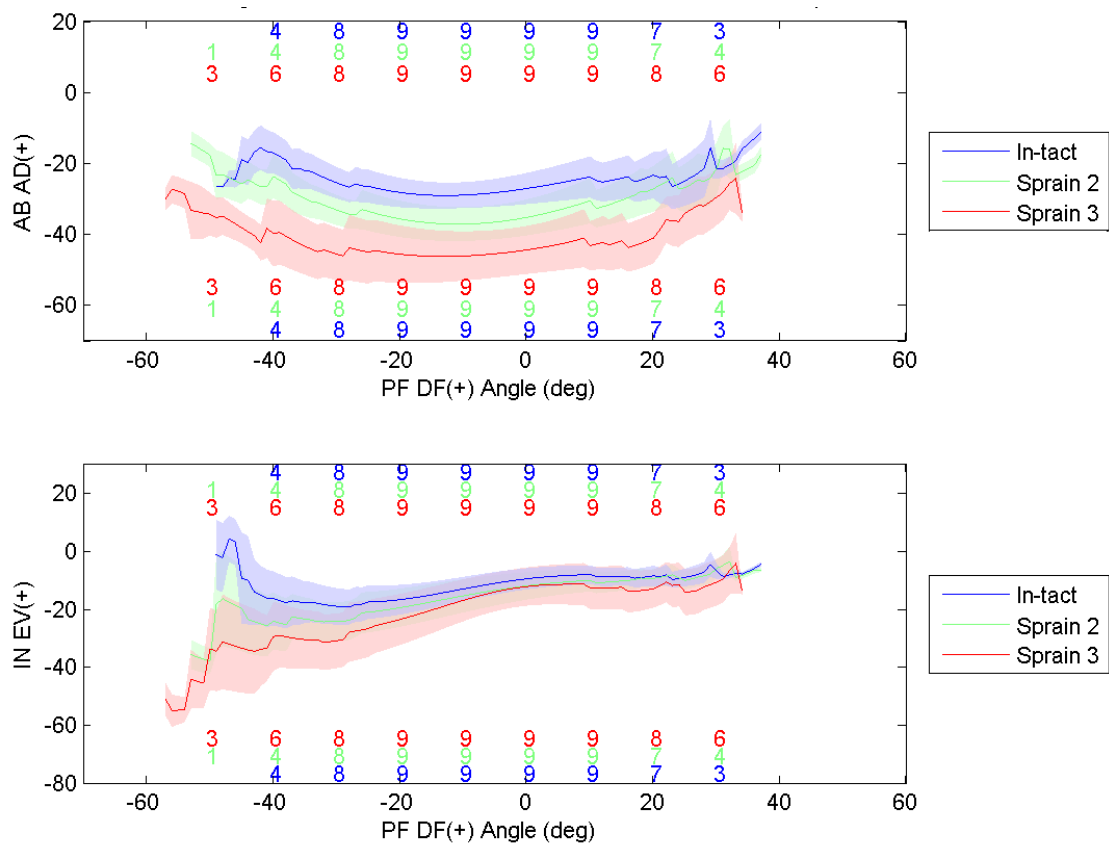


Fig. C.23: Resulting range of motion from 3 Nm ABAD torque in the AJC.

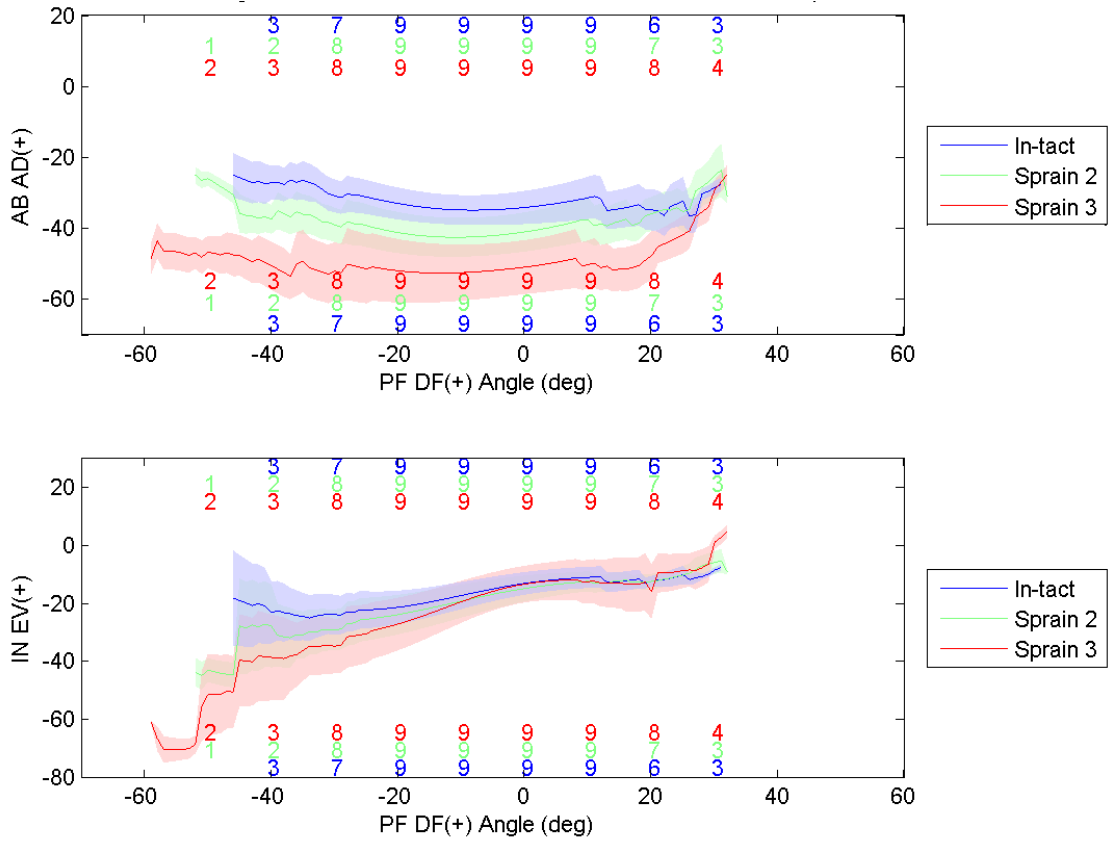


Fig. C.24: Resulting range of motion from 6 Nm ABAD torque in the AJC.

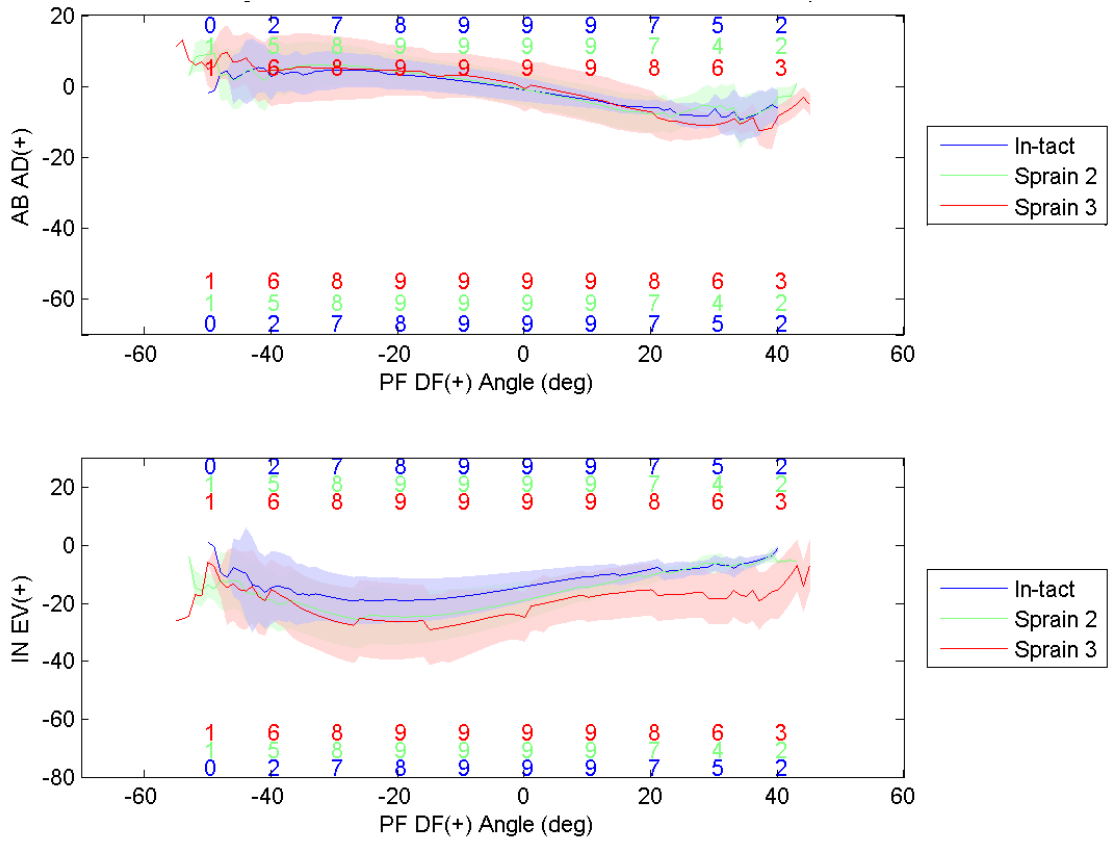


Fig. C.25: Resulting range of motion from 3 Nm INEV torque in the AJC.

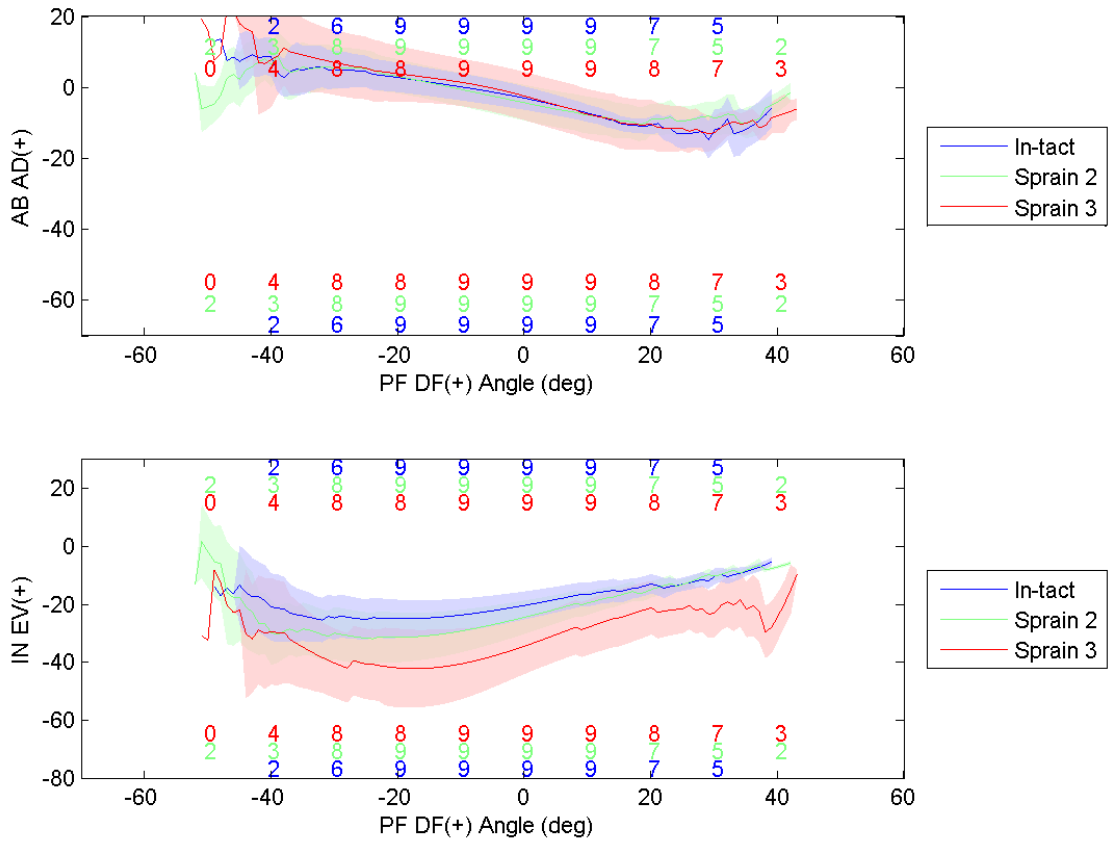


Fig. C.26: Resulting range of motion from 6 Nm INEV torque in the AJC.

C.5.2 TCJ

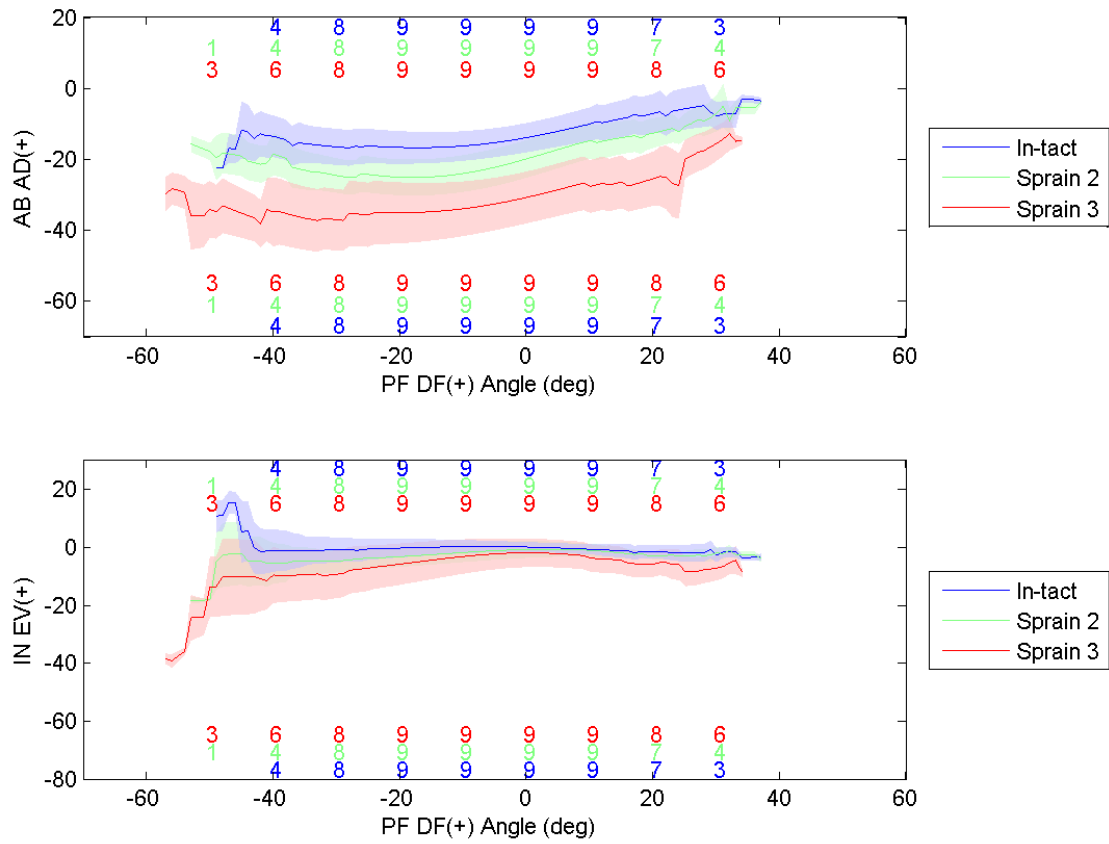


Fig. C.27: Resulting range of motion from 3 Nm ABAD torque in the TCJ.

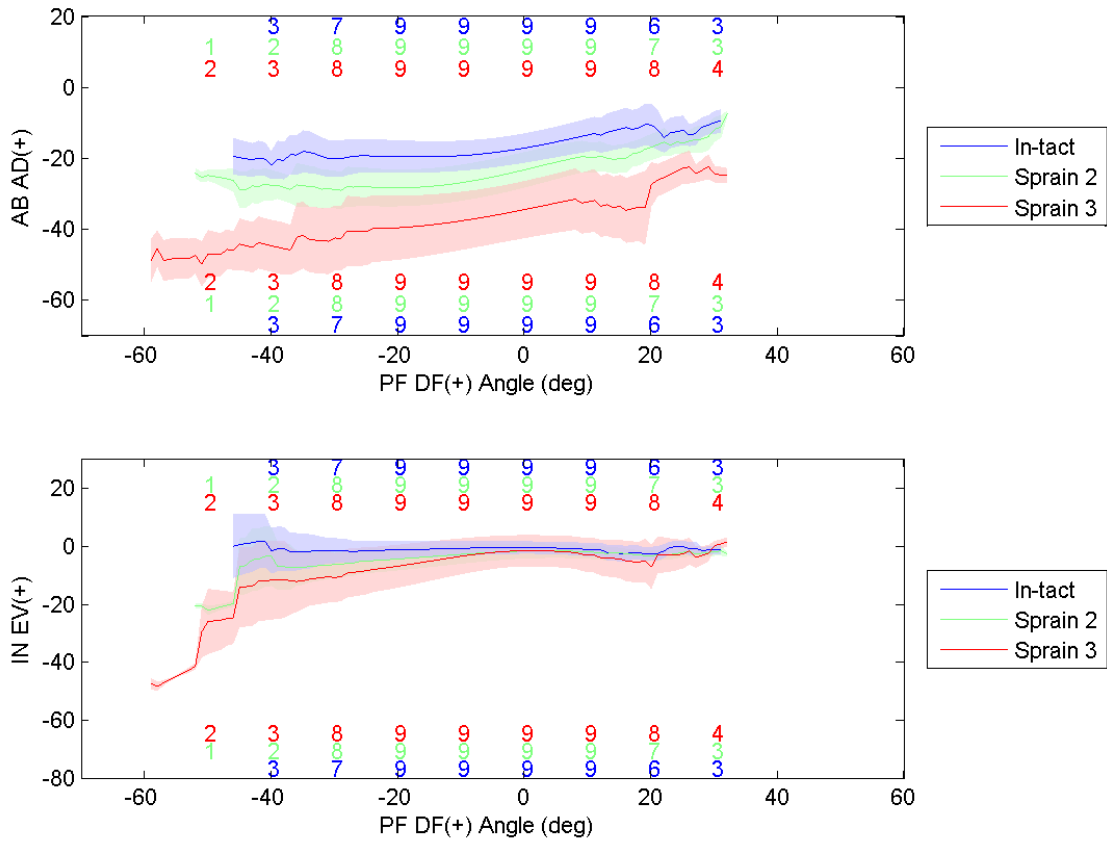


Fig. C.28: Resulting range of motion from 6 Nm ABAD torque in the TCJ.

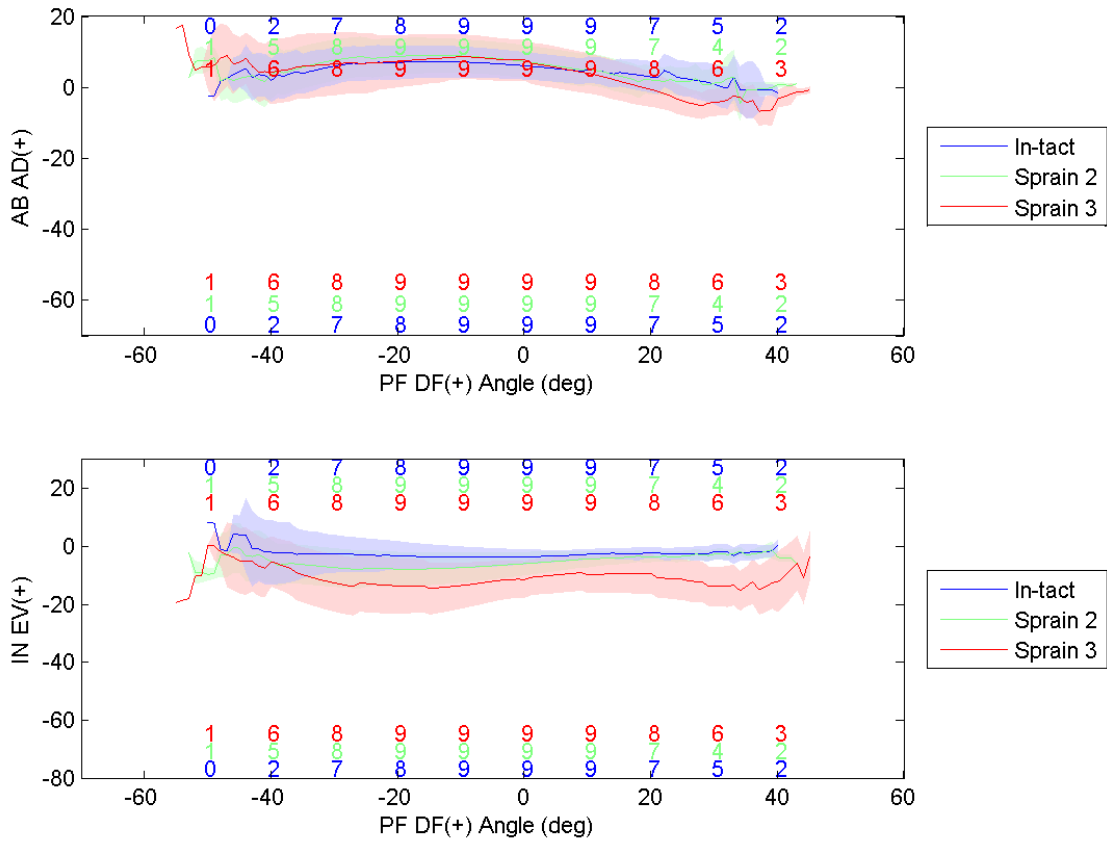


Fig. C.29: Resulting range of motion from 3 Nm INEV torque in the TCJ.

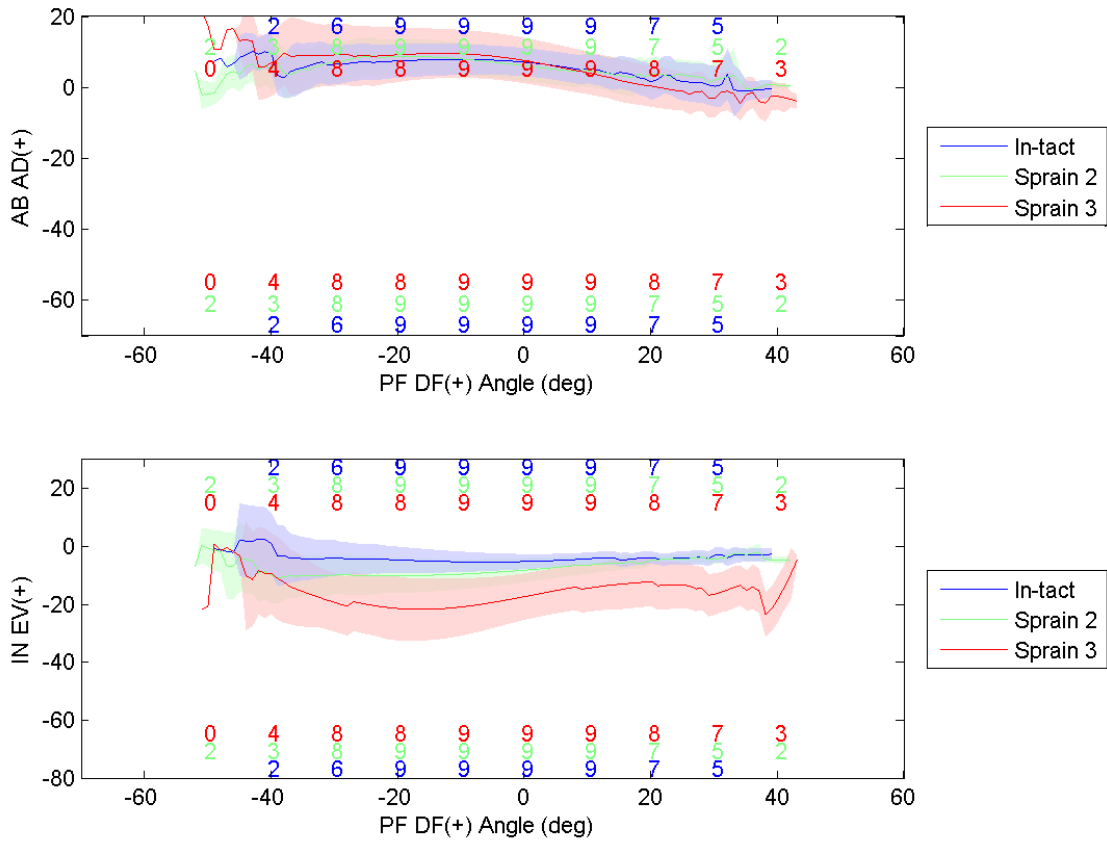


Fig. C.30: Resulting range of motion from 6 Nm INEV torque in the TCJ.

C.5.3 STJ

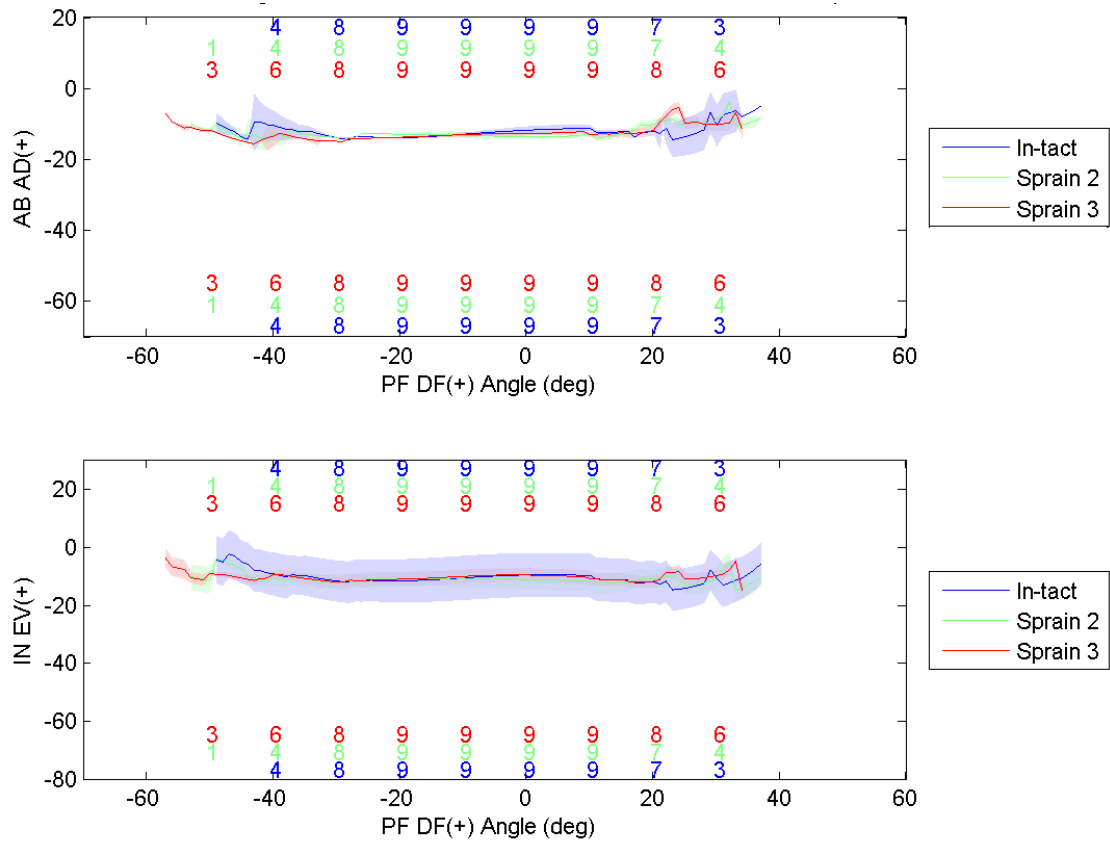


Fig. C.31: Resulting range of motion from 3 Nm ABAD torque in the STJ.

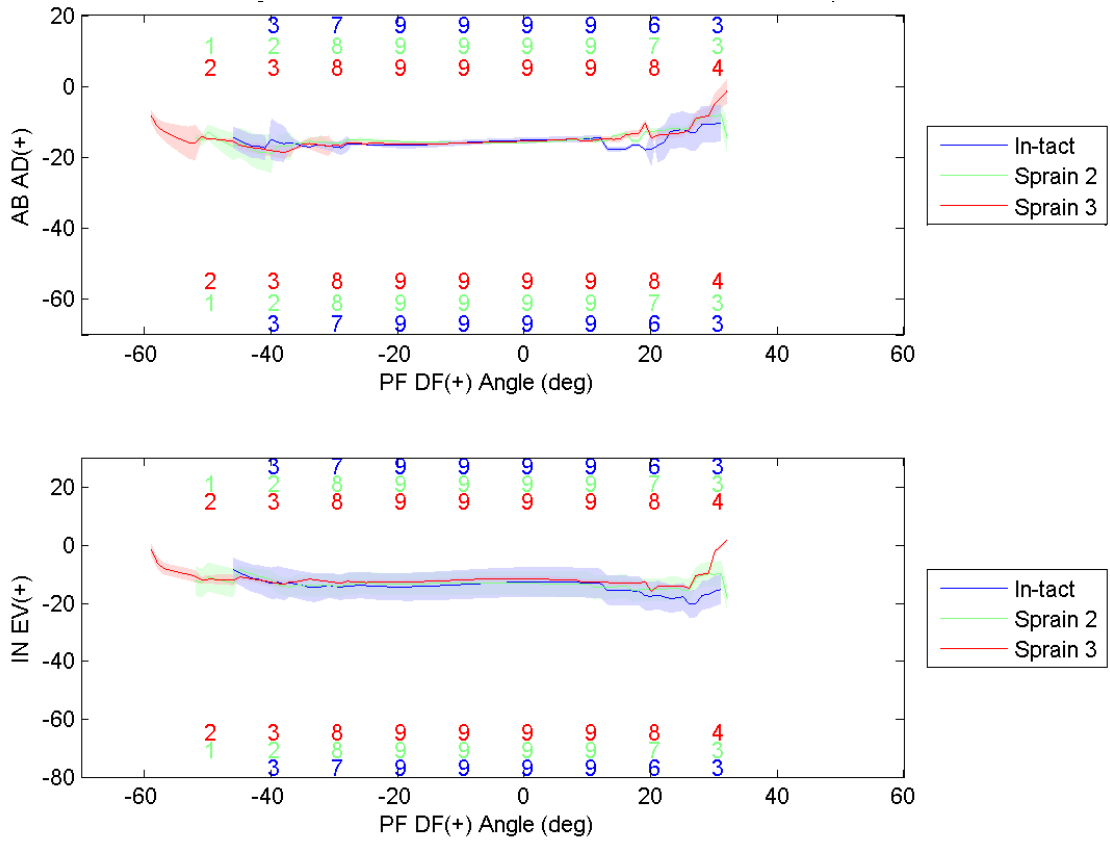


Fig. C.32: Resulting range of motion from 6 Nm ABAD torque in the STJ.

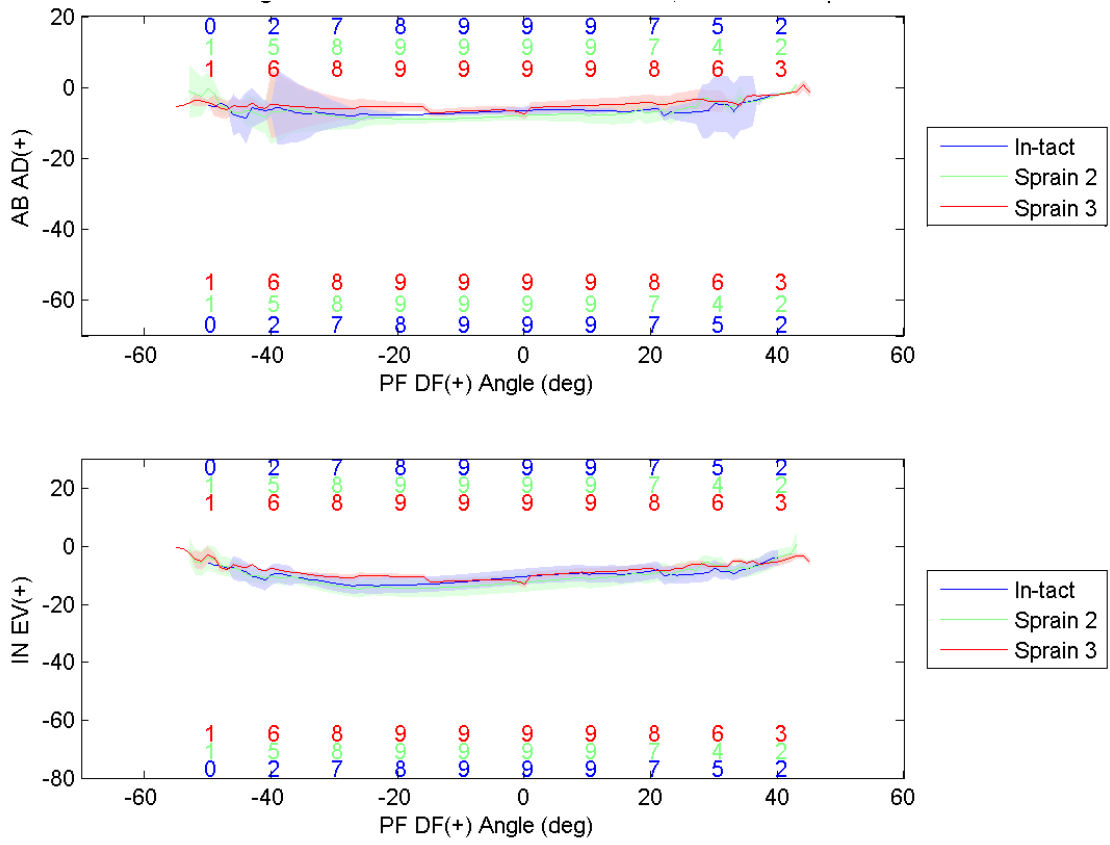


Fig. C.33: Resulting range of motion from 3 Nm INEV torque in the STJ.

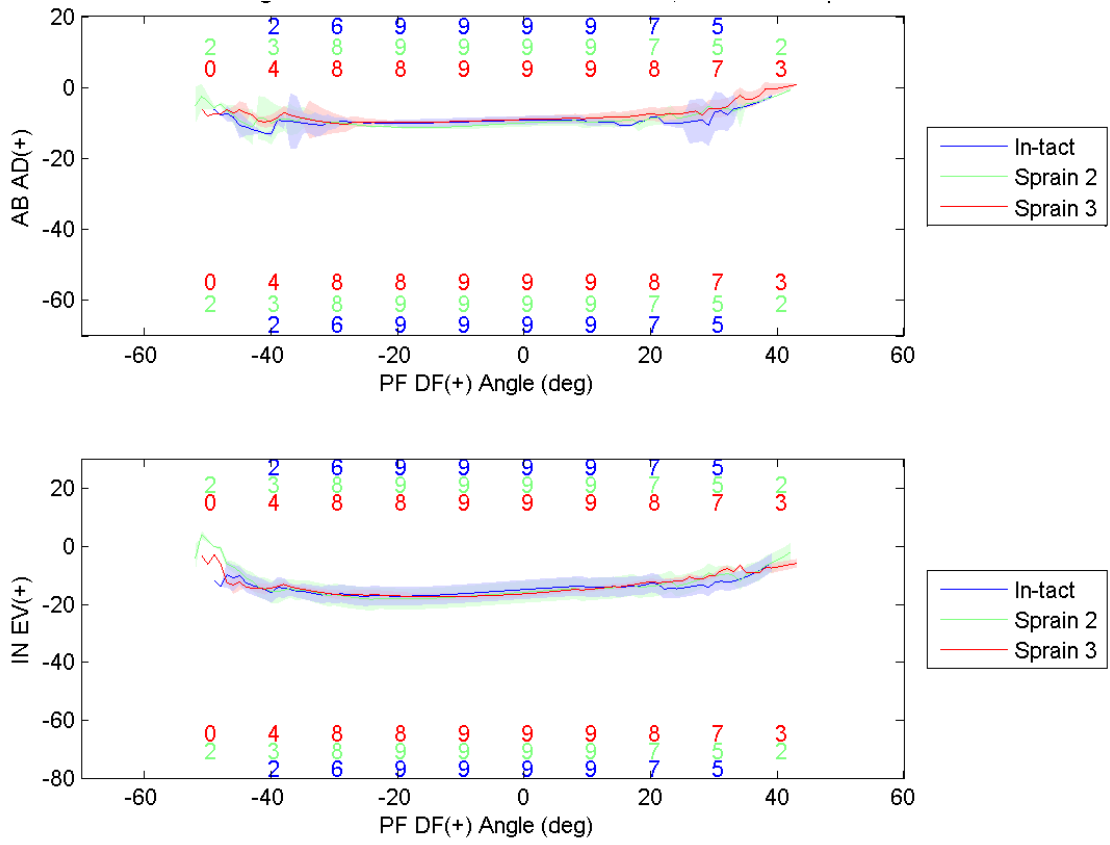


Fig. C.34: Resulting range of motion from 6 Nm INEV torque in the STJ.

C.6 Off Axis Loading

Off-axis loading is the cross talk seen when applying a torque to the ankle of either INEV or ABAD rotation. Invariably when one is applied there is some application in the other direction due to the constraint of the ankle from the ligaments. Because of this tendency there were some instances where the off-axis loading was three to five times that of the primary axis loading. What this means is that if 4Nm of ABAD torque was applied, there could be 16Nm of INEV torque and vice versa. To address this issue, a cutoff threshold was set at 1.5 times the primary axis loading, so if there were 4Nm of ABAD torque, then any corresponding INEV torque above 6Nm would be thrown out.

Off axis loading is showing two comparable sets of data (Fig. C.35; Fig. C.36). The color and size of the points are varied to show the amount of off axis loading. The size and color of the points were set such that higher values are more red and larger, but they are scaled to the data found in each set. A cutoff threshold of 0.5 times the on axis torque loading did not have enough data points to process the line fits completely. An off-axis cutoff threshold of 1.5 was chosen because it had a sufficient amount of data to generate acceptable curve fits, and the off axis loading is in the general range of the primary loading.

C.6.1 ABAD Motion

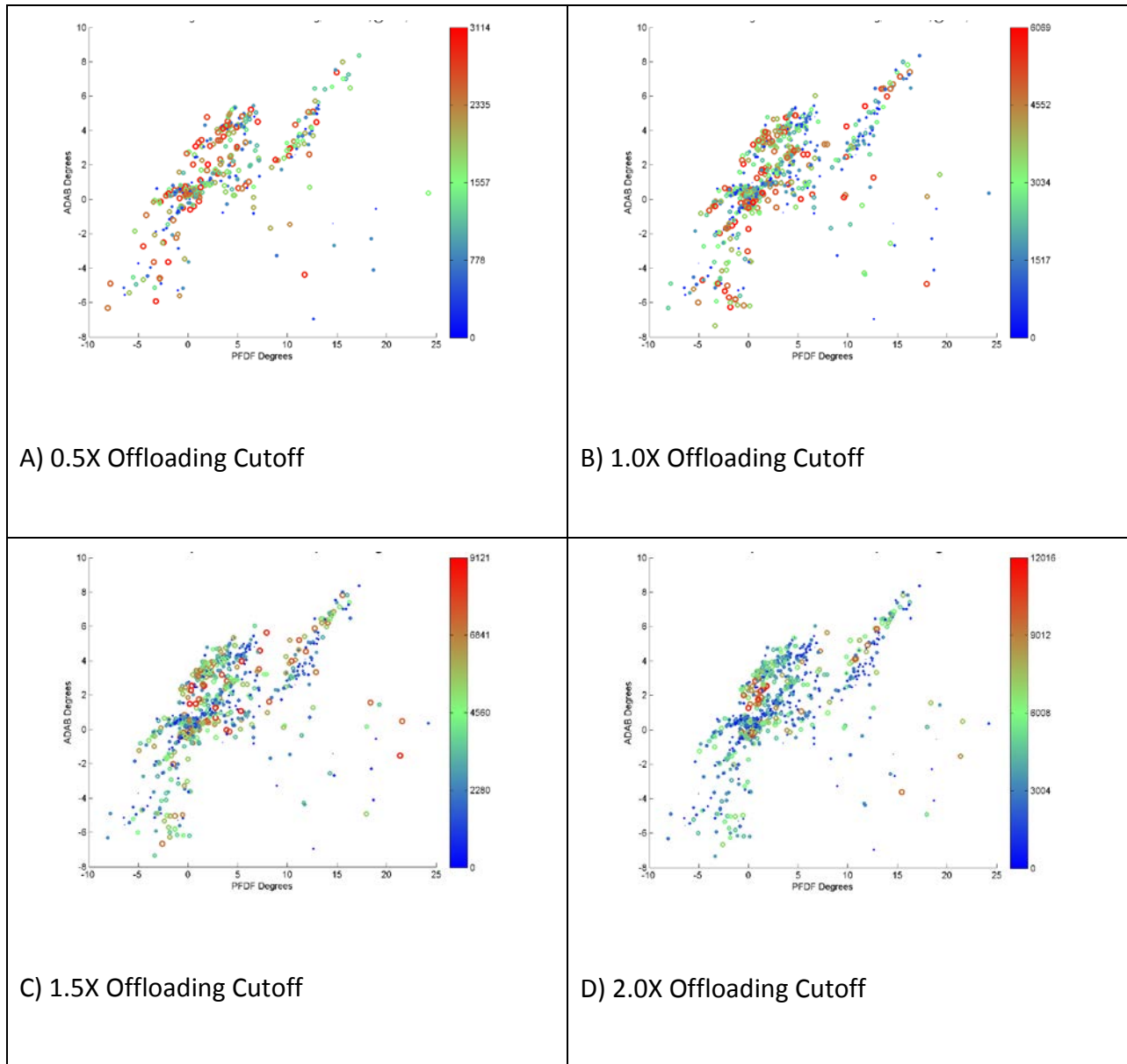


Fig. C.35: Varying levels of off-axis loading for an applied ABAD motion.

C.6.2 INEV Motion

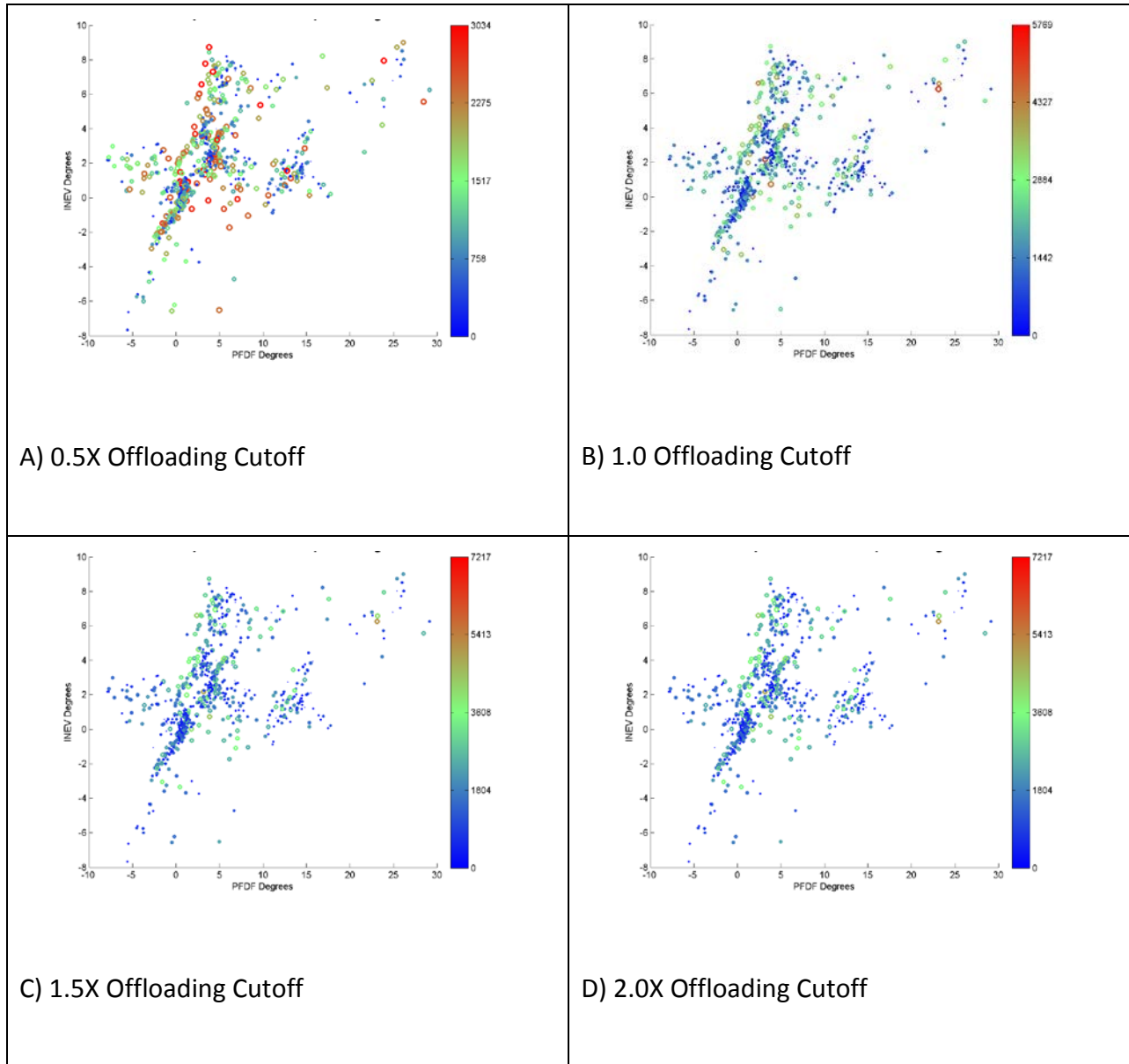


Fig. C.36: Varying levels of off-axis loading for an applied INEV torque.

Appendix D Sensitivity analysis

D.1 Neutral Position Repeatability

As a test to determine the repeatability and the reliability of the effect of the neutral position on the data, three tests were performed. In the first test the ankle was put into a neutral position 25 times, and the variations on the position recorded. In the second test a rotation matrix that perturbed the orientation was applied to the neutral position effectively adjusting the neutral position. For the third test all neutral position snapshots for each ankle were analyzed for variation during the one second of collection (100 points).

Five individuals placed the ankle independently into a neutral position to verify the repeatability and interoperator variation. For these 25 runs the average standard deviations are as follows; PFDF (0.098), ABAD (0.288), INEV (0.140). Based on these results the variation at three standard deviations of the neutral position is less than 1 degree for all rotations. The larger variation for the ABAD motion can be accounted for in the use of a bubble level which gave the orientation for PFDF, and INEV, but not ABAD. Interoperator variability between runs was acceptably small with an average standard deviation of; PFDF (0.063), ABAD (0.145), INEV (0.079).

Runs were analyzed for sensitivity to variation in the starting neutral position by varying the neutral position in PFDF, ABAD and INEV by $\pm 3^\circ$ (Fig. D.1). The two tests: ABAD w/ PFDF and INEV w/ PFDF in the Tibia-Calcaneus frame characterized a broad range of motion that is relevant to the study. PFDF orientation was completely independent of ABAD and INEV in both runs. When the ABAD axis was varied there was approximately a 1° effect on the INEV

axis while in deep PF. When the INEV axis was varied there was approximately a 1° effect on the ABAD axis as well. When the INEV axis was varied there was a pronounced degree of offsetting equal to approximately 1° from neutral and was most pronounced in deep PF. ABAD only varied by $1/2^\circ$ also in deep PF.

In the third test all neutral positions were analyzed. Each neutral position was collected as 1 second of data (100 data points for each ankle), and was analyzed for variation in average position and standard deviation for the 3 angles of motion (**Error! Reference source not found.**). The average variation was 0.004° , 0.023° and 0.016° for PFDF, ABAD, and INEV respectively across all ankles. The standard deviation across the ankles was 0.021° , 0.024° , and 0.059° . This puts the standard deviation to less than 0.2° of motion when considering three standard deviations. The range of motion for each angle varied by about 0.1° with a similar standard deviation.

D.2 Fixed CS Construction Sensitivity

To test the sensitivity of the coordinate system construction to the probed surface points that are used to define the PFDF axis, the probed points representing the surface geometry of the talus was split into 3 groups; All points, $1/2$ points randomly removed, and the remaining $1/2$ points. The number of probed points was different for each ankle, but most were in the range of approximately 500 data points. The results from calculating the FE axis shows zero variation between axes based on the points input. **Therefore the method of using the probed surface points is very repeatable, and insensitive to user variation.**

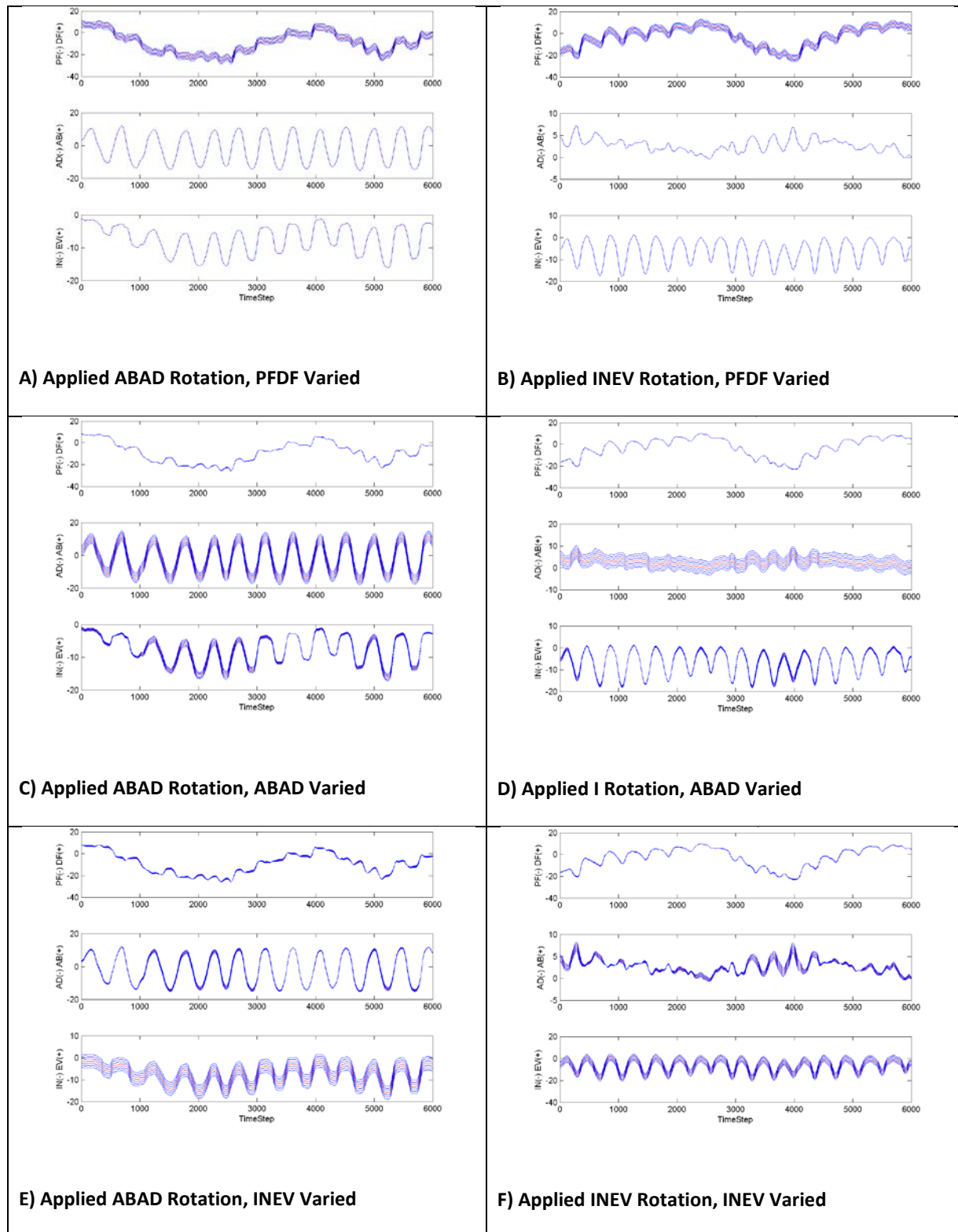


Fig. D.1: Repeatability where the neutral position was varied by +/- 3 degrees in 1 degree increments.

Tbl. D.1: Numerical results from repeatability study. Average change in orientation during neutral position was less than 0.03 degrees, while the range of motion was less than 0.10 degrees.

Ankle	Average			Std			Max			Min			Range		
	PDFD	ADAB	INEV	PDFD	ADAB	INEV	PDFD	ADAB	INEV	PDFD	ADAB	INEV	PDFD	ADAB	INEV
1	-0.035	0.026	0.035	0.028	0.052	0.082	0.005	0.103	0.189	-0.075	-0.029	-0.061	0.079	0.132	0.249
2	0.013	0.015	0.007	0.027	0.058	0.024	0.063	0.118	0.034	-0.014	-0.051	-0.029	0.077	0.170	0.063
3	0.018	0.009	-0.013	0.019	0.011	0.015	0.045	0.021	0.004	-0.001	-0.025	-0.035	0.046	0.046	0.039
4	0.010	-0.065	0.003	0.029	0.029	0.022	0.065	-0.036	0.036	-0.023	-0.122	-0.030	0.088	0.086	0.067
5	0.004	-0.055	0.069	0.019	0.035	0.029	0.031	-0.021	0.147	-0.018	-0.117	0.044	0.049	0.096	0.103
6	-0.033	-0.012	-0.024	0.109	0.077	0.073	0.219	0.116	0.103	-0.141	-0.113	-0.120	0.359	0.229	0.223
7	-0.008	0.006	0.010	0.003	0.002	0.016	0.002	0.010	0.031	-0.014	0.002	-0.010	0.016	0.008	0.041
8	-0.020	-0.034	-0.032	0.016	0.024	0.011	0.023	-0.005	-0.018	-0.039	-0.086	-0.065	0.062	0.081	0.046
9	-0.010	-0.059	0.072	0.023	0.038	0.024	0.023	-0.013	0.111	-0.050	-0.128	0.042	0.072	0.114	0.069
TotAvg	-0.004	-0.023	0.016	0.029	0.036	0.031	0.054	0.027	0.072	-0.038	-0.077	-0.024	0.091	0.104	0.096
TotStd	0.020	0.034	0.034	0.028	0.021	0.024	0.059	0.058	0.063	0.041	0.045	0.049	0.092	0.059	0.072

Appendix E Statistical Analysis

Tbl. E.1: Statistical significance of injury modes in the ankle joints based on two torque loading levels (3 and 6 Nm). A confidence interval was constructed from the comparison of group means where a significant difference in means was indicated by a 1. The comparison was done for intact (intact_N), sprain level 2 (S2_N), and sprain level 3 (S3_N), where N is the torque loading level.

	Ankle Condition		AD					AB					IN					EV				
	Mode 1	Mode 2	-10	0	10	min	max	-10	0	10	min	max	-10	0	10	min	max	-10	0	10	min	max
AIC	Intact_3	S2_3	0	0	0	0	0	0	0	0	0	0	0	0	0	0	0	0	0	0	0	0
	Intact_3	S3_3	1	1	1	1	1	1	1	1	1	0	1	1	0	1	1	1	0	0	0	0
	S2_3	S3_3	0	1	0	0	1	0	0	0	0	0	0	0	0	0	0	1	0	0	0	0
	Intact_6	S2_6	0	0	0	0	0	0	0	0	0	0	0	0	0	0	0	0	0	0	0	0
	Intact_6	S3_6	1	1	1	1	1	1	1	1	1	1	1	1	0	0	0	0	0	0	0	0
	S2_6	S3_6	0	0	1	0	0	1	1	1	1	0	1	1	0	0	0	0	0	0	0	0
TCJ	Intact_3	S2_3	0	0	0	0	0	0	0	0	0	0	0	0	0	0	0	0	0	0	0	0
	Intact_3	S3_3	1	1	1	1	1	1	1	0	1	0	1	1	0	1	1	1	1	0	0	0
	S2_3	S3_3	1	1	1	1	1	0	0	0	0	0	1	1	0	0	0	1	1	0	0	0
	Intact_6	S2_6	0	0	0	0	0	0	0	0	0	0	0	0	0	0	0	0	0	0	0	0
	Intact_6	S3_6	1	1	1	1	1	1	1	1	1	0	1	1	1	0	0	0	0	0	0	0
	S2_6	S3_6	1	1	1	1	1	1	0	0	1	0	1	1	0	0	0	0	0	0	0	0
STJ	Intact_3	S2_3	0	0	0	0	0	0	0	0	0	0	0	0	0	0	0	0	0	0	0	0
	Intact_3	S3_3	0	0	0	0	0	1	1	0	1	0	0	0	0	0	0	0	0	0	0	0
	S2_3	S3_3	0	0	0	0	0	0	0	0	0	0	0	0	0	0	0	0	0	0	0	0
	Intact_6	S2_6	0	0	0	0	0	0	0	0	0	0	0	0	0	0	0	0	0	0	0	0
	Intact_6	S3_6	0	0	0	0	0	1	1	0	1	0	0	0	0	0	0	0	0	0	0	0
	S2_6	S3_6	0	0	0	0	0	0	0	0	1	0	0	0	0	0	0	0	0	0	0	0

Appendix F Computational Programs

Abbreviations used in the coding of the program are different than the abbreviations published in the present study. The rotations of the ankle had a different notation as follows: FE - PFDf; AA - INEV; IE - ABAD

F.1 Ankle Processing, and Kinematics Transformation Builder Pseudo code

The pseudo code represented here was used to construct the processing of the kinematic output from the Optotrak and its conversion into the G&S coordinate frames.

Author: Jim West

Date: 5/7/2010

Description: This is the pseudo code for the AnkleProcessMaster function to completely process all the data from a kinematic run

Notes:

Axis Directions: AA (X Axis), IE (Y Axis), FE (Z Axis)

Units: Forces (N), Moments (N-mm), Distances (mm)

AnkleProcessMaster Pseudocode

```
    Define Variables
    Setup Data Paths
    If 'ankle.mat' exists then load data file
    Else
        Load the excel spreadsheets to determine the trials to run, and their names
        (fcn_processExcelSheet)
            Find the name of the ankle being processed
            Import the data sheet files
            Determine if the ankle is left or right
            Determine whether the probed maleolus points are in the tibia or the calcaneus
frame
            Determine if/where a reprobing has been done
            Create a name for each run
            Determine the new cycles to run based on the filtering done above and the trial
runs that are listed as "Not good".
            Select the run type for each run
            Setup paths to structure directories
            Load RB numbering sequence
            Determine where the neutral position data is and build a Neutral Position Transformation
            Load the probed point data (fcn_loadProbePointData)
            Generate Fixed Coordinate System for Each Bone
                Find the ankle center and axis using a sphere fit to the talus-tibia domes with
an optimization for a cylinder fit
                Transformation for Tibia, Talus, and Calcaneus
                This will have the UnitVector Directions and the Center of each bone
            Loop
                Process Probed Points if first run, or determine if new probed points are
required (fcn_loadProbePoints)
                    If required, load and replace old probed points file with new one
                    Read in file for kinematic and force data and convert if necessary to SI (N-mm)
                    Stretch the force data to fit the kinematic data (fcn_fitForceData)
                    Interpolate force data linearly to fit
                    Filter the force data
                Determine if there are missing data (NaN values) in the sets and filter them out
(fcn_removeNaNValues)
                Determine if Force Jumper was set incorrectly, if so:
```

```

        If not set correctly run the scaling script fcn_rescaleForceData to fix
the data.
        Translate and Rotate the force data to the ankle joint (fcn_lcForceConverter)
        Rotate 45 degrees about LCz axis and move to known LC transformation
position (fcn_LCtransformAJC)
        create transformation from LC --> Tibia
        Transform the forces
        Transform the torques and add the forceTorques
        Output fDataMoved
(fcn_removeHysteresis2) Remove Hysteresis from Pure IE, AA, FE, IE w FE, and AA w FE runs
        by generating a logical index
        Apply Hysteresis index to Kinematic and Force Data runs (fcn_logIndexArray)
        Output fDataHystRem and kDataHystRem
        Process G&S Transformations between each of the three bones
        Cal rel Tib; Tal rel Tib; Cal rel Tal
    End Loop
    Save Output as 'ankle.mat'
Endif

```

F.2 Ankle Processing, and Kinematics Transformation Builder Matlab Code

This is the code that corresponds to the Pseudocode above. It is broken up into several functions that work together to output the final product.

F.2.1 APM.m

This initializes the paths directory, verifies that data is where it should be, and clears all data. After this has been run, then fcn_ankleProcessMasterLoadData is called to load and crunch the data set.

```

%{
The master program:
1. Loads Ankle Data
2. Manipulates Ankle Data
3. Saves Ankle Data as a New Data Set
4. Performs any required output
%}

%% Clear all Variables
clear ankle

%% Setup Paths and Load the Data
AnkleInitPaths; %Initialize paths to different function directories.
% ankle.path = uigetdir('C:\Users\yuanchueh\Documents\School\Biomechanics Lab (Research
Project)\AnkleData\Data\', 'Select the ankle to process');
% ankle.path = 'C:\Users\yuanchueh\Documents\School\Biomechanics Lab (Research
Project)\AnkleData\Data\6-17-2010_BB18';
% ankle.path = 'C:\Users\yuanchueh\Documents\School\Biomechanics Lab (Research
Project)\AnkleData\Data\4-14-2010_BBUnknown';
% ankle.path = 'C:\Users\yuanchueh\Documents\School\Biomechanics Lab (Research Project)\AnkleData\5-
05-2010_BB22';

dataPath = 'C:\Users\yuanchueh\Documents\School\Biomechanics Lab (Research Project)\AnkleData\Data';
cd(dataPath);

```

```

dirStructure = dir; %Creates a list of all the files in the current directory
dirStructure(1) = []; dirStructure(1) = []; %Removes the '.' and the '..' from the directory list.

if strcmp(dirStructure(length(dirStructure)).name, 'Figures')
    dirStructure(length(dirStructure)) = []; %Remove the figures directory
end
if strcmp(dirStructure(length(dirStructure)).name, 'AllAnklesForGraphing.mat')
    dirStructure(length(dirStructure)) = []; %Remove the figures directory
end

for i = 1:length(dirStructure)
    cd([dataPath, '\', dirStructure(i).name, '\']);
    if exist('ankle.mat','file') == 2
        display('This Ankle Is Already Loaded');
    else
        display(['Loading Ankle: ', dirStructure(i).name]);
        fcn_ankleProcessMasterLoadData([dataPath, '\', dirStructure(i).name]);
    end
end
end

```

F.2.2 *fcn_AnkleProcessMasterLoadData.m*

This is function performs the heavy processing of the data. It takes all the raw input data, and prepares it for processing. After processing it is saved to an output file called ankle.mat. Each specimen has its own .mat file.

```

function [ankle] = fcn_ankleProcessMasterLoadData(anklepath)
%% This is the master code file that will import and process ankle data
%{
By Jim West
Notes on Data:
    Optotrak Kinematic Marker Output: mm
    Force Sensor Output: lbs, in-lbs

Version 0.1, 2/3/2010
    Import and process basic data
    Added variables
Version 0.2 2/7/2010
    Graph probe points for visualization purposes
    Setup coordinate system version 1 for tibia, calcaneus and talus

Version 0.3 2/8/2010
    Full processing to the G&S function is complete, and full output graphs
    are created in both 2D and 3D for analysis
    It is not clear at this point whether the directions of all the vectors
    are correct or not. This will need to be addressed

Version 0.4 2/9/2010
    Added coordinate transformation code to view the probed points overlaid
    on each other.

Version 0.5 3/20/2010
    Updated code to new standards now that I know what I'm probing.

Version 0.6 4/19/2010
    Added code to output a concave object mesh for use in 3dsmax
    Cleaned up path coding. Added some new functions to clean up the main
    process
    fcn_initializeData to initialize the program
    fcn_PlotProbedPoints was added to plot the points in a subplot

```

fcn_PP2RB has been streamlined to work with both the GUI and this program.

Version 0.7 4/25/2010

Streamlined the loading operation to search for a processed ankle.mat file. If it exists it is loaded, otherwise the raw data is processed and a processed ankle.mat is saved to the folder for future use.

Version 0.8 5/7/2010

Revising program to be more streamlined and to follow the pseudocode path so that future revisions will be easier to control.

Version 0.9 5/16/2010

Complete work on repathing the functions and layout. The loading process is streamlined, and intuitive. Added the ability to reprobe during testing, and have the process load the next probed set for the upcoming data
Load, linearly interpolate, and filter the force data
All that is left now is to determine the best method of finding the ankle center

Version 1.0 6/29/2010

Final version of Ankle Process Master which has been converted to a function to accept the ankle path and load the data file. This was done so that work could be done on manipulating the data in future functions.

Version 1.1 7/29/2010

Combined the fcn_ankleProcessMasterPhase2Changes with this one to create one file that performs all all necessary processing. All thats left is to calculate the G&S angles and displacements

```

%}
%% Define Variables
    global lineWidth;
    global fontSize;
        lineWidth = 2;
        fontSize = 20;

    AnkleInitPaths; %Initialize paths to different function directories.
    distBetweenPoints = 25; %Used for hysteresis checking...This is the distance between consecutive x
points on the force data to require before a new peak is counted.

    ankle.probePointsDir = 1; %This is the probed point directory to use, based on the amount of reprobng
that was required during trials.
    ankle.fData = cell(1); %Cell to store the force data
    ankle.kData = cell(1); %Cell to store the kinematic data
%    ankle.gsData = cell(1,length(ankle.kData));%Initialize the cell array

%% Setup Paths and Load the Data
%    ankle.path = uigetdir(cd, 'Select the ankle to process');
%    ankle.path = 'C:\Users\yuanchueh\Documents\School\Biomechanics Lab (Research Project)\AnkleData\4-
30-2010_BB19';
%        ankle.path = 'C:\Users\yuanchueh\Documents\School\Biomechanics Lab (Research
Project)\AnkleData\Data\4-14-2010_BBUnknown';
%    ankle.path = 'C:\Users\yuanchueh\Documents\School\Biomechanics Lab
(Research Project)\AnkleData\5-05-2010_BB22';
    ankle.path = anklepath; clear anklepath;
    cd(ankle.path);
    %Test to see if the ankle.mat file exists and loads the data depending
    %on its existence. If it doesn't exist the data must be processed from
    %scratch.

    if exist([ankle.path '\ankle.mat'],'file') == 2 %If the file exists then load it.
        tic
        load('ankle.mat'); %Load the existing data set into the program.
        display(['It took ' num2str(toc) ' seconds to load the data from file']);
    else %The data needs to be processed because no processed data file exists.
        %Setup paths and get directory information
        ankle.kPath = [ankle.path '\Exported6d'];
        ankle.fPath = [ankle.path '\ForceData'];

```

```

%Load the excel spreadsheets to determine the trials to run, and their names
ankle = fcn_processExcelSheet(ankle); %Read in the excel data sheet

%Select the list of files to process
cd(ankle.kPath); %Changes the working directory to the data directory
kDirStructure = dir; %Creates a list of all the files in the current directory
kDirStructure(1) = []; kDirStructure(1) = []; %Removes the '.' and the '..' from the directory
list.
    kDirStructure = kDirStructure(ankle.log.Cycles); %Selects only the cycles to process
cd(ankle.fPath); %Changes the working directory to the force data
fDirStructure = dir; %Creates a list of all the files in the current directory
fDirStructure(1) = []; fDirStructure(1) = []; %Removes the '.' and the '..' from the directory
list.
    fDirStructure = fDirStructure(ankle.log.Cycles); %Selects only the cycles to process
cd(ankle.path);

%% Define RB Index Parameters
ankle.rb.probeStart = 2;                ankle.rb.ProbeStop = 13;
ankle.rb.tibStart = ankle.rb.probeStart+13; ankle.rb.tibStop = ankle.rb.ProbeStop+13;
ankle.rb.talStart = ankle.rb.tibStart+13; ankle.rb.talStop = ankle.rb.tibStop+13;
ankle.rb.calStart = ankle.rb.talStart+13; ankle.rb.calStop = ankle.rb.talStop+13;

%% Create Transformations to the Neutral Position from the Rigid Bodies
ankle.neutralData = xlsread([ankle.kPath, '\',
(kDirStructure(ankle.log.Neutral(ankle.log.Cycles)).name)]); %Read the neutral data file
ankle.pos.ntib =
fcn_transformationBuilder(ankle.neutralData(50,ankle.rb.tibStart:ankle.rb.tibStop));
ankle.pos.ntal =
fcn_transformationBuilder(ankle.neutralData(50,ankle.rb.talStart:ankle.rb.talStop));
ankle.pos.ncal =
fcn_transformationBuilder(ankle.neutralData(50,ankle.rb.calStart:ankle.rb.calStop));
display(' Neutral data loaded');

%Load the probed point data
ankle = fcn_loadProbePointData(ankle);

%% Generate Fixed Coordinate System: Check to see if this has been done before
if exist([ankle.path '\pref.mat'],'file') == 2 %If the file exists then load it.
    load([ankle.path '\pref.mat']); %Load the existing data set into the program.
    ankle.transCS = transCS;
    ankle.transGS = transGS;
else %The data needs to be processed because no processed data file exists.
    if strcmp(ankle.name,'5-12-2010_BB10R');
        [transCS transGS] = fcn_buildFixedCS5_BB10R(ankle); %Rotation Format is [FE IE AA]
    elseif strcmp(ankle.name,'4-30-2010_BB19');
        [transCS transGS] = fcn_buildFixedCS5_BB19(ankle); %Rotation Format is [FE IE AA]
        plotUnitVectors = true;
        fcn_plotProbedPointCloud(ankle, 1, 'tibia', plotUnitVectors);
        display('Press a key to continue');
        ginput(1)
    else
        [transCS transGS] = fcn_buildFixedCS5(ankle); %Rotation Format is [FE IE AA]
    end
    ankle.transCS = transCS;
    ankle.transGS = transGS;
    %Save the Preferences File
    cd(ankle.path)
    save('pref.mat', 'transCS', 'transGS');
end
%% This will iterate through every ankle that should be processed
loadBar = waitbar(length(ankle.cycles2run),'Loading Trial: ');
for runNum = 1:length(ankle.cycles2run)
    tic %Begin timer
    waitbar(runNum/length(ankle.cycles2run),loadBar,[ankle.name, ' Loading Trial: ',
num2str(runNum), ' of ', num2str(length(ankle.cycles2run))])
    %% Load Data
    %If it needs to be reprobbed then it will iterate to the next
    %probed points directory. This is initialized previously for the neutral run
    if (ankle.log.Reprobe(runNum) == true) %The first Run or a run tagged for reprobng.

```



```

        ankle.probePointsDir = ankle.probePointsDir+1;
        ankle = fcn_loadProbePointData(ankle); %Load the probed point data
        display(['Trial Number ', num2str(ankle.cycles2run(runNum)), ' was reprobed']);
    end

    %Import kinematic and force run data for the ankle
    cd(ankle.kPath); ankle.kData{runNum} = xlsread([ankle.kPath, '\',
kDirStructure(runNum).name]); %Read in this trial numbers kinematic data
    cd(ankle.fPath); ankle.fData{runNum} = dlmread([ankle.fPath, '\', fDirStructure(runNum).name],
'\t'); %Read in this trial numbers force data
    %Convert fData from English (lb, in-lb) to metric (N, N-mm)
    ankle.fData{runNum}(:,1:3) = ankle.fData{runNum}(:,1:3)*4.4482216228; %Forces in N
    ankle.fData{runNum}(:,4:6) = ankle.fData{runNum}(:,4:6)*112.98482933; %Torques in N-mm

    %Fit and interpolate the force data to match the size of the
    %kinematic data if there is a discrepancy
    [ankle.fData{runNum}, output.forceError{runNum}] = fcn_fitForceData(ankle.kData{runNum},
ankle.fData{runNum});
    %Search for NaN values. If found, then remove them from the force and kinematic data runs
    [ankle.kData{runNum}, ankle.fData{runNum}] = fcn_removeNaNValues(ankle.kData{runNum},
ankle.fData{runNum});

    %% Customized Actions for certain runs
    %Only run this for one trial...It will remove the first 15 seconds of data
    if strcmp(ankle.name,'4-14-2010_BBUnknown') && (ankle.cycles2run(runNum) == 67)
        tempLength = length(ankle.fData{runNum});
        ankle.fData{runNum} = ankle.fData{runNum}(1500:tempLength,:);
        ankle.kData{runNum} = ankle.kData{runNum}(1500:tempLength,:);
    end

    %Check to see if the jumper was set correctly
    %The following 3 strings are the names of the 3 runs that had the force jumper incorrectly
    set.
    if ~isempty(strfind(ankle.name,'BB21')) || ~isempty(strfind(ankle.name,'DRC07')) ||
~isempty(strfind(ankle.name,'DRC09'))
        %Multiply all values by 4 to fix the matrix jumper setting
        for runNum = 1:length(ankle.fData)
            ankle.fData{runNum} = ankle.fData{runNum}*4;
        end
    end

    %% Process Force Data
    %Translate the Force Data to be in the Ankle Joint Center,
    %where F and T are forces and torques
    %--> The columns are F_FE(X-1), F_IE(Y-2), F_AA(Z-3), T_FE(X-4), T_IE(Y-5), T_AA(Z-6)
    ankle.fDataMoved{runNum} = fcn_lcForceConverter(ankle.fData{runNum}, ankle.probeTibLC(5:7,:),
ankle.transCS.tib);

    %If the ankle is DRC07 and the run number is greater than or equal to 29 then the data needs
    to be translated
    if (ankle.cycles2run(runNum) >= 29) && ~isempty(strfind(ankle.name,'DRC07'))
        display(['DRC07, run number: ', num2str(runNum)]);
        fe=4; ie=5; aa=6;%Column Order: fe=1, ie=2, aa=3
        %This is a correction factor because for this one run all
        %the runs were translated above the 0 axis. These were
        %found by averaging the first 10 values on runs that were
        %unloaded at the beginning
        drc07FETTranslate = 54529.3537; %Run 37
        drc07IETTranslate = -6657.3503; %Run 37
        drc07AATTranslate = -31587.0874; %Run 37%
        ankle.fDataMoved{runNum}(:,fe) = ankle.fDataMoved{runNum}(:,fe)+drc07FETTranslate;
        ankle.fDataMoved{runNum}(:,ie) = ankle.fDataMoved{runNum}(:,ie)+drc07IETTranslate;
        ankle.fDataMoved{runNum}(:,aa) = ankle.fDataMoved{runNum}(:,aa)+drc07AATTranslate;

    %If the ankle is BB18 and the runNumber is 42. It will sync up the force and kinematics data
    elseif strcmp(ankle.name,'6-17-2010_BB18') && (ankle.cycles2run(runNum) == 42)
        % Fix the Lagging Fdata on BB18, run Number 42
        phaseLag = 69;
        addZeros = zeros(phaseLag,6);

```

```

    ankle.fDataMoved{runNum} = [addZeros; ankle.fDataMoved{runNum}];
    ankle.fDataMoved{runNum}(6001:length(ankle.fDataMoved{runNum}),:) = [];
end

%Align the force data to match GS output. For left ankles IE and FE need to be flipped
if strcmpi(ankle.LorR(1), '1')
    %Column Order: fe=1, ie=2, aa=3
    fe=1;
    ie=2;
    aa=3;
    ankle.fDataMoved{runNum}(:,fe) = ankle.fDataMoved{runNum}(:,fe)*-1; %flip Force FE
    ankle.fDataMoved{runNum}(:,ie) = ankle.fDataMoved{runNum}(:,ie)*-1; %flip Force IE
%   ankle.fDataMoved{runNum}(:,aa) = ankle.fDataMoved{runNum}(:,aa)*-1; %flip Force AA
    ankle.fDataMoved{runNum}(:,fe+3) = ankle.fDataMoved{runNum}(:,fe+3)*-1; %flip Torque FE
%   ankle.fDataMoved{runNum}(:,ie+3) = ankle.fDataMoved{runNum}(:,ie+3)*-1; %flip Torque IE
    ankle.fDataMoved{runNum}(:,aa+3) = ankle.fDataMoved{runNum}(:,aa+3)*-1; %flip Torque AA

end

%Generate the logical indices for hysteresis:
%For tibia frame tranCSTib = AA, IE, FE
switch ankle.case{runNum}
    case {'Pure IE', 'IE w FE'} %Torque Unloading on the IE(y) Axis
%       col = 5; %IE Torque
        col=5;
        dispAx = 'IE';
        [ankle.log.ForceHysteresis{runNum}          ankle.hystErr(runNum)] =
fcn_removeHysteresis2(ankle.fDataMoved{runNum}(:,col),distBetweenPoints,runNum);
        case {'Pure AA', 'AA w FE'} %Torque Unloading on the AA(x) Axis
%       col = 4; %AA Torque
        col=6;
        dispAx = 'AA';
        [ankle.log.ForceHysteresis{runNum}          ankle.hystErr(runNum)] =
fcn_removeHysteresis2(ankle.fDataMoved{runNum}(:,col),distBetweenPoints,runNum);
        case {'Pure FE'} %Torque Unloading on the FE(z) Axis
%       col = 6; %FE Torque
        col=4;
        dispAx = 'FE';
        [ankle.log.ForceHysteresis{runNum}          ankle.hystErr(runNum)] =
fcn_removeHysteresis2(ankle.fDataMoved{runNum}(:,col),distBetweenPoints,runNum);
        otherwise %This would be Neutral, Const IE, and Const AA
            display(['   Nothing required to be removed on ', ankle.cyclesName{runNum}]);
            ankle.log.ForceHysteresis{runNum} = true(length(ankle.fDataMoved{runNum}),1);
            ankle.hystErr(runNum) = false;
        end
        title(['Hysteresis-Run ', num2str(ankle.cycles2run(runNum)), ' ', ankle.case{runNum}]);
        if exist('dispAx')
            display(['   Hysteresis removed on ', dispAx, ' Axis on ', ankle.cyclesName{runNum}]);
        end
        clear dispAx
        close(gcf)

%Remove Hysteresis from both the force and kinematic runs:
%   ankle.kDataHystRem{runNum} = ankle.kData{runNum}(ankle.log.ForceHysteresis{runNum},:);
%   ankle.fDataHystRem{runNum} = ankle.fDataMoved{runNum}(ankle.log.ForceHysteresis{runNum},:);
    display(['   Completed Run Number: ', num2str(runNum)]);

%Check to see if any runs are ill-conditioned and had errors

if isempty(ankle.fDataHystRem{runNum})
    display(['There was a serious error with run number ', num2str(runNum), '!!!']);
end

%Generate Logical Indices for Ankle Condition
[ankle.log.cond1, ankle.log.cond2, ankle.log.cond3] = fcn_logAnkleCond(ankle);

%Process Grood and Suntay Angles and Translations for a run of data for all data collected -
This is used for validation

```

```

[gsAnglesAll gsDispAll] = fcn_processGS(ankle.kData{runNum}, ankle.transGS, ankle.rb,
ankle.LorR);
    ankle.gsAnglesAll.tibcal{runNum} = gsAnglesAll.tibcal;
    ankle.gsAnglesAll.tibtal{runNum} = gsAnglesAll.tibtal;
    ankle.gsAnglesAll.talcal{runNum} = gsAnglesAll.talcal;
    ankle.gsDispAll.tibcal{runNum} = gsDispAll.tibcal;
    ankle.gsDispAll.tibtal{runNum} = gsDispAll.tibtal;
    ankle.gsDispAll.talcal{runNum} = gsDispAll.talcal;

    %Process Grood and Suntay Angles and Translations with hysteresis removed
    [gsAngles gsDisp] = fcn_processGS(ankle.kDataHystRem{runNum}, ankle.transGS, ankle.rb,
ankle.LorR);
    ankle.gsAngles.tibcal{runNum} = gsAnglesAll.tibcal(ankle.log.ForceHysteresis{runNum},:);
    ankle.gsAngles.tibtal{runNum} = gsAnglesAll.tibtal(ankle.log.ForceHysteresis{runNum},:);
    ankle.gsAngles.talcal{runNum} = gsAnglesAll.talcal(ankle.log.ForceHysteresis{runNum},:);
    ankle.gsDisp.tibcal{runNum} = gsDispAll.tibcal(ankle.log.ForceHysteresis{runNum},:);
    ankle.gsDisp.tibtal{runNum} = gsDispAll.tibtal(ankle.log.ForceHysteresis{runNum},:);
    ankle.gsDisp.talcal{runNum} = gsDispAll.talcal(ankle.log.ForceHysteresis{runNum},:);

    %% Verify Result
    if runNum > 1
        xmin = 0; xmax = 60;
        ymin = -45; ymax = 45; ydelta = 15;
        yminF = -15; ymaxF = 15; yFdelta = 5;
        time = 0:length(ankle.fDataMoved{runNum})-1; time = time/100;
        figure(runNum); clf;
        subplot(3,1,1);
        %
        plotyy(time,gsAnglesAll.tibcal(:,fe),time,ankle.fDataMoved{runNum}(:,fe+3)/1000,'plot'); hold on;
        %
        set(get(ax(1),'Ylabel'),'String','FE Degrees')
        %
        set(get(ax(2),'Ylabel'),'String','FE Torque (N-mm)')
        %
        ylabel('FE Degrees ');
        %
        axis(ax(1),[xmin xmax ymin ymax]);
        %
        axis(ax(2),[xmin xmax yminF ymaxF]);
        %
        title([ankle.name, ' ', ankle.cyclesName{runNum}]);
        %
        set(ax,'xtick',[])
        %
        set(ax(1),'ytick',ymin:ydelta:ymax);
        %
        set(ax(2),'ytick',yminF:yFdelta:ymaxF);
        %
        subplot(3,1,2);
        %
        plotyy(time,gsAnglesAll.tibcal(:,ie),time,ankle.fDataMoved{runNum}(:,ie+3)/1000,'plot'); hold on;
        %
        set(get(ax(1),'Ylabel'),'String','IE Degrees')
        %
        set(get(ax(2),'Ylabel'),'String','IE Torque (N-mm)')
        %
        ylabel('IE Degrees ');
        %
        axis(ax(1),[xmin xmax ymin ymax]);
        %
        axis(ax(2),[xmin xmax yminF ymaxF]);
        %
        set(ax,'xtick',[])
        %
        set(ax(1),'ytick',ymin:ydelta:ymax);
        %
        set(ax(2),'ytick',yminF:yFdelta:ymaxF);
        %
        subplot(3,1,3);
        %
        plotyy(time,gsAnglesAll.tibcal(:,aa),time,ankle.fDataMoved{runNum}(:,aa+3)/1000,'plot'); hold on;
        %
        set(get(ax(1),'Ylabel'),'String','AA Degrees')
        %
        set(get(ax(2),'Ylabel'),'String','AA Torque (N-mm)')
        %
        xlabel('time'); ylabel('AA Degrees ');
        %
        axis(ax(1),[xmin xmax ymin ymax]);
        %
        axis(ax(2),[xmin xmax yminF ymaxF]);
        %
        set(ax(1),'ytick',ymin:ydelta:ymax);
        %
        set(ax(2),'ytick',yminF:yFdelta:ymaxF);
        %
        set(gcf,'WindowStyle','docked');
        %
    end

    %Indicate position of process
    n(runNum) = toc;
    display(['Trial, ' num2str(ankle.cycles2run(runNum)), ' loaded in ', num2str(n(runNum)), '
seconds.']);

end
close(loadBar)

```

```

display(['Total time to process all trials was ', num2str(sum(n)/60), ' minutes.']);

%% Save the file to the run folder
display('File is being saved')
cd(ankle.path);
save('ankle.mat', 'ankle'); %Save the ankle structure to the hard drive for later retrieval
clear runNum n kDirStructure fDirStructure
display('Processed ankle data has been saved!!!')
end

% print_verifyKinematicAndForceData

display(['Ankle Process Master has been completed on ', ankle.name]);

```

F.2.3 *fcn_transformationbuilder.m*

The purpose of this function is to take the optotrak data and convert it into a transformation matrix.

```

function [transformationMatrix] = fcn_transformationBuilder(rigidPos)
%Author: Jim West
%Date: 4/5/2010
%Use: trMatrixOut = fcn_transformationBuilder(kinemPosOfRBn[1x12])
%Description: This needs a 12 column matrix of kinematic data, and it builds a
%transformation matrix for the current rigid body relative to the optotrak
%camera origin. The data should be exported as ASCII 6D and Rotation Matrix
i=1;
r00=rigidPos(i,1);
r01=rigidPos(i,2);
r02=rigidPos(i,3);
r10=rigidPos(i,4);
r11=rigidPos(i,5);
r12=rigidPos(i,6);
r20=rigidPos(i,7);
r21=rigidPos(i,8);
r22=rigidPos(i,9);
x=rigidPos(i,10);
y=rigidPos(i,11);
z=rigidPos(i,12);
transformationMatrix = [1 0 0 0; ...
                        x r00 r01 r02; ...
                        y r10 r11 r12; ...
                        z r20 r21 r22]; %Origin relative to RigidBody Transformation Matrix

```

F.2.4 *fcn_transformmcs.m*

The purpose of this function is to transform data points from one CS to another.

```

function [ calCSrelRef talCSrelRef tibCSrelRef ] = fcn_transformCS(fixedCS, pos, reference )
%Description: Convert and transform a Fixed CS to a moving animation frame.
% Example would be building a fixed CS for the tibia, and then defining that
% CS at each point in time for the position of the Tibia.
%Author: Jim West
%Date: 7/18/2010
%Use: [ calCSrelRef talCSrelRef tibCSrelRef ] = fcn_transformCS(fixedCS, pos, points, reference )
% Output: calCSrelRef talCSrelRef tibCSrelRef are transformation matrices

```

```

% with the resultant position and rotation matrix
% Input:
%   fixedCS = a structure with 3 transformation matrices .cal, .tal, and
%   .tib being the fixed coordinate system of the bone.
%   pos = a structure with 3 transformation matrices .cal, .tal, and .tib
%   being the current transformation matrix describing the position of
%   each rigid body in space.
%   reference = One of the following strings
%   cal - all points relative to the calcaneus rigid body
%   tal - all points relative to the talus rigid body
%   tib - all points relative to the tibia rigid body
%   calor - all points relative to the calcaneus rigid body oriented at zero
%   talor - all points relative to the talus rigid body oriented at zero
%   tibor - all points relative to the tibia rigid body oriented at zero

if nargin <=2
    reference = 'cal';
elseif nargin == 3
    %do nothing
else
    error('Incorrect number of inputs');
end

%Generate Fixed CS:
fixedCS.ori = eye(4);
switch reference
    case 'cal'
        calCSrelRef = fixedCS.cal;
        talCSrelRef = (pos.cal\pos.tal)*fixedCS.tal;
        tibCSrelRef = (pos.cal\pos.tib)*fixedCS.tib;
    case 'tal'
        calCSrelRef = (pos.tal\pos.cal)*fixedCS.cal;
        talCSrelRef = fixedCS.tal;
        tibCSrelRef = (pos.tal\pos.tib)*fixedCS.tib;
    case 'tib'
        calCSrelRef = (pos.tib\pos.cal)*fixedCS.cal;
        talCSrelRef = (pos.tib\pos.tal)*fixedCS.tal;
        tibCSrelRef = fixedCS.tib;
    case 'calor'
        calCSrelRef = fixedCS.cal\fixedCS.ori*fixedCS.cal;
        talCSrelRef = fixedCS.cal\fixedCS.ori*(pos.cal\pos.tal)*fixedCS.tal;
        tibCSrelRef = fixedCS.cal\fixedCS.ori*(pos.cal\pos.tib)*fixedCS.tib;
    case 'talor'
        calCSrelRef = fixedCS.tal\fixedCS.ori*(pos.tal\pos.cal)*fixedCS.cal;
        talCSrelRef = fixedCS.tal\fixedCS.ori*fixedCS.tal;
        tibCSrelRef = fixedCS.tal\fixedCS.ori*(pos.tal\pos.tib)*fixedCS.tib;
    case 'tibor'
        calCSrelRef = fixedCS.tib\fixedCS.ori*(pos.tib\pos.cal)*fixedCS.cal;
        talCSrelRef = fixedCS.tib\fixedCS.ori*(pos.tib\pos.tal)*fixedCS.tal;
        tibCSrelRef = fixedCS.tib\fixedCS.ori*fixedCS.tib;
end

```

F.3 Algorithm for Finding Ankle Axes and Center Pseudo Code

The pseudocode represented here was used to define an algorithm which would repeatably fit a cylinder to the dome of the talar points using an optimization procedure that was repeated until conversion. This cylinder was then used for construction of the CS of the talus.

Note: A sphere was fit to the points to find the center.

```
Minimize Variation in R, std dev
ctr(x y z) + direction (xo yo zo unit vectors)
  Use sphere / ellipsoid finder to find the center
  Iterate change in degree of a line going through the center
Ri=dist from the point to the line

Processing Loop:
Transform the points to an XY grid facing the Z axis
Do until SlopeChange is equal to the PositionChange
  Start Loop
  SlopeChange:
    Iterate a series of 8 points bounding a square around the initial guess
    Draw a line to each point and determine the lowest standard deviation between the points
and the newly created line
    If the initial guess and the new point are different than move the new point to be the new
initial point and repeat the process until it is no longer walking
  PositionChange:
    Move the line found previously to an 8 point bounded box around the initial guess
    Draw a line to each point and determine the lowest standard deviation between the points
and the newly created line
    If the initial guess and the new point are different than move the new point to be the new
initial point and repeat the process until it is no longer walking
  End Loop
Compare the position solution with the slope solution
If the solutions are different repeat the loop
When the points overlap decrease the bounding box and repeat for the number of iterations required
```

F.4 Algorithm for Finding Ankle Axes and Center Matlab Code

F.4.1 fcn_buildFixedCS5.m

```
function [tranCS tranGS] = fcn_buildFixedCS5(ankle)
% This program will build a fixed CS for each bone
%To keep track of CS units will have a suffixed .tal, .tib, .cal to denote
%reference frame.
%Version 1: Function works but the output CS are not orthogonal, so there
%is a problem in the transformations.
%Version 2: Transforming the points to the Tibia frame first, and then
%building the CS.

%Initialize Variables:
figTemp = 10;
dStep = 2; %Angle change in degrees can be 0.5 to 4 with little change in precision
numLoops = 6; %The ideal number of loops is 5
indexTal = 4; %
indexTib = 1; %The tibia talus articulating surface on the Tibia.
indexCal = 3; %The dome that the talus sits on for the calcaneus

%% Build Transformation Matrices with Origin at [0 0 0] for Converting Unit Vectors
tranTib = ankle.pos.ntib;
    tranTib(2:4,1) = [0; 0; 0];
tranTal = ankle.pos.ntal;
    tranTal(2:4,1) = [0; 0; 0];
tranCal = ankle.pos.ncal;
    tranCal(2:4,1) = [0; 0; 0];

%% Create FE(x) axis off of talar dome points
%Load talar dome points and remove unnecessary points from talar dome
%surface:
pointsTalDome.tal =
ankle.probeTal(ankle.probeTalPoints(indexTal,1):ankle.probeTalPoints(indexTal,2),2:4);
%    pointsTalDome.tal = fcn_removeTalarDomePoints(pointsTalDome.tal,figTemp); pause(.1)
    pointsTalDome.tal = fcn_removeDomePoints(pointsTalDome.tal,figTemp); pause(.1)

    pointsTalDome.tib = fcn_transformPoints(tranTal,tranTib,pointsTalDome.tal); %Convert points to Tibia
Frame

%Setup Initial Points and Guesses in the Tibia Frame looking for 2
%points defining the FE axis, one through the center
%Find the first guess for center of talus in the tibia frame.
[P1tal.tib] = ellipsoid_fit(pointsTalDome.tib, 3); P1tal.tib = P1tal.tib'; %Center of fit sphere
P2talIndex = 5; %This is the probe set to use
P2guessPoints.tal =
ankle.probeTal(ankle.probeTalPoints(P2talIndex,1):ankle.probeTalPoints(P2talIndex,2),2:4);%Center of range
of points perpendicular to talar dome
P2tal.tal = mean(P2guessPoints.tal);
P2tal.tib = fcn_transformPoints(tranTal,tranTib,P2tal.tal); %Convert P2 to the Tibia Frame

%Optimize the initial guesses in relation to the talar dome by finding
%the line going through the cylinder of points
[outP1tal.tib, outP2tal.tib] = fcn_findAnkleAxis10(P1tal.tib, P2tal.tib, pointsTalDome.tib, dStep,
's', numLoops);

%Create FE Unit CS Axis:
unitFE.tib = fcn_createUnitVector(outP2tal.tib-outP1tal.tib); %Convert the output points into a F/E
unit vector in Tibia Reference Frame

%% IE(y) axis off of the tibia probed points:
%Load tibia surface points and remove unnecessary points from tibial dome surface:
%    pointsTib.tib =
ankle.probeTib(ankle.probeTibPoints(indexTib,1):ankle.probeTibPoints(indexTib,2),2:4);
```

```

%      pointsTib.tib = fcn_removeDomePoints(pointsTib.tib,figTemp); pause(.1); %Trim Tibia Dome Points:
This will be used for either finding the center of the tibia for the IE axis line, and/or used for finding
a center around the rotation of the bone.
%      display('choose again');
%      pointsTib.tib = fcn_removeDomePoints(pointsTib.tib,figTemp); pause(.1); %Trim Tibia Dome Points:
This will be used for either finding the center of the tibia for the IE axis line, and/or used for finding
a center around the rotation of the bone.

%Setup Tibia Coordinate System:
P1tib.tib = ankle.probeTib(1,2:4); %Center of Proximal Tibia Bone
P2tib.tib = ankle.probeTib(4,2:4); %Center of Distal Tibia Talus Articulating Surfcae
%      P2tib = mean(pointsTib); %An alternate way as opposed to probing the point by hand
%Create the IE(y) Axis:
unitIE.origTib = fcn_createUnitVector(P1tib.tib-P2tib.tib);

%% AA(z) axis
unitAA.tib = fcn_createUnitVector(cross(unitFE.tib,unitIE.origTib)); %Abduction/Adduction Axes
unitIE.tib = fcn_createUnitVector(cross(unitAA.tib,unitFE.tib)); %Internal/External Rotation

%% Convert to Talus and Calcaneus Reference Frames:
unitFE.tal = fcn_createUnitVector(fcn_transformPoints(tranTib,tranTal,unitFE.tib));
unitFE.cal = fcn_createUnitVector(fcn_transformPoints(tranTib,tranCal,unitFE.tib));
unitIE.tal = fcn_createUnitVector(fcn_transformPoints(tranTib,tranTal,unitIE.tib));
unitIE.cal = fcn_createUnitVector(fcn_transformPoints(tranTib,tranCal,unitIE.tib));
unitIE.origTal = fcn_createUnitVector(fcn_transformPoints(tranTib,tranTal,unitIE.origTib));
unitIE.origCal = fcn_createUnitVector(fcn_transformPoints(tranTib,tranCal,unitIE.origTib));
unitAA.tal = fcn_createUnitVector(fcn_transformPoints(tranTib,tranTal,unitAA.tib));
unitAA.cal = fcn_createUnitVector(fcn_transformPoints(tranTib,tranCal,unitAA.tib));

%% Find center of Tibia for placement of CS:
[P1tib.tib, P1tib_radius] = ellipsoid_fit(ankle.probeTib(ankle.probeTibPoints(indexTib,1):ankle.probeTibPoints(indexTib,2),2:4), 3);
P1tib.tib = P1tib.tib'; %Center of fit sphere

%% Find center of Calcaneus for placement of CS:
pointsCalDome = ankle.probeCal([ankle.probeCalPoints(indexCal,1):ankle.probeCalPoints(indexCal,2)],2:4);
[P1cal.cal, P1cal_radius] = ellipsoid_fit(pointsCalDome, 3); P1cal.cal = P1cal.cal'; %Center of fit sphere
P1tal.tal = fcn_transformPoints(tranTib,tranTal,outP1tal.tib');

%% Build output Transformation Matrices
% Original Matris is built as FE(X), IE(Y), AA(Z)
tranCS.tib = [1 0 0 0; P1tib.tib', unitFE.tib', unitIE.tib', unitAA.tib'];
tranCS.tal = [1 0 0 0; P1tal.tal', unitFE.tal', unitIE.tal', unitAA.tal'];
tranCS.cal = [1 0 0 0; P1cal.cal', unitFE.cal', unitIE.cal', unitAA.cal'];

%Edited to be consistent with the Wu representation (2002) of the CS
%directions: AA(X), IE(Y), FE(Z) for the fixed bones:
% The notation is proximal(XYZ), distal(xyz)
% For the tib-cal: e1=Z, e3=x
tranGS.tibcal.tib = [1 0 0 0; P1tib.tib', unitFE.tib', unitIE.tib', unitAA.tib'];
tranGS.tibcal.cal = [1 0 0 0; P1cal.cal', unitFE.cal', unitIE.cal', unitAA.cal'];
tranGS.tibcal.tal = eye(4);
% For the tib-tal: e1=Z, e3=y
tranGS.tibtal.tib = [1 0 0 0; P1tib.tib', unitFE.tib', unitAA.tib', unitIE.tib'];
tranGS.tibtal.tal = [1 0 0 0; P1tal.tal', unitFE.tal', unitAA.tal', unitIE.tal'];
tranGS.tibtal.cal = eye(4);
% For the tal-cal: e1=Y, e2=x
tranGS.talcal.tal = [1 0 0 0; P1tal.tal', unitIE.tal', unitFE.tal', unitAA.tal'];
tranGS.talcal.cal = [1 0 0 0; P1cal.cal', unitIE.cal', unitFE.cal', unitAA.cal'];
tranGS.talcal.tib = eye(4);

```


F.4.2 fcn_findAnkleAxis10.m

This is the actual optimization algorithm used to find the optimal orientation of the cylinder.

```
function [outP1, outP2, dev ] = fcn_findAnkleAxis10(P1, P2, points, dStep, flag, numLoops)
%% Algorithm for finding Ankle Axes and Center
%{
Minimize Variation in R by finding the min std dev
ctr(x y z) + direction (xo yo zo unit vectors)
    Use sphere / ellipsoid finder to find the center
    Iterate change in degree of a line going through the center
Ri=dist from the point to the line
Create a bounding cube with 27 points around the line

USE: P1 and P2 are origin and guess point
points are the probed surface
flag is used to define the type of comparison done.
    's' : standard deviation
    'm' : mean
    'r' : range
Version 2: Will walk at a set dStep, and when it finds itself in the same
position will then iterate at smaller levels.

Version 3: between versions, adding the translation functions, but it didn't really work.

Version 4: This function gets rid of the angle change and performs a transformation matrix on the points
to align them on an XY axis alignment

Version 5: Removed translation function and added ouput data to the fields

Version 6: cleaned up code, and making a simpler version without
transformations to test a simpler case. Created a new breakoff function
called fcn_findDistancePoint2Line to simplify this code.

Version 7: Creating the program into a complete loop system to iterate and
repeat until conversion has been reached. The program function appears to be
functional now and operating correctly.

Version 8: The program will now be able to translate the points

Version 9: Changing order of operations and fixed points being used incorrectly.

Version 10: Final Working Version: Cleaning up code, and removing unnecessary components
%}

tic
if nargin == 5
    numLoops = 5;
elseif nargin == 4
    numLoops = 5;
    flag = 's';
elseif nargin == 3
    numLoops = 5;
    flag = 's';
    dStep = .1;
elseif nargin < 3
    error('Not enough input arguments');
end

if numLoops > 10;
    error('Your iteration loop is set dangerously high');
end
```

```

switch flag
    case {'s', 'm', 'r'} %The input is fine
        otherwise; error('The flag is not set correctly. Please set to s, m, or r');
end

%% Define Variables:
% Find the 9 variations of the line orientation
signIndex = [-1 1; 0 1; 1 1; -1 0; 0 0; 1 0; -1 -1; 0 -1; 1 -1]; %The sign index dictates whether to
use positive or negative angles when defining the new test grid. Each matrix pair represents an x,y
combination. For example [-1,0] is in the negative x direction with no y direction.
slopeIterCount = 0; posIterCount = 0;
plotColorCounter = 0;
testP2{1} = 0;

%% Transform the points to an XY grid facing the Z axis
%Generate coordinate system transform to translate test points
unitx = mean(points)-P1; unitx = unitx./sqrt(dot(unitx,unitx)); %Finds the average center of the
points. This will be used to create a unit vector
unitz = P2-P1; unitz = unitz./sqrt(dot(unitz,unitz));
unity = cross(unitz,unitx); unity = unity./sqrt(dot(unity,unity));
unitx = cross(unity,unitz); unitx = unitx./sqrt(dot(unitx,unitx));
%Transformation of points to align to an XY coordinated plane
transOrigin2XY = [1 0 0 0; [0 0 0]' unitx' unity' unitz'];

%% Transform Points to new Position
newP2 = transOrigin2XY\[1 P2]'; P2 = newP2(2:4)';
newP1 = transOrigin2XY\[1 P1]'; P1 = newP1(2:4)'; %This will only be used for a [0 0 0] center

%Transform all the input points to the new coordinate frame
newP = zeros(length(points),4);
for i = 1:length(points); newP(i,:) = transOrigin2XY\[1 points(i,:)]'; end;
p = newP(:,2:4);

%% Initialize the P1 and P2 for Slope and Position analysis
posCurP1 = P1; posCurP2 = P2;
posPrevP1 = P1; posPrevP2 = P2;
slopePrevP1 = posCurP1; slopeCurP1 = posCurP1;
slopePrevP2 = posCurP2; slopeCurP2 = posCurP2;

%% Do until SlopeChange is equal to the PositionChange
for loopCount = 1:numLoops %This loop sizes the step size. This is the number of step sizes to make
while (abs(sum(slopeCurP1-posCurP1)) > 0) && (abs(sum(slopeCurP2-posCurP2)) > 0) || (slopeIterCount ==
0) %Do this while the selections for P1 and P2 are not equal. When they are equal it has converged
    %% SlopeChange: Find best fit for P2 to find the right slope
    plotColorCounter = plotColorCounter+1; %When the loop cycles iterate the color
    % display(['plotColorCounter=', num2str(plotColorCounter), ', P1=',num2str(slopeCurP1), ', P2=',
num2str(slopeCurP2)]);
    slopeIterCount = 0;
    %Initialize the positions for the next loop
    slopePrevP1 = posCurP1; slopeCurP1 = posCurP1;
    slopePrevP2 = posCurP2; slopeCurP2 = posCurP2;

    while (abs(sum(slopeCurP2-slopePrevP2)) > 0) || (slopeIterCount == 0) %This will loop until the
points are overlapping and no longer walking
        slopeIterCount = slopeIterCount+1;
        slopePrevP2 = slopeCurP2; %Set the currentP2 to the previousP2

        %Iterate a series of 8 points bounding a square around the initial guess
        for testPoint = 1:length(signIndex)
            slopeTestP2{testPoint} = [slopePrevP2(1)+dStep*signIndex(testPoint,1)
slopePrevP2(2)+dStep*signIndex(testPoint,2) slopePrevP2(3)]; %Slope Test for XY Frame: A test point
generated.

            %Draw a line to each point and determine the lowest standard deviation between the points
and the newly created line
            distance2Line = fcn_findDistancePoint2Line(slopeCurP1,slopeTestP2{testPoint}',p); %Find
the distance of the points from the current line

```

```

        switch flag
            case 's' %Standard Deviation Method
                dev(testPoint) = std(distance2Line);
            case 'm' %Mean Method
                dev(testPoint) = mean(distance2Line);
            case 'r' %Range Method
                dev(testPoint) = range(distance2Line);
        end
        [ans,indexCurPoint] = min(dev); %Selects the index for the minimum deviation value for all
        guessed points in the square quadrant.
    end
    slopeCurP2 = slopeTestP2{indexCurPoint}'; %Sets the closest test point as the current point to
    test against for the next round
end
%% PositionChange: Translate best fit line to find the best fit center
posPrevP1 = slopeCurP1; posCurP1 = slopeCurP1;
posPrevP2 = slopeCurP2; posCurP2 = slopeCurP2;
plotColorCounter = plotColorCounter+1; %When the loop cycles iterate the color
posIterCount = 0;

while (abs(sum(posCurP1-posPrevP1)) > 0) || (posIterCount == 0) %This will loop until the points
are overlapping and no longer walking
    posIterCount = posIterCount+1;
    posPrevP1 = posCurP1; %Set the previous point to the current point and iterate the loop
    posPrevP2 = posCurP2;

    %Build the bounding box of 8 points and move the line to each change in step size
    for testPoint = 1:length(signIndex)
        %Position Test for XY Frame:
        posTestP1{testPoint} = [posPrevP1(1)+dStep*signIndex(testPoint,1)
posPrevP1(2)+dStep*signIndex(testPoint,2) posPrevP1(3)];
        posTestP2{testPoint} = [posPrevP2(1)+dStep*signIndex(testPoint,1)
posPrevP2(2)+dStep*signIndex(testPoint,2) posPrevP2(3)];

        %Find the distance of the points from the current line
        distance2Line = fcn_findDistancePoint2Line(posTestP1{testPoint}',posTestP2{testPoint}',p);

        switch flag
            case 's' %Standard Deviation Method
                dev(testPoint) = std(distance2Line);
            case 'm' %Mean Method
                dev(testPoint) = mean(distance2Line);
            case 'r' %Range Method
                dev(testPoint) = range(distance2Line);
        end

        %Select the lowest deviation point
        [ans,indexCurPoint] = min(dev); %Selects the index for the minimum deviation value for all
        guessed points in the square quadrant.
    end

    %Sets the closest test point as the current point to test against for the next round
    posCurP1 = posTestP1{indexCurPoint}';
    posCurP2 = posTestP2{indexCurPoint}';
end
end
dStep = dStep/5; %Change the angle for the next cycle
slopeIterCount = 0;
posIterCount = 0;
end

%Generate Outputs with Transformations
outP1 = transOrigin2XY*[1 posCurP1]'; outP1 = outP1(2:4);
outP2 = transOrigin2XY*[1 posCurP2]'; outP2 = outP2(2:4);

display(['Time: ', num2str(toc),'(s). The origin is ', num2str(outP1)',', the direction is ',
num2str(outP2)', 'the dStep is: ', num2str(dStep)]);

```

F.5 Grood and Suntay Processing Code

F.5.1 fcn_processGS.m

This function was written to take the kinematic data, and the existing CS transformations and construct the G&S output kinematics. The last part of the function adjusts the positiveness/negativeness of the outputs to correlate them correctly to a right or left ankle.

```
function [gsAngles gsDisp] = fcn_processGS(kData, transGS, rb, LorR)%Grood and Suntay calculation program.
% Proximal(Tibia) (FE) (Flexion+)
% Distal (Calcaneus) (AA) (Adduction+)

%% Custom Jim G&S Program
%Initialize Variables
%Define the columns where the angles and displacements are kept.
    fe.tibcal=1;    ie.tibcal=2;    aa.tibcal=3;
    fe.tibtal=1;    ie.tibtal=3;    aa.tibtal=2;
    fe.talcal=2;    ie.talcal=1;    aa.talcal=3;

for curFrame = 1:length(kData)
    pos.tib = fcn_transformationBuilder(kData(curFrame,rb.tibStart:rb.tibStop));
    pos.tal = fcn_transformationBuilder(kData(curFrame,rb.talStart:rb.talStop));
    pos.cal = fcn_transformationBuilder(kData(curFrame,rb.calStart:rb.calStop));
    [trCalRelTib(:, :, curFrame) ans ans] = fcn_transformCS(transGS.tibcal, pos, 'tiber');
    [ans trTalRelTib(:, :, curFrame) ans] = fcn_transformCS(transGS.tibtal, pos, 'tiber');
    [trCalRelTal(:, :, curFrame) ans ans] = fcn_transformCS(transGS.talcal, pos, 'talor');
end

%Perform G&S angle and displacement calculations for the 3 bone
%conditions, then filter the data
[gsAngles.tibcal gsDisp.tibcal] = fcn_gs(trCalRelTib);
gsAngles.tibcal = fcn_filterGSData(gsAngles.tibcal);
gsDisp.tibcal = fcn_filterGSData(gsDisp.tibcal);

[gsAngles.tibtal gsDisp.tibtal] = fcn_gs(trTalRelTib);
gsAngles.tibtal = fcn_filterGSData(gsAngles.tibtal);
gsDisp.tibtal = fcn_filterGSData(gsDisp.tibtal);

[gsAngles.talcal gsDisp.talcal] = fcn_gs(trCalRelTal);
gsAngles.talcal = fcn_filterGSData(gsAngles.talcal);
gsDisp.talcal = fcn_filterGSData(gsDisp.talcal);

%Adjust the angles and displacements to fit the following condition:
%Angles: Flexion(+), Adduction(+), External Rotation(+)
%Displacements: Lateral(+), Anterior(+), Distraction(+)
if strcmpi(LorR(1), 'l')
    %Cal Rel Tib:
    gsAngles.tibcal(:, fe.tibcal) = -gsAngles.tibcal(:, fe.tibcal);
    gsAngles.tibcal(:, ie.tibcal) = -gsAngles.tibcal(:, ie.tibcal);
    gsDisp.tibcal(:, ie.tibcal) = -gsDisp.tibcal(:, ie.tibcal);
    gsDisp.tibcal(:, aa.tibcal) = -gsDisp.tibcal(:, aa.tibcal);
    %Tal Rel Tib:
    gsAngles.tibtal(:, ie.tibtal) = -gsAngles.tibtal(:, ie.tibtal);
    %Cal Rel Tal:
    gsDisp.talcal(:, aa.talcal) = -gsDisp.talcal(:, aa.talcal);
    gsDisp.talcal(:, ie.talcal) = -gsDisp.talcal(:, ie.talcal);
    gsAngles.talcal(:, fe.talcal) = -gsAngles.talcal(:, fe.talcal);
    gsAngles.talcal(:, ie.talcal) = -gsAngles.talcal(:, ie.talcal);
end
```

```

        gsAngles.talcal(:,aa.talcal) = -gsAngles.talcal(:,aa.talcal);
elseif strcmpi(LorR(1),'r')
    %Cal Rel Tib:
    gsDisp.tibcal(:,ie.tibcal) = -gsDisp.tibcal(:,ie.tibcal);
    %Tal Rel Tib:
    gsDisp.tibtal(:,ie.tibtal) = -gsDisp.tibtal(:,ie.tibtal);
    gsAngles.tibtal(:,fe.tibtal) = -gsAngles.tibtal(:,fe.tibtal);
    %Cal Rel Tal:
    gsDisp.talcal(:,ie.talcal) = -gsDisp.talcal(:,ie.talcal);
    gsAngles.talcal(:,aa.talcal) = -gsAngles.talcal(:,aa.talcal);
else
    error('The ankle is not designated Left or Right, set LorR');
end

```

F.5.2 fcn_gs.m

This function performs the actual G&S math and outputs the angles and displacements.

```

function [angles disp] = fcn_gs(trDistRelProx)
%Grood and Suntay calculation program.
%Author: Jim West
%Date: 7/30/2010
%Description: This function will take an input transformation matrix in the
%form of [1 0 0 0; [origin(1x3)]' [rotMatrix(3x3)]. The input needs to be
%conditioned to be distal relative to fixedOrigin proximal meaning the
%proximal should be at [1 0 0 0; 0 1 0 0; 0 0 1 0; 0 0 0 1].
%Note: The input transformation matrix can be 3 dimensional where you have
% the index as (trDistRelProx[4x4], timePoint). This is so that you can build
% up an array of time points and process it all at once. However it can also
% just be run on a single transformation as part of a loop as well.

%% Custom Jim G&S Program
% ***** CALCULATE GROOD-SUNTAY CLINICAL ROTATIONS AND TRANSLATIONS *****
%Grood-Suntay clinical rotations
% len = length(trDistRelProx);
[r c len] = size(trDistRelProx);
alpha = nan(len,1);
beta = nan(len,1);
gamma = nan(len,1);
q1 = nan(len,1);
q2 = nan(len,1);
q3 = nan(len,1);

for curFrame = 1:len
    alpha(curFrame) = rad2deg(atan2(trDistRelProx(4,3,curFrame),trDistRelProx(4,4,curFrame))); %Rotation
    about e1, FE (e1=FE for me)
    beta(curFrame) = rad2deg(pi/2-acos(trDistRelProx(4,2,curFrame))); %Rotation about e2, AA (e2=IE for
    me)
    gamma(curFrame) = rad2deg(atan2(trDistRelProx(3,2,curFrame),trDistRelProx(2,2,curFrame))); %Rotation
    about e3, IE (e3=AA for me)

    %Grood-Suntay clinical translations, NOTE: T_te_fe(1,3) is the same as cos(Beta) in the GS Paper
    q1(curFrame) = (trDistRelProx(2,1,curFrame) +
    trDistRelProx(4,1,curFrame)*trDistRelProx(4,2,curFrame));%-n.q1;
    q2(curFrame) = (trDistRelProx(3,1,curFrame));%-n.q2; %IE
    q3(curFrame) = (-trDistRelProx(4,1,curFrame) -
    trDistRelProx(2,1,curFrame)*trDistRelProx(4,2,curFrame));%-n.q3; %AP
end

%Generate Output
angles = [alpha, beta, gamma];
disp = [q1, q2, q3];

```

F.5.3 *fcn_filtergsdata.m*

The purpose of this function is to smooth the resulting G&S output and remove any jitters from the data.

```
function [ dataFilt, dataError ] = fcn_filterGSData(data)
% Filter the G&S data
[r c] = size(data);
n = 2; %Order of filtfilt
wn = .025; %Cutoff Frequency
dataFilt = zeros(size(data)); %Create an array to hold the data
[b,a] = butter(n, wn); %Create the butterworth filter with order n, and natural frequency wn
for i = 1:c %This will filter Fx, Fy, Fz, Tx, Ty, and Tz from the force data columns.
    dataFilt(:,i) = filtfilt(b,a,data(:,i));
end

dataError = abs(mean((dataFilt-data)./data*100));
```

F.6 *Graphical Interfaces*

F.6.1 *gui_bonePositionGrapher3.fig*

This program was written in Matlab to verify the CS construction, and to verify that the transformations were being done correctly. This program has the capability to playback the recorded animation at various speeds, to view any specific frame, and to display from any coordinate view. For example you can make the tibia at the origin and view the animation relative to the tibia, talus or calcaneus.

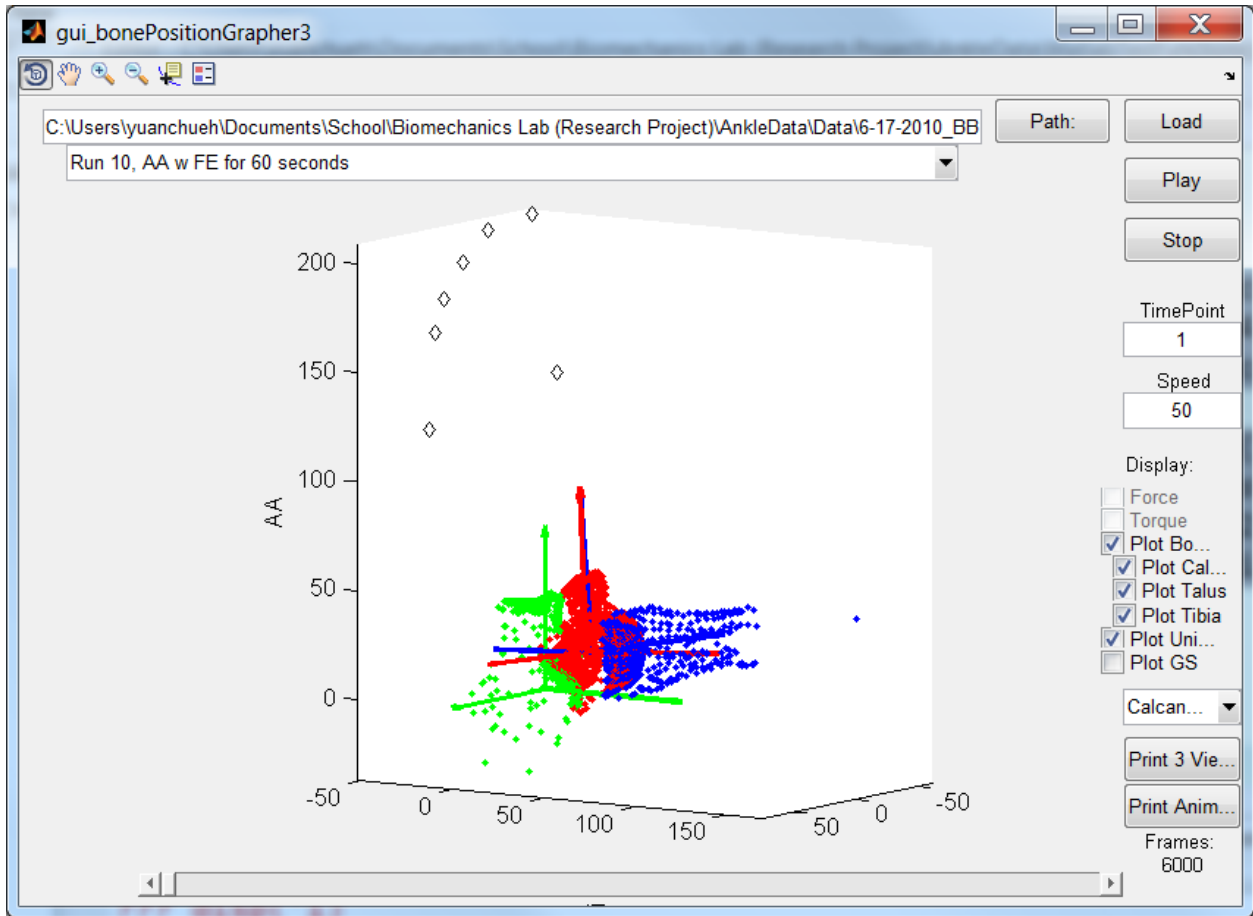


Fig. F.1: Example view of the bone position grapher written in Matlab and used to validate the kinematics.